Universities High Voltage Network (UHVnet)

2nd UHVnet Colloquium
(In association with the Institute of Physics Dielectrics Group)

"High Voltage Measurement and Insulation Research"

Glasgow Caledonian University

Wednesday 21st January 2009

IET Collective inspiration

IOP Institute of Physics

Glasgow Caledonian University

Agenda

9:30 – 10:00	Registration and Refreshments Registration: Foyer of CPD (Continuous Professional Development) Building
10:00 – 10:15	Professor Manu Haddad, Chair of UHVnet, Cardiff University *"Introduction to UHVnet"* *Room A005*
10:15 – 11:00	Dr Erik de Jong, KEMA *"Flex Power Grid Laboratory - Assisting grid integration of distributed generation"* *Room A005*
11:00 – 11:30	Professor Chengke Zhou, Glasgow Caledonian University *"Partial Discharge Monitoring in Medium Voltage Cables - Experience in Data Denoising"* *Room A005*
11:30 – 12:00	Professor Phil Moore, University of Strathclyde *"Advances in radiometric monitoring of partial discharges"* *Room A005*
12:00 – 12:45	Lunch *CDP Building*
12:45 – 14:45	Research Student Poster Presentation Sessions, UHVnet Universities *Posters from UHVnet students/researchers, IoP students/researchers, etc.* *CPD Building*
14:45 – 15:15	Dr Jenny Cooper, National Grid, plc *"HV challenges in the transmission network"* *Room A005*
15:15 – 15:30	Professor Manu Haddad, Chair of UHVnet, Cardiff University *Closing comments and discussion* *Room A005*

Please visit the UHVnet Website at: www.uhvnet.org.uk

Speaker presentations can also be found on the UHVnet website

2nd UHVnet Colloquium Booklet Contents

Professor Manu Haddad, Chair of UHVnet

Chairman's Introduction to the 2nd UHVnet Colloquium

Welcome to the 2nd UHVnet colloquium. The first colloquium was organised back in 2005 at Cardiff University, and was attended by some 70 delegates with over half of them from industry. 33 papers were presented in the areas of insulation ageing and condition monitoring of high voltage plant. This second colloquium focuses on disseminating postgraduate research students' work in the areas of measurements and condition monitoring.

The Universities High Voltage network, UHVnet, was founded some 5 years ago to provide a dissemination and networking forum for researchers and engineers investigating aspects of high voltage phenomena, and high voltage equipment and systems. This is also aimed at facilitating direct and effective exchange of expertise amongst network members and industry, and at establishing closer collaboration between university research groups and industrial partners including both manufacturers of high voltage equipment and electricity utilities. UHVnet is now open to new members from academia and industry.

The current UHVnet consists of seven university partners having strong high voltage engineering research groups; they are based at the following universities: Southampton, Cardiff, Leicester, Manchester, Liverpool, Strathclyde and Glasgow Caledonian. These groups cover most topics of high voltage research, and their members are well established international experts in their areas of research.

The primary objective of UHVnet is to maintain the Health of the High Voltage Discipline in the UK. Furthermore, UHVnet has the following specific objectives:

i. To increase visibility and dissemination of work carried out in universities in the high voltage area;
ii. To ensure future health of discipline by attracting younger researchers, and establish a community of networked researchers;
iii. To improve training and learning for postgraduate students and researchers, and ensure continuity;
iv. To develop academic links between academic institutions and contribute to the innovation and engagement agenda;
v. To highlight contributions and establish a high profile for the discipline to attract /influence industry and government research funding;
vi. To develop and undertake multi partner initiatives to address major issues faced by industry, and
vii. To raise the international profile of the group.

Flexible Power Grid Laboratory.

Assisting grid integration of distributed generation

UHVnet colloquium, 21 January 2009
Glasgow Caledonian University, Glasgow, U.K.

Anton Linssen
Erik de Jong

Experience you can trust.

Content.

- Introduction - trends towards future networks
  - Grid integration of distributed generation
  - Flex Power Grid Lab
- Research subjects
  - Intelligent grid components
  - Fault ride-through
  - Power quality
  - Pre-qualification and standardisation
- Summary & Conclusions

Trends towards future networks.

- New emerging technologies / innovations
  - Bulk to 'greener' decentralised power (solar, wind)
  - Integration of PE and ICT applications in grid
  - Smart grids (DER / integrated network control)
  - New (privatised) equipment (intDS)
- Challenges:
  - PQ aspects
  - Stability aspects
  - Standardisation
  - Efficiency

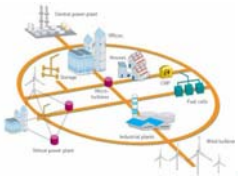

Power grids of the future.

Existing power system:

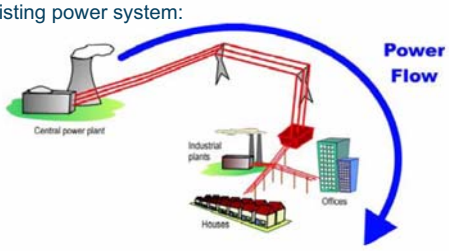

Power grids of the future.

Existing power system is mutating

≈15% of EU power demand in 2010 delivered by renewable energy sources (RES):

- Wind
- Solar
- Biomass
- Gas-based micro technologies

Including storage (Peak shaving, etc)

Power grids of the future.

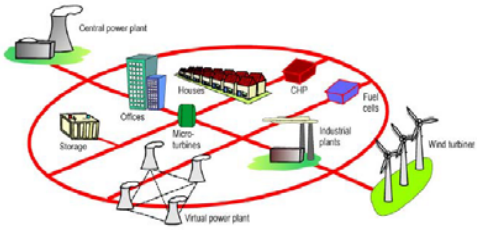

Power grids of the future.

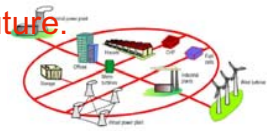

≈small to medium sized (100kW – 50 MW) conversion technology

- High-speed micro & mini power turbines
- Reciprocal machines
- Fuel cells
- Combined Heat & Power systems

Grid integration of renewables.

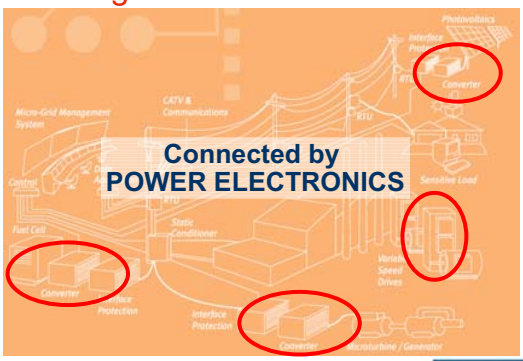

Introduction - Flex Power Grid Lab.

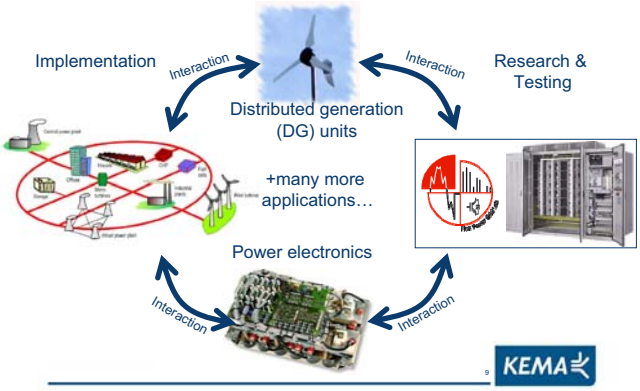

Key figures makes test facility unique.

- Voltage level up to ***3.3 kV***
- ***DC to 75 Hz*** frequency range
- Continuous power up to ***1 MVA***
- Up to ***>25th*** harmonics
- ***4 Quadrant*** operation
- Synchronisation with other source
- Controllable power exchange

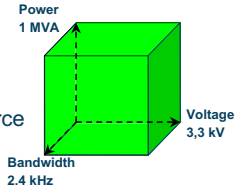

A free programmable polluted grid

Programmable GRID parameters.

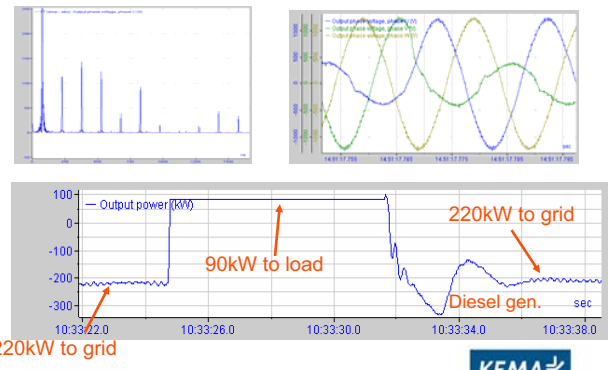

Content.

- Introduction - trends towards future networks
  - Grid integration of distributed generation
  - Flex Power Grid Lab
- Research subjects
  - Intelligent grid components
  - Fault ride-through
  - Power quality
  - Pre-qualification and standardisation
- Summary & Conclusions

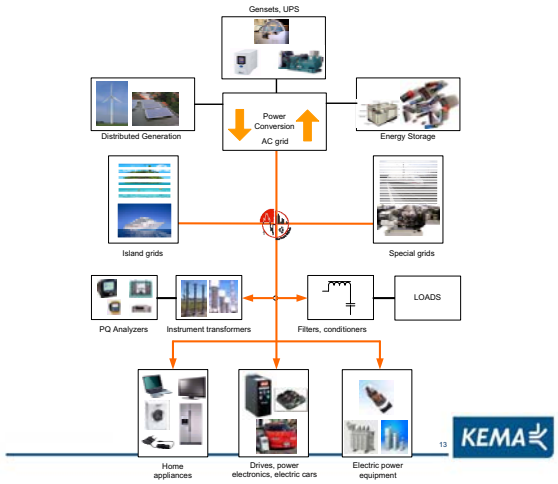

Intelligent components.

Intelligent distribution station

- Aggregation of Customer Demand and Supply
- Guaranteeing Power Quality
- Information Gateway between Customers and Transmission Grid
- Control Gateway between Customers and Transmission Grid

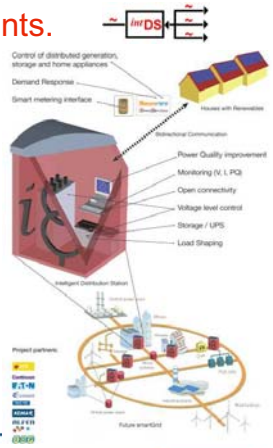

Intelligent components.

Intelligent distribution station

- Aggregation of Customer Demand and Supply
- Guaranteeing Power Quality
- Information Gateway between Customers and Transmission Grid
- Control Gateway between Customers and Transmission Grid

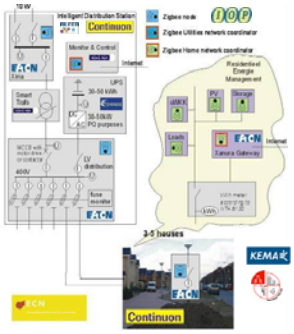

Fault ride-through.

- Disconnection criteria

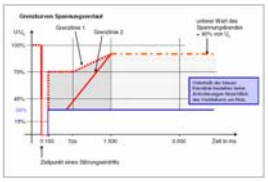

- Reactive power support
  - Req. by German grid code from 1 Jan. '09

PQ research and testing.

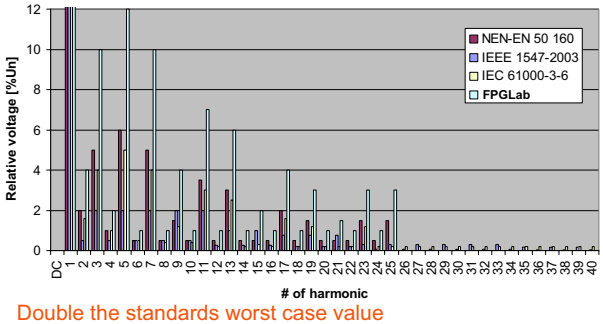

Double the standards worst case value

Relative phase angels freely and individually adjustable

PQ research and testing.

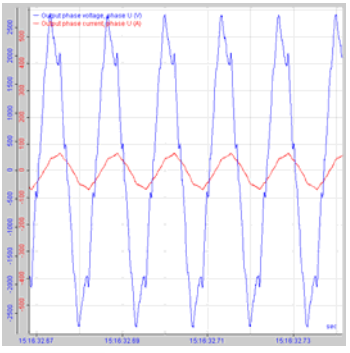

f=75 Hz

EN50160 (mix)

5,0% 3rd harm.
6,0% 5th harm.
5,0% 7th harm.
1,5% 9th harm.
3,5% 11th harm.
1,5% 19th harm.

R||L Load (PF=0.7)

300kVA @ 3300Vrms

PQ research and testing.

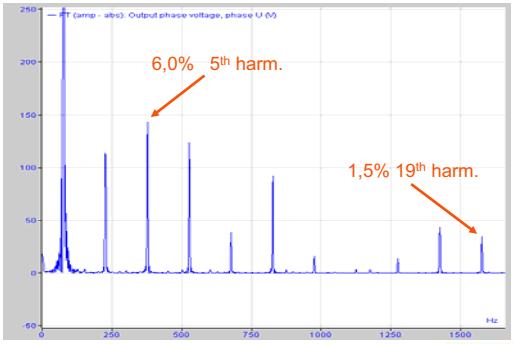

PQ research and testing.

At medium voltage level and full power:

- PQ immunity analysis
- Thermal analysis
- Audible noise analysis
- EMI analysis

Standardisation.

Pre-qualification and standardisation
- DERLab consortium

- International white paper on grid inverters
  - Research needs
  - Standardisation needs

Content.

- Introduction - trends towards future networks
  - Grid integration of distributed generation
  - Flex Power Grid Lab
- Research subjects
  - Intelligent grid components
  - Fault ride-through
  - Power quality
  - Pre-qualification and standardisation
- Summary & Conclusions

Summary & Conclusion.

- Grid integration of RES & DER high on political agenda
- Dynamic, active grids are evolving (Smartgrids)
  - Increasing small scale generation in the grid
  - Power flow in multiple directions
  - Increasing ICT to control the grid
- Ancillary services by grid coupled power electronics provide opportunities (also during grid-fault conditions)
- Testing and standardisation requirements still lagging

Visit our website for more details.

The Flex Power Grid (FPG) Lab offers unique services for DG and RES grid integration, power conversion equipment, and power monitoring and control devices by offering a predefined grid or load in the MV range.


KEMA
Thank you for your attention.
Anton.Linssen@kema.com
+31 26 356 6071
Erik.deJong@kema.com
+31 26 356 2794
www.kema.com
Experience you can trust.

GLASGOW CALEDONIAN UNIVERSITY

Partial Discharge Monitoring in Medium Voltage Cables --- Experience in Data Denoising

Prof. Chengke Zhou
Dr. D.M.Hepburn, Mr. M.Michel*, Mr. X. Song

Glasgow Caledonian University / *EDF Energy

Talk Overview:-

- The need for PD-based condition monitoring of MV cables
- On-line vs. Off-line monitoring
- Noise in on-line cable condition monitoring signals
- Wavelet-based data processing
- Conclusions/Future Work

Why Condition Monitor MV plant?

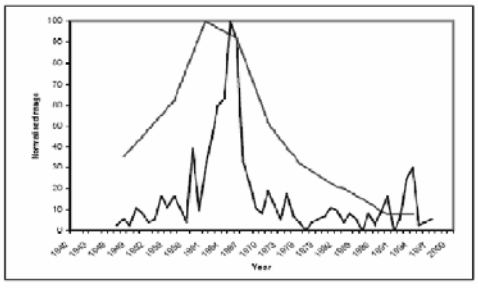

Typical UK MV Plant Install Rate (1940 to 2000)

Why Condition Monitor MV plant?

Asset	Asset type	Design life (years)
Transformers	>11kV	50
	11kV ground mounted	45
	11kV pole mounted	45
Switchgear	Indoor	45
	Outdoor	40
Cables	132kV	60
	33kV	60
	6.6kV / 11kV	70

UK utility "Design life" of MV plant

Why Condition Monitor MV plant?

- Existing MV plant continues to age
- Current replacement rate is not fast enough to stop MV plant failure
- Condition monitoring is required because it
  - Provides early warning of incipient fault
  - Allows asset replacement programme to be prioritised
  - Avoids expensive unplanned outage

Cable PD pre- & post-replacement

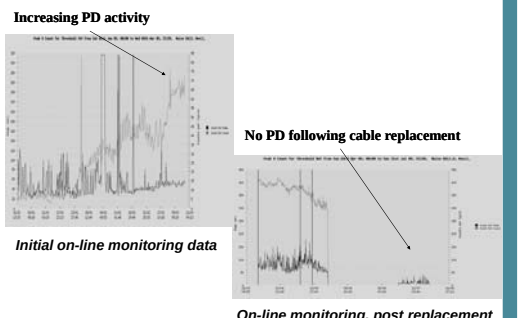

Initial on-line monitoring data

On-line monitoring, post replacement

On-line vs Off-line cable PD detection

On-line: system permanently installed

Off-line: test van often employed.

PD monitoring – On-line vs. Off-line

- Off-Line monitoring – mature technology:
  - Both the repetition rate at which PD are excited and the discharge magnitude can be correlated with applied voltage;
  - The cable under test must be taken out of service;
  - Specialists needed to set up, perform tests and to reinstate system;
  - The high costs of operating a cable van system;
  - Offers only snapshots of cable condition and only under the specific testing conditions (1 phase energised at one time).
- On-line monitoring – increasing application:
  - Continuous monitoring of system possible;
  - All 3 phases are energised, i.e. under standard operational situation;
  - Once installed, does not require the costly interventions associated with off-line testing;
  - Seen as an easier and less expensive solution, providing an economical advantage;
  - No established theory for diagnostics.

PD activity vs. Time

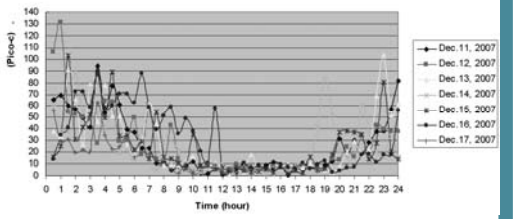

Variation in PD activity in one cable

Challenges in on-line monitoring

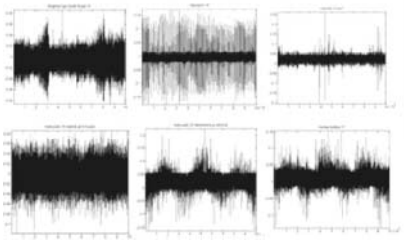

Variation in on-line signal from MV cables:
PD activity, RF noise and external pulsative signals

On-line data frequency spectrum

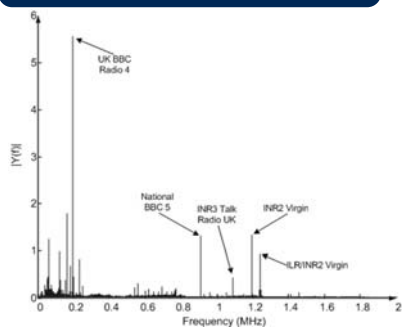

FFT of data signal from one end of 1022m MV cable

Variation in detected pulse shape

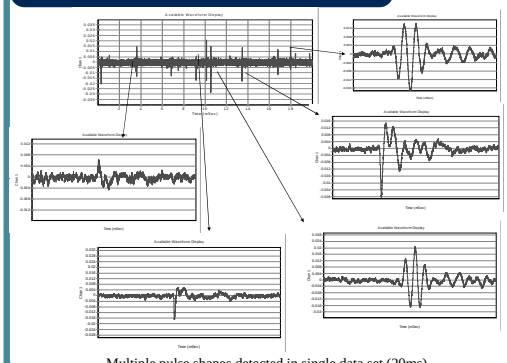

Multiple pulse shapes detected in single data set (20ms)

Typical waveforms from on-line cable PD detection systems

Noise from Exciter pulses

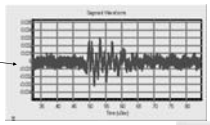

PD from local switchgear

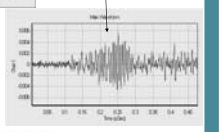

PD from 11 or 33kV paper insulated cable

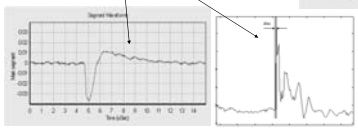

Wavelet-based denoising

- PD test result interpretation often encounters severe problems in practical, on-site testing ---- NOISE !

Very Noisy Signal

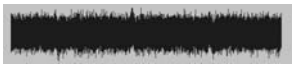

Misleading Interpretation!!

'Clean' Signal

Wavelet-based denoising

- Wavelet denoising procedure
  - Apply DWT to noisy signal
    - to produce noisy wavelet coefficients
  - Threshold the wavelet coefficients
    - to eliminate those associated with noise and retain those related to PD pulses
  - Reconstruct signal - cleaned data !

Applications

- **Applied to IEC-60270 detecting system**
- Applied to ultrasonic detecting system
- Applied to CT-based detecting system

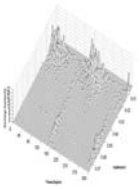

$\varphi - q - N$ Analysis

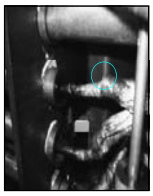

PD Source Location

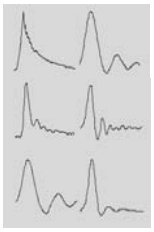

PD Pulse Shape Analysis

Problems with DWT

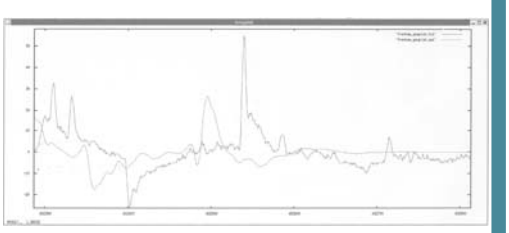

Second Generation Wavelet Transform or Lifting scheme

- Better adaptability
- Calculation --- quicker
- Less memory is required
- More accurate in pulse shape reconstruction

Examples of Adaptability

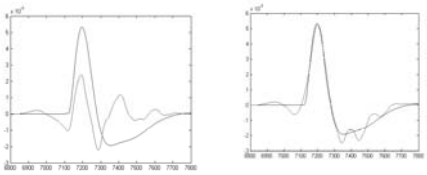

DWT SGWT

Application of SGWT to PD data denoising

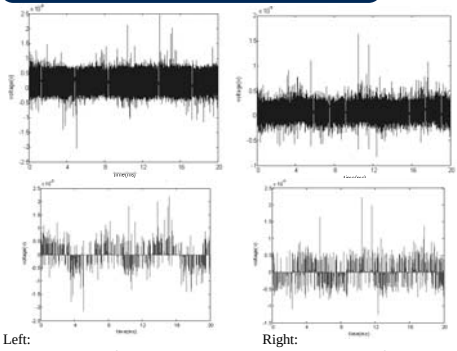

Left:
HFCT at one end of a 1022m cable

Right:
HFCT at other end of cable 1 hour later.

Frequency spectra from cable ends

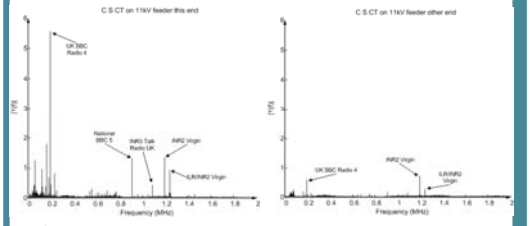

Left:
FFT from one end of cable

Right:
FFT from other end of same cable

Zooming-in

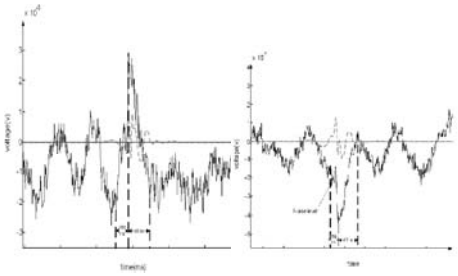

This is the category… Lifestyle etc.

PD source localisation

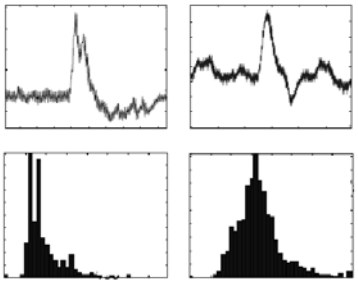

Top: individual pulses observed at the two ends of the cable

Bottom: PD count vs pulse risetime.

Cable Mapping Results

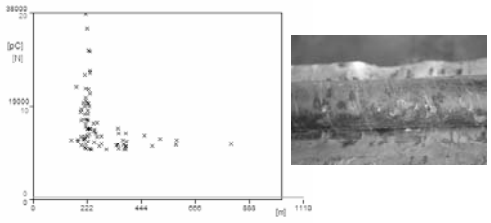

Off-line cable mapping results revealed that the source of PD is around 222 metres from one end and 800 metres from the other.

Multiple PD sources

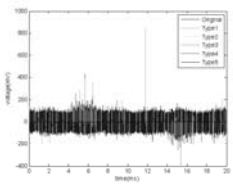

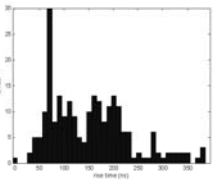

Left hand Figure:
Blue: original data.
Red: pulse type 1.
Light blue: pulse type 2.

Right hand Figure:
PD count vs risetime.

PD pattern and pulse shape may contain location and defect type information.

Conclusions

- Data acquired from on-line cable monitoring systems contain significant levels of noise.
- The most significant noise sources are RF and pulsative noise.
- SGWT based algorithm is effective in signal denoising
- Pulse shape and PD pattern may offer valuable information on PD fault type and source location

Future Work

Knowledge Discovery from On-line Cable Condition Monitoring Systems: Insulation Degradation and Ageing Diagnostics

Prof. C. Zhou, Dr. D.M. Hepburn (GCU),
Dr. M.Judd and Dr. W.H.Siew (Strathclyde)

- Develop an innovative data mining technique and apply the technique to acquire knowledge on insulation condition and aging mechanism of power plant items directly from on-line Partial Discharge (PD) monitoring systems;
- Validate the results by extensive laboratory and on-site experiments which will be expected to generate new knowledge on
  - understanding of relationship between PD current pulse and physical degradation,
  - the traveling loss of PD signals and
  - the correlation between measurable quantities with the insulation degradation and associated risks

Future development --- Knowledge extraction

- Knowledge rules for on-line and off-line monitoring are different
  - The electric field distribution is different in the two cases.
  - During off-line PD testing the equipment used is generally connected to one cable-end while the other end is left open.
  - On-line systems monitoring underground cables are fully connected with other parts of the network.
  - The operating temperature of the cable depends directly on the load.
  - PD activity in power plant depends on time varying factors such as thermal and mechanical stress. Off-line testing cannot provide information on the effect of these factors, only giving snapshots and only under the specific testing conditions.
  - Knowledge for diagnostics in on-line monitoring has to be acquired from on-line monitoring data.

Innovative simulations

Concluding remarks

- MV plant items are ageing
- Reported plans indicate replacement will occur long after design life is completed
- PD based on-line condition monitoring is gaining importance in management of the ageing assets
- Challenges remain in maximising the benefit of on-line monitoring systems
- Bright future for further technical innovations

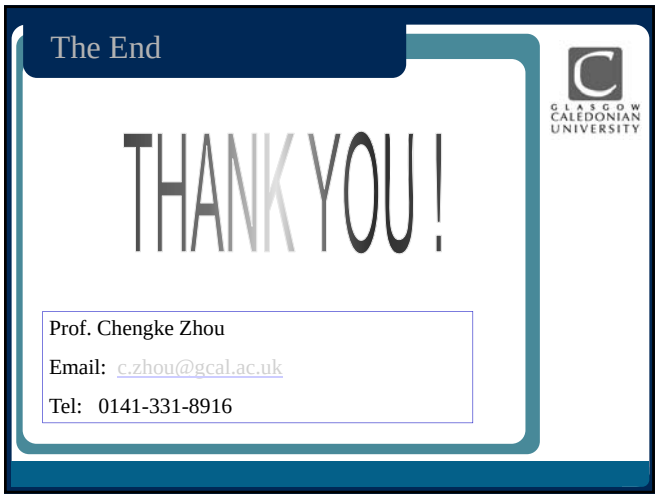
The End
THANK YOU !
GLASGOW CALEDONIAN UNIVERSITY
Prof. Chengke Zhou
Email: c.zhou@gcal.ac.uk
Tel: 0141-331-8916

INSTITUTE FOR ENERGY AND ENVIRONMENT

University of Strathclyde Engineering

Advances in radiometric monitoring of partial discharges

Prof Philip Moore
Electrical Plant & Diagnostics Group
Department of Electronic and Electrical Engineering

Structure of presentation

- Basic principle
- Gas-insulated substations
- Air-insulated substations
- Transformer monitoring

Basic Principle

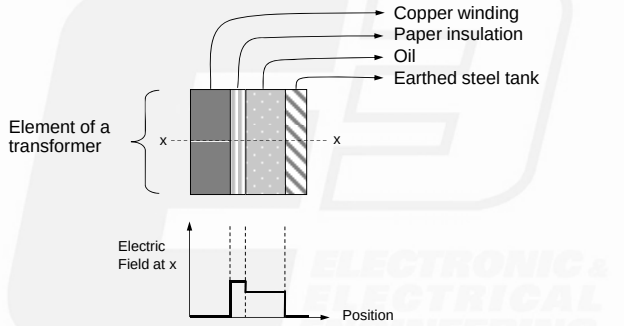

Basic Principle

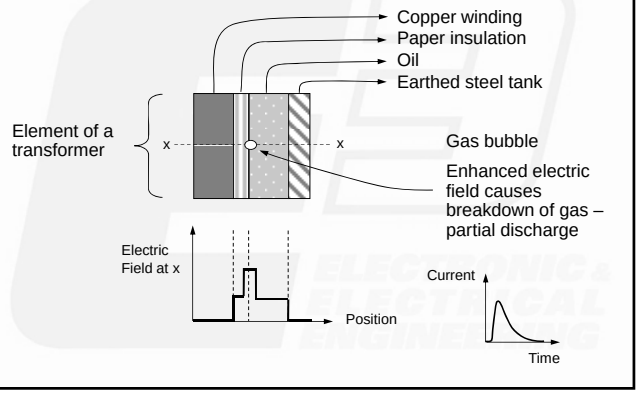

Partial discharge current

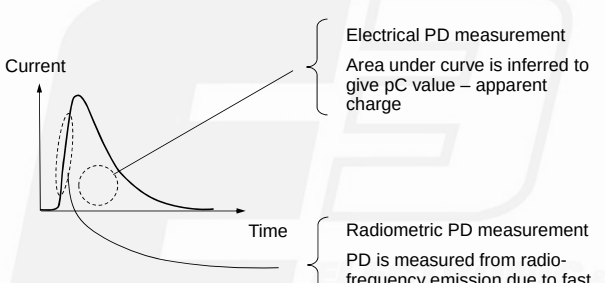

Radiometric PD measurement

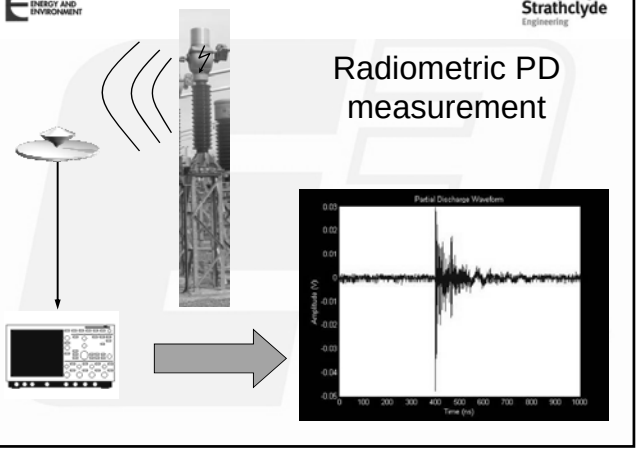

Gas Insulated Substations

DMS

Gas insulated substations

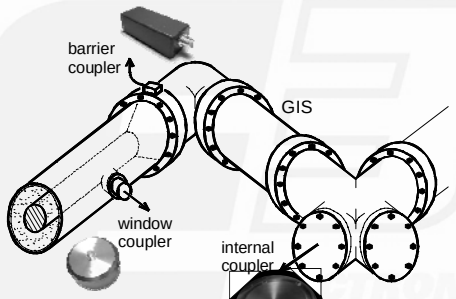

- Pioneered during 1980s
- CIGRE procedure for verifying sensitivity of UHF detection systems in 1998

Locating Defects by the Time-of-Flight Method

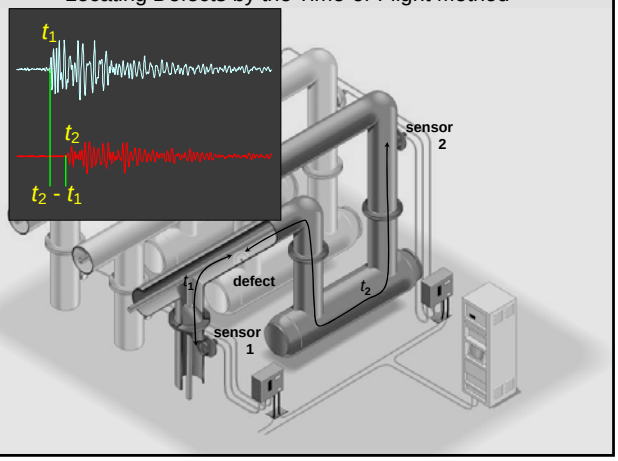

Air Insulated Substations

- PD source location
- Fixed PD monitoring systems
- Relocatable monitoring systems
- Substation PD surveys

elimpus

PD source location

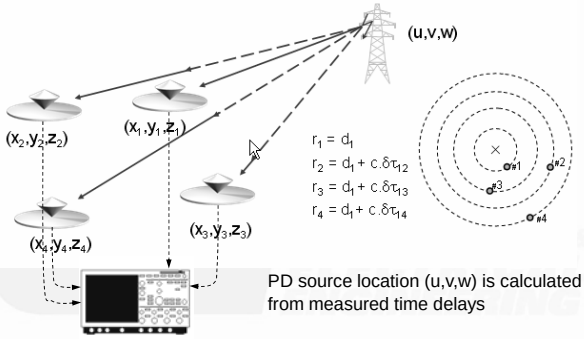

PD source location (u,v,w) is calculated from measured time delays

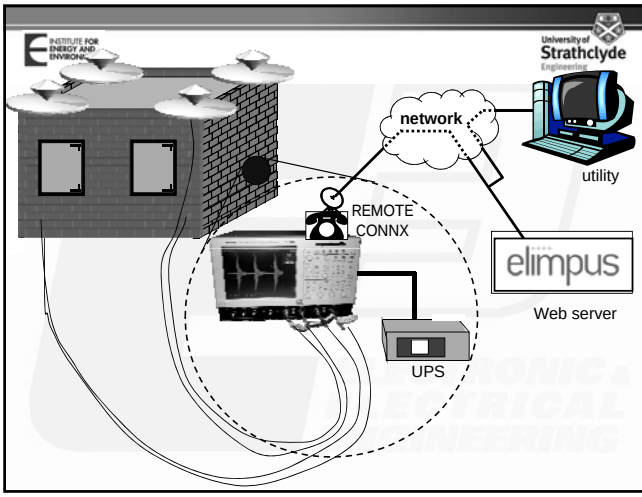

Fixed PD monitoring system

Substation A – recorded data

- In a typical month, system triggered by 12,000 records
- Around 11,000 (~90%) of these records were *non-impulsive*; typically mobile phone transmissions
- An algorithm was developed to discard non-impulsive records
- System is also sensitive to switchgear operations

Substation A – recorded data

Breakdown of impulsive records for month of February 2003

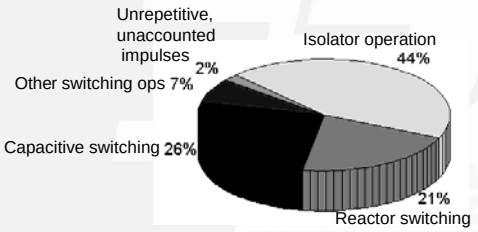

Substation A – recorded data

Breakdown of impulsive records for month of January 2003

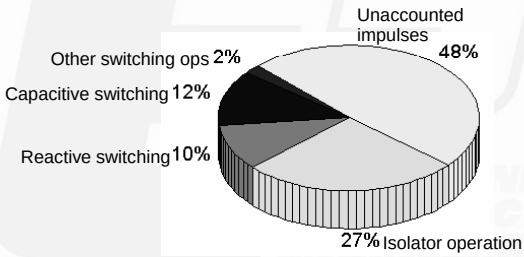

Substation A – recorded data

Breakdown of unaccounted impulses for month of January 2003

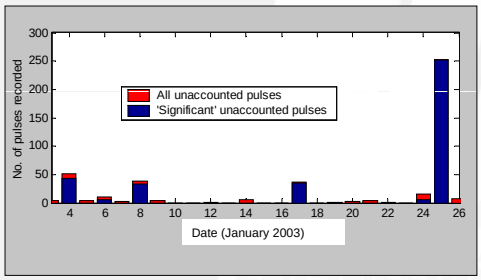

What happened on 26 January 2003?

Substation A – 26 Jan 2003

PD Location

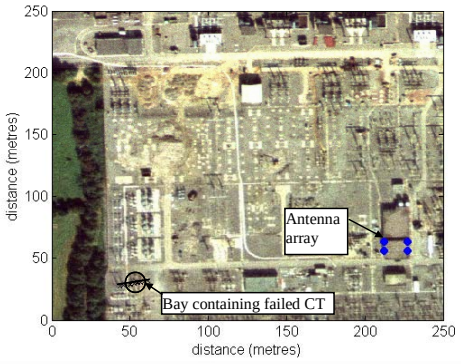

Current Installations

- 4 systems in UK
- 5 systems in USA
- 1 system in Australia

Automated PD Analysis

- Screening for
  - Circuit breaker/isolator operations
  - Mobile phone triggers
- Adaptive sensitivity
- Automated location
- Automated classification

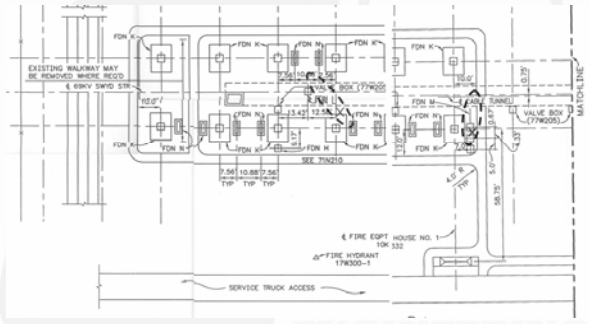

Day history for discharge 2

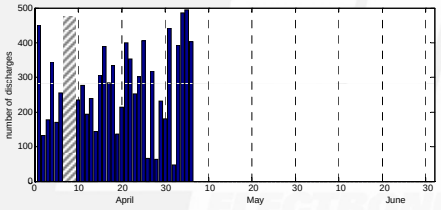

No data for these days

69 kV VT after disassembly

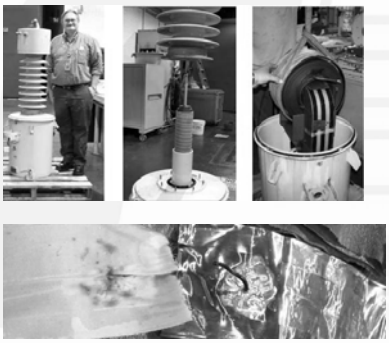

Relocatable monitoring system

Substation PD surveys

Typical result – 275 kV substation

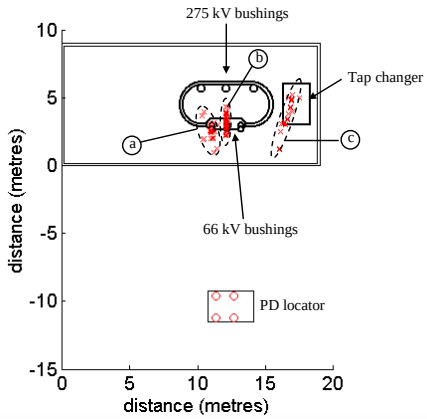

Mobile PD Locator - Experience

- Transformer bushings
- Through bushings
- Cable sealing ends
- Tap changers
- Current/voltage transformers
- Isolators
- Post insulators

Transformer monitoring

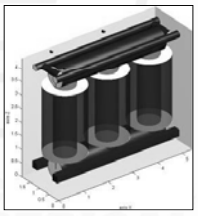

Locating PD in a power transformer

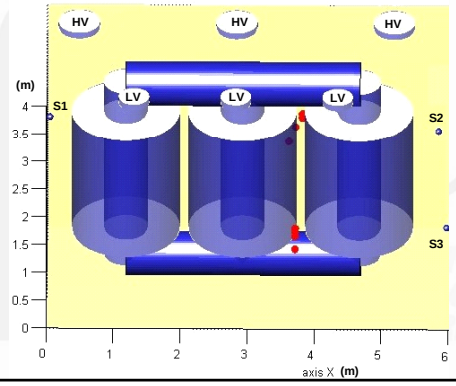

Externally coupled signals

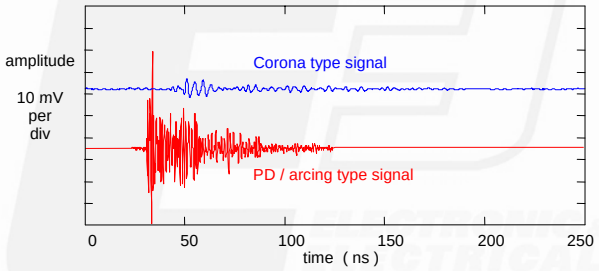

Example

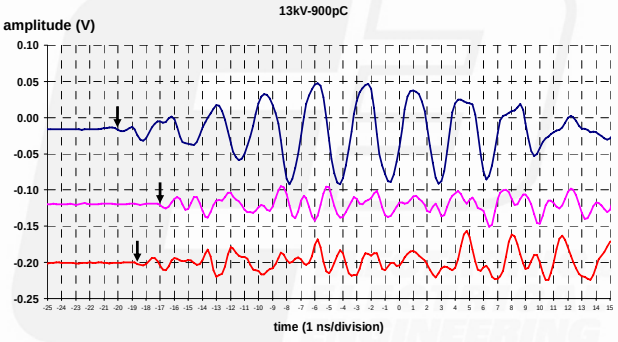

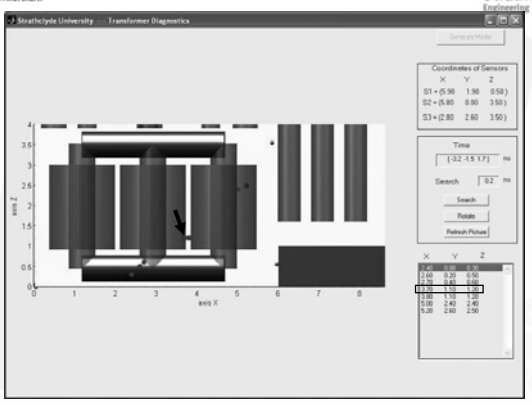

Transformer couplers

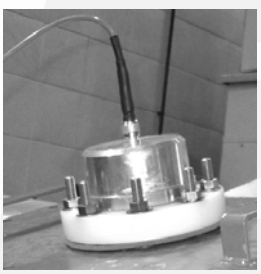

UHF sensor for DN80 oil valve on power transformer (images courtesy of LDIC GmbH)

Advantages of radiometric PD monitoring

- Proven technology
- Ability to locate source of PD
- Safe – no electrical contact
- Easy to apply

Acknowledgements

- Dr Martin Judd
- Dr Iliana Portugues

HV Challenges in the Transmission Network

Jenny Cooper

nationalgrid
The power of action.

Who is National Grid?

National Grid is one of the world's largest utilities, focused on delivering energy safely, reliably, efficiently and responsibly .

We own and operate gas and electricity transmission and gas distribution networks in the UK and US and electricity distribution networks in the US.

Our core skills lie primarily in the management of large and complex energy delivery networks.

National Grid's goal is to be the world's premier utility through focus on

- **Performance**
- **Integration**
- **Reliability**
- **Safety**

National Grid UK Electricity Transmission

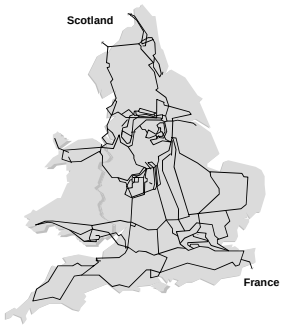

Key Statistics

- Operating voltages 132, 275 & 400kV
- 341 substations
- 190 Grid Supply Points
- 128 generating unit connections
- Installed capacity: 67 GW
- Maximum demand: 53.29 GW
- Energy transmitted: 308.7 TWh
- 14,102 circuit km of OHL
- 985 km of cables
- 21,890 Transmission towers
- 2,751 circuit breakers
- 727 transformers

National Grid UK Gas National Transmission System (NTS)

Key Statistics

Operating pressures 70-94 bar

Miles of NTS pipeline - 6800km

Compressor Stations - 25

Beach Gas Reception Terminals - 6

Off-takes to Distribution networks - 106

LNG Storage Sites (Unregulated) - 5

End Consumers - 21.2 Million

Peak Demand (04/05) - 418 million cubic meters

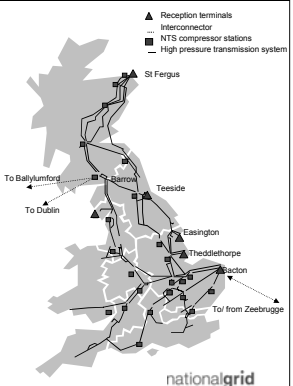

Generic Challenges for the Electricity and Gas Transmission Networks in 2009

- Asset replacement of the energy networks
- Changing sources of energy supply
- UK Emissions targets
- Implementation of new technology
- Energy policy, planning and regulatory framework

Transformers Asset Age Profiles

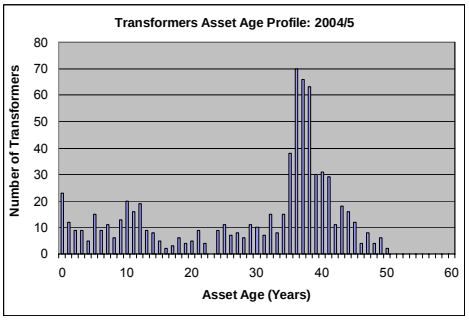

With many outages highly restricted it is critical to understand the condition of plant before ……

7

nationalgrid
The power of action.

Asset Management Maturity Model

'Reactive based' (e.g. repair/replace on fail)	'Interval based' (e.g. maintain at a set interval, replace at asset life)	'Condition based' (e.g. maintain/replace based on condition)	'Risk & Criticality based' (e.g. maintain/replace assets with the highest risk and greatest importance)

Increasing maturity of asset management based on research to predict lifetime of assets

8

nationalgrid
The power of action.

Changing Sources of Electricity

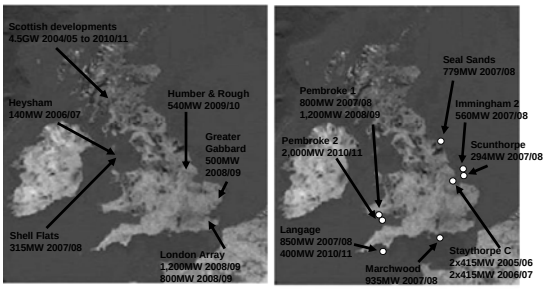

Potential wind developments **Potential gas-fired plant**

9

nationalgrid
The power of action.

To Complete the Picture - Changing Sources of Gas

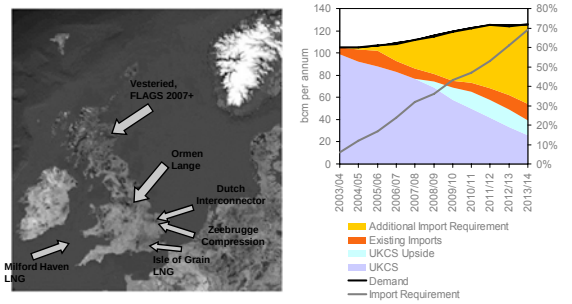

10

nationalgrid
The power of action.

Renewables and carbon dioxide reduction targets are challenging.

15% of final energy demand to be met from renewable sources by 2020 (EU Directive)

Target to reduce CO_2 emissions to 80% below 1990 levels by 2050

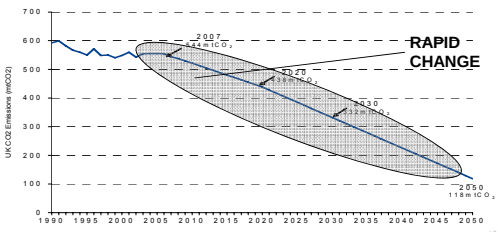

11

nationalgrid
The power of action.

Heat, transport and electricity are major CO_2 polluters and must be addressed

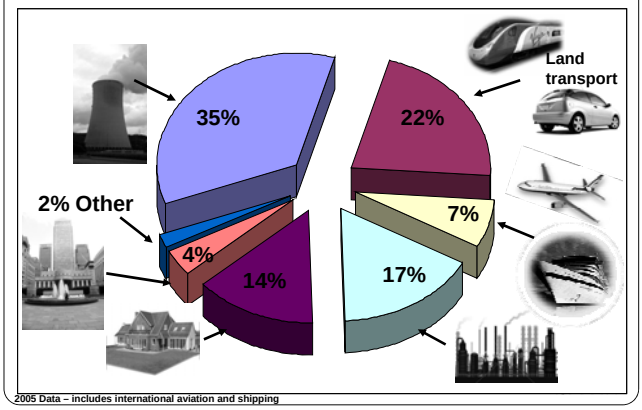

2005 Data – includes international aviation and shipping

There are two strategies to meet the 15% renewables target

Renewables 'slices' must "add up" to 15% by 2020

1742TWh
UK Final Energy Demand

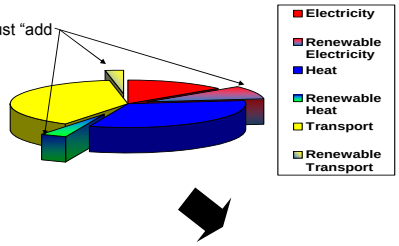

"Make the pie smaller"

(reduce demand for energy across the three sectors)

"Make the renewable slices bigger"

Increase the contribution from renewables in each sector

Business As Usual - 2020/21 Capacity Mix (GW) – A problem!

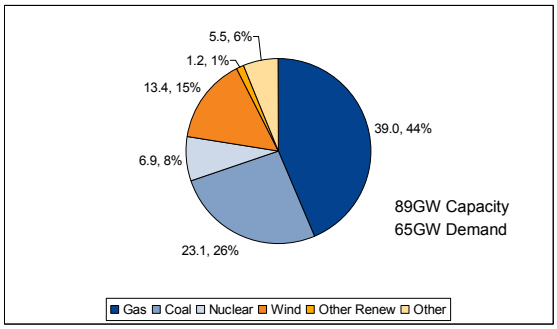

The Challenge of UK Renewable and emissions targets

National Grid has developed Green 'hypotheses' which assume;

- 100% domestic compliance
- EU 15% target for renewables in GB met in 2020
- emissions reduce along a trajectory towards CO_2 target by 2050

Developing these hypotheses helps us understand the drivers, needs and trade-offs.

Low Carbon Electricity

A collaborative effort amongst the big stakeholders to connect wind by 2020

Low Carbon Energy

Significant behavioural change amongst all parties which leads to green action.

Introducing Low Carbon Electricity

We have developed two separate "hypotheses" describing plausible routes to achieving the 2020 targets and beyond

- Low Carbon Electricity
- Low Carbon Energy

Our first hypothesis requires

- Significant supplies from wind, means new fossil fuel with CCS and new nuclear
- Improvements in energy efficiency create demand reductions…
- …but demand reductions are netted off by some electrification of heat, followed by transport

Low carbon Electricity – 2020/21 Capacity Mix (GW)

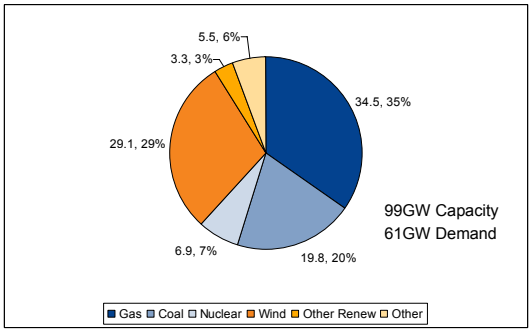

Introducing low carbon energy

Back to the two separate "hypotheses" describing plausible routes to achieving the 2020 targets and beyond

- Low Carbon Electricity
- Low Carbon Energy

Our second hypothesis requires

- more significant contribution from heat and transport
- greater balance across all energy sectors
- significant behavioural change amongst all parties which leads to green action

Low Carbon Energy 2020

Electricity

Lower renewables share (~27%) of electricity demand

- **compare with 35% in 'Low Carbon Electricity'**

Reduced requirement for offshore wind development

- **15 GW wind in total, with 4 GW offshore**

Demand

The population driven to become climate-aware and everyone 'does their bit'

- **Insulation, SMART, efficient appliances**

Combined effect is that energy demand falls by 15%

Capacity Mix

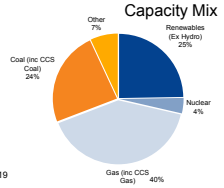

Description of UK/EU target:

- **20% of electricity demand to be met by renewable sources (UK).**
- **15% of all energy met by renewable sources which equates to an average of 34-40% of electricity demand (EU)**

Projected outcome: 27%

CO_2 emissions reduction of at least 26% (relative to 1990 levels)

Circa 35% -40%

nationalgrid

19

Low Carbon Energy 2020

Heat

More industrial and district CHP (new build)

- biomass and gas-fired

Ground source heat pumps

Some electrification, e.g. storage heating

Transport

Some modal change (e.g. private to public transport)

Electrification of rail and some urban commercial fleet

10% Biofuel target met

Capacity Mix

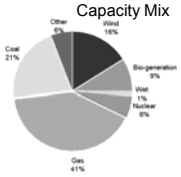

Description of UK/EU target:

- **20% of electricity demand to be met by renewable sources (UK).**
- **15% of all energy met by renewable sources which equates to an average of 34-40% of electricity demand (EU)**

Projected outcome: 27%

CO_2 emissions reduction of at least 26% (relative to 1990 levels)

Circa 35% -40%

nationalgrid

20

Low Carbon Energy 2030

Heat

More CHP into existing buildings

More ground source heat pumps

More electrification, e.g. storage heating

Transport

Continued modal change

Electrification of private vehicles

- Plug-in hybrids?

Capacity Mix

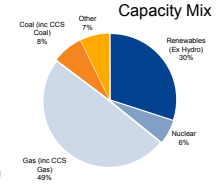

Renewable target not currently set for 2030

CO_2 emissions reduction of at least 44% (relative to 1990 levels)

Circa ~ 50%

nationalgrid
The power of action.

21

Hypotheses Summary (renewables share of total final energy demand)

YEAR 2020		
ELECTRICITY	9%	5%
HEAT	3%	7%
TRANSPORT	3%	3%
TOTAL	15%	15%

nationalgrid
The power of action.

22

2008 to 2020 Flows

2008 flows – No problems!

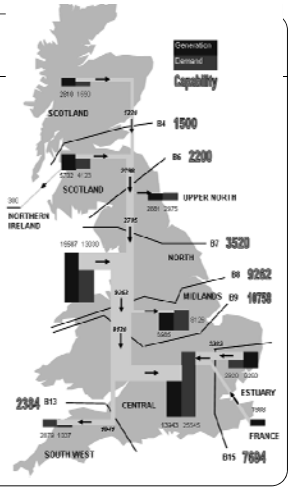

23

2008 to 2020 Flows

2020 Potential Flows

Very heavy flows from North Scotland, through Scotland and Upper North England

High volume of offshore wind farms off East Coast

Potential for Central Wales renewable generation

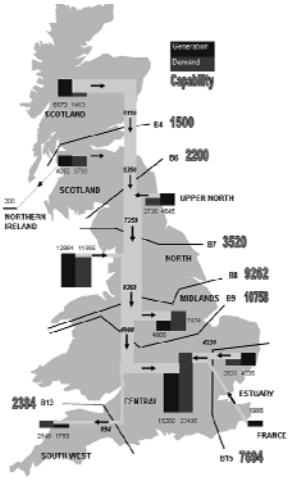

24

Getting Renewables from Scotland

Possible solutions, Offshore HVDC – providing additional capacity

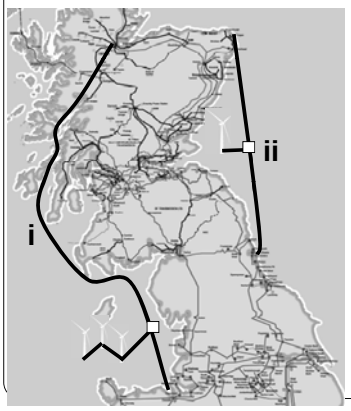

Accommodates 10 GW of renewables from Scotland

Option of connecting 4 GW of offshore wind

Challenges in HVDC cables and associated technology including control devices

Beauly – Deny line is a pre-requisite

nationalgrid
The power of action.

Getting Renewables from Scotland

Alternative option – Incremental Onshore Reinforcements – getting more out of existing capacity

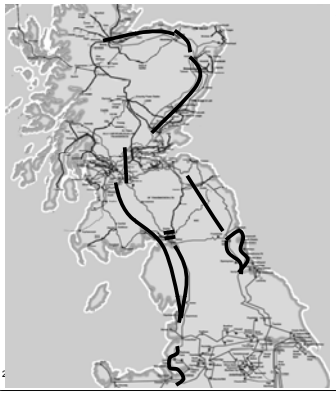

Accommodates 10 GW of renewables from Scotland

Option of connecting 2 GW of offshore wind

Use of FACTS (Flexible AC Transmission systems) devices to improve stability limits.

Increased operating voltage

Convert HVAC to HVDC

Improved control systems to improve stability limits – HTS, semiconductors.

Connecting East Coast offshore wind

Possible solution to series of east coast radial connections

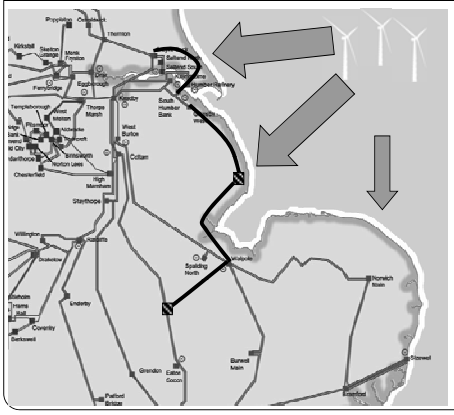

Facilitating large volumes of wind off of the East coast in a congested part of the network

Required Investment to accommodate offshore generation

New lines AC/DC

Rating of Switchgear

- **Fault level 80KA +**
- **Continuous rating 5000A+**

nationalgrid
The power of action.

2030 Challenges and opportunities

135 GW of electricity demand

- Higher volume of Intermittency
- Significant increase in power flows
- Power flows more volatile with 'active' transmission limits
- Greater integration with European Transmission

But…

New technologies

- Dynamic demand
- DC networks
- Extending onshore networks to offshore
- More Sophisticated energy management systems
- Active distribution networks
- Novel energy storage
  - Domestic heat storage
  - Novel flow batteries

Active Monitoring by National Grid

28

nationalgrid
The power of action.

Where is the combined market for new materials solutions driving short to long term?

- **Construction – current materials and materials from other industry sectors**
- **Resilience to climate change issues – flooding, higher temperatures, wind**
- **Condition monitoring and assessment – sensors and knowledge**
- **Low loss materials – overhead line conductors, coatings for pipes, will HTS ever be reliable enough for transmission?**
- **Alternative energy networks – will hydrogen or carbon dioxide networks emerge, will the materials technology need to evolve or adapt new pipelines?**
- **Alternative transformer and circuit breaking options – non-mineral oils or different transformer designs, an alternative technology or gas to sulphur hexafluoride**
- **More flexible plant – control devices based on HTS or semiconductor technology, multipurpose pipes, composites**
- **Smart materials – self healing materials based on nanotechnology research**

29

nationalgrid
The power of action.

Conclusions for electricity transmission

- **WE will have to drive the Transmission system harder then ever before.**
- **If we are to meet renewable targets we need to start developing transmission system now.**

SO

- WE **ALL have some exciting challenges ahead that need the support of HV research and technology.**
- HOW **do WE ALL ensure that HV technology is available to required timescales?**

30

nationalgrid
The power of action.


Thank you
Jenny Cooper
nationalgrid
The power of action.

Numerical Simulation of Partial Discharge Acoustic Signals in Oil

S. A. Ashraf [1*], B. G. Stewart[2], C. Zhou[2], D.M. Hepburn[2] and J.M. Jahabar[1]

[1]Faculty of Electrical Engineering, Salalah College of Technology, Salalah-211, OMAN
[2]School of Engineering and Computing, Glasgow Caledonian University, Glasgow, UK
***email: saa99@lycos.com.**

Abstract: **The work presented here is the simulation study of partial discharge (PD) Acoustic Emission (AE) signal propagation in a metal oil tank. Partial differential equations (PDE) describing the AE wave have been developed and solved using the Finite Element Method (FEM). The study described in this paper helps to investigate the propagation behaviour and signal attenuation of the AE waves in oil at different temperatures. Reflection and refraction of the waves are simulated and displayed. This is an important result in relation to the interpretation and understanding of practically measured PD signals emitted in a model tank. It is shown that the attenuation of acoustic signal depends upon the location of the discharge and the temperature of the oil medium. Fast exponential decay of the PD AE wave amplitude has been observed with higher temperature. Animation of simulation results provides a clearer picture of the propagation and attenuation of the AE signal. The PD AE wave pressure distribution over time can also be seen clearly.**

Index Terms **–Acoustic Emission, Finite Element Method, Partial Discharges**

I. INTRODUCTION

Partial Discharge (PD) measurement is used as an important tool for determining the condition of insulation systems of high voltage (HV) devices. Understanding the condition of the insulation components allows Asset Managers to improve the reliability of the transmission and distribution network. The interpretation of the signals produced in the various measurement techniques helps to extract information about the insulation defects. PD occurs when the local electrical field intensity exceeds the dielectric strength of the dielectric involved, resulting in localized ionization and breakdown. It is defined by the IEEE as an electrical discharge that only partially bridges the insulation between conductors and that may or may not occur adjacent to a conductor [1]. These PDs can be detected by a variety of techniques. One of them is the Acoustic Emission (AE) technique which is non-invasive and immune to electromagnetic noise. Under normal operating high voltages, the presence of any defect in an insulation medium can cause local field enhancement near the defect site causing PDs in the insulation and consequently local perturbation in the medium due to the release of energy in the form of burst/impulsive pulses (acoustic energy) that radiate in all directions from the discharging source. The released energy can be detected by mounting an AE sensor over the outer surface of the HV structure. The AE method provides information on the existence, size, and first of all the location of PD occurrence, which cannot be obtained by using other methods [2-4].

A great deal of research work has already been carried out on acoustic PD detection and its practical applications have been undertaken by many researchers [1-10]. Studies of AE signals presented in the current literature are often carried out in the form of experimental investigations. Unfortunately there is a lack of understanding of acoustic modes of propagation within HV insulation systems. As such there is also little published work related to modeling and simulation of propagation modes of acoustic wave from PD activity. The idea behind the simulation study is to deduce how PD AE waves travel in a basic metal model tank and to visualize how the wave is attenuated and reflected from the tank walls before the scheme can be applied to real transformers [5-10]. Specifically, this paper investigates the simulation of PD AE wave propagation behaviour and signal attenuation in transformer oil at different temperatures to demonstrate the physical changes in the AE waves which may be expected in real-life situations.

II. GOVERNING EQUATION

PD activity appears as a small "explosion" within an insulating medium. PD emits light, heat, electromagnetic radiation and AE signals. It will excite, in the case being considered here, the surrounding fluid medium and therefore induce ultrasonic pressure waves. These signals can be considered as an impulse having a steep wave front. In reality, the pressure waves are more complex due to interference of longitudinal, shear and surface waves and also with the reflected waves from the tank walls but for an initial evaluation, the simplest form of signal emission is considered. These signals travel towards sensors through various propagation materials such as oil and metal. The standard partial differential equation (PDE) that governs the propagation of an acoustic wave within a 2-D homogenous media is given by [8]:

$$\frac{\partial^2 P}{\partial t^2} - C^2\left[\frac{\partial^2 P}{\partial x^2} + \frac{\partial^2 P}{\partial z^2}\right] = \delta(r-R)\,f(t) \quad \text{-- (1)}$$

In equation (1), P is the pressure wave field *(Pa)*, t is the time *(s)* and C is the acoustic wave velocity *(ms^{-1})*. $\delta(r)$ is

the Dirac Delta function associated with the position of the PD source in space, R is the specific observation radius and $f(t)$ is the source function used in the numerical simulation of acoustic propagation. The function $f(t)$ which represents the PD source is often expressed [8] as follows:

$$f(t) = P_0 \beta t e^{-\beta * t} \sin \omega t \quad \text{------ (2)}$$

where P_0 is the maximum amplitude of the acoustic source, ω is the angular frequency and β is the attenuation factor which determines how fast the peak amplitude decays. Equation (1) can be solved and simulated using Finite Element Methods (FEM) [5-7]. FEM is a versatile and powerful numerical procedure which analyzes complex structures for various scientific and engineering fields.

III. PROBLEM FORMULATION

The proposed simulation is based on a specific small scale propagation geometry in order to simulate PD AE waves from a point source as shown in Figure 1. The main objective of this paper is to demonstrate 2-D propagation characteristic of the acoustic wave within the oil. An oil filled steel tank of size 30cm by 35cm is considered with steel thickness presumed to be 0.5cm. The oil is filled up to 27cm from the bottom of the tank. A point-to-point electrode is placed in the oil tank as shown in Figure 1. Mesh densities are increased at sharp points/junctures as well as at the boundaries to improve the accuracy of the simulations. A low resolution mesh has also been used in the main oil area in order to speed up the calculations. The mesh generation of the model consists of 214 nodes and 380 elements.

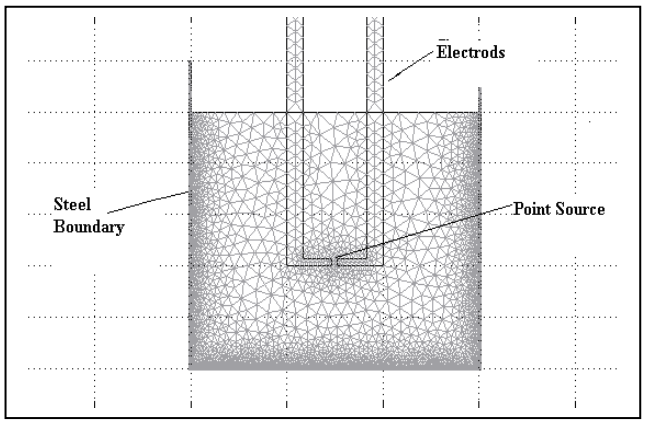

Fig.1 Investigative 2-D oil filled steel tank

The PD is simulated as a point source with mathematical form at the centre point of the oil region in the model tank. Both of the electrodes have conical needles 16 mm long with 3 mm diameter at one end and a sharp end of 40μm. It is also assumed that the pressure formula for the "explosion" of the PD moves with a spherical wave front at any time t expressed through equation (2) [8].

The oil, within the steel tank is modelled as Class-I type transformer mineral oil according to the IEC60296 Standard. The temperature is presumed to be 20^0C with a corresponding density of 998 kgm^{-3} and viscosity 13.0 cSt. The wave velocity in the oil is 1415 m/s [3].

IV. SIMULATION RESULTS AND DISCUSSION

The variation of the pressure of the PD AE wave and its reflection from the tank boundary can therefore be modelled, providing a clear picture of the behaviour and characteristic nature of the waves at any point in the oil and at any time after the PD has occurred. The examples of the results from simulation are shown in Figures 2, 3, 4, 5 and 6. These are the series of screen shots. The first shows the pressure at t = 0 prior to PD. The second, the pressure just after at t = 10 μs, the third at 50 μs, the fourth at 100 μs, and the fifth at 200 μs.

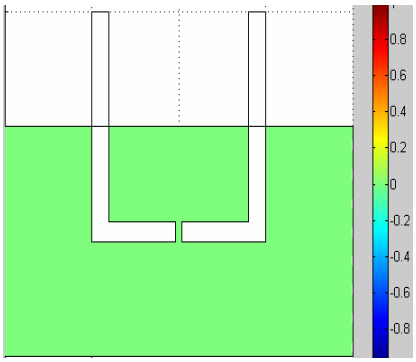

Fig 2: Propagation of the PD AE wave in oil at t = 0

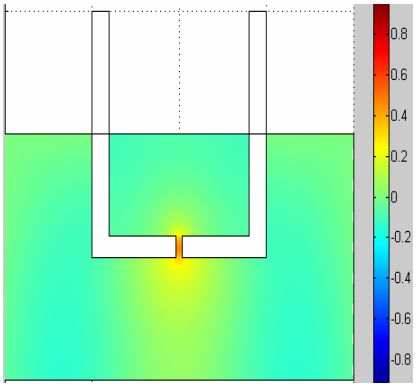

Fig 3: Propagation of the PD AE wave in oil at t =10μs

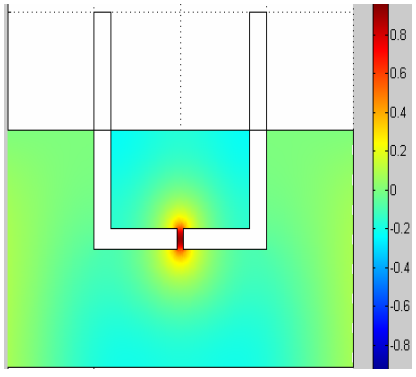

Fig 4: Propagation of the PD AE wave in oil at t = 50μs

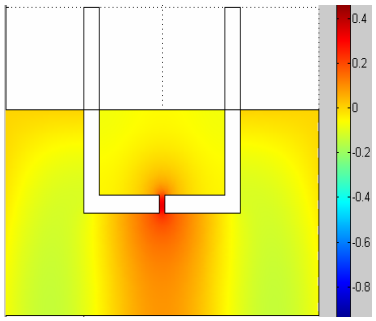

Fig 5: Propagation of the PD AE wave in oil at t =100µs

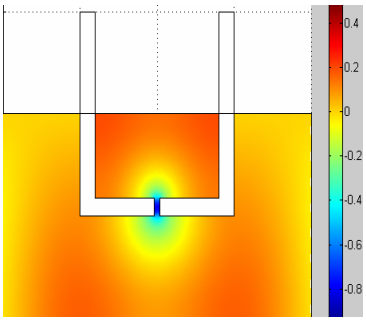

Fig 6: Propagation of the PD AE wave in oil at t =200µs

Normal pressure is characterised by the green colour, with pressure changes being displayed by the changes in colour. Fig.2 shows the snapshot at t = 0 prior to PD. Fig.3 shows the pressure distribution at 10µs just after the initiation of the PD. The initial impulse started at the centre of the electrodes with red colour which means high pressure. The peak pressure with dark red colour is where the PD impulse occurs. Fig.4 shows the PD shock wave pressure at 50µs with dark red colour again indicating high pressure. In Fig. 5, as the wave travels in the oil, the colour changes from red to yellow to light green to light blue indicating that the pressure is decreasing. In this diagram the shades of light green/blue colour indicate that the wave is propagating towards the steel boundary with decreasing pressure. Fig.6 shows the PD pressure at 200µs propagating with red colour towards tank boundaries. When an acoustic wave propagates from one medium to another which has different acoustic impedances, reflection and refraction will take place. The reflection of the wave is characterised as the light yellow colour near the tank boundaries in Fig 6. The colour change is due to attenuation of the wave which results in reduction of the propagated energy.

Fig. 7 shows the variation of pressure of the PD AE wave over time in µs within the oil tank starting at the PD location (15 cm, 0, 10 cm). The pressure variation graph shows the first peak pressure due to the occurrence of PD at nearly 90µs after the start of the discharge. The second peak at 115µs shows the reduced pressure due to propagation in the oil region whereas the third peak at nearly at 130µs shows much reduced pressure. It is clear that the pressure of the PD decays in due course of time. It can be observed in the above Figure. 7, that when wave move further from the PD source, amplitude of the peak pressure has been reduced. Fast exponential decay of the PD AE wave amplitude is observed.

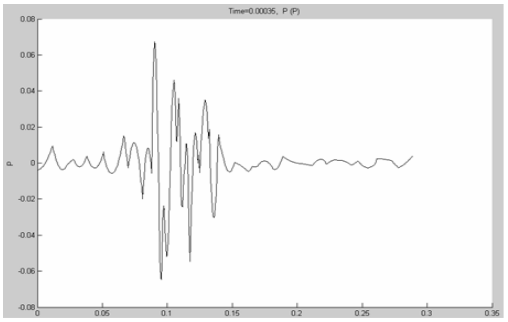

Fig 7: Variation of pressure of PD AE wave over time

V. EFFECT OF TEMPERATURE

The temperature of transformer oil is an important factor for PD acoustic wave propagation as this influences the way in which the AE will propagate through the oil medium since viscosity and density are both temperature dependent. With an increase in temperature the density and viscosity of the oil reduces thus any the signal monitored at the tank wall will change. In the simulation study, the temperature of the transformer oil was increased gradually from 20^0C to 100^0C. The results of attenuation of PD AE wave was measured at the PD location (15 cm, 0, 10 cm). The x is the distance from the PD source to the inner boundary of the tank in all directions. The variation of peak pressure amplitude P with different temperature is shown in Fig.8, Fig.9 and Fig.10 respectively.

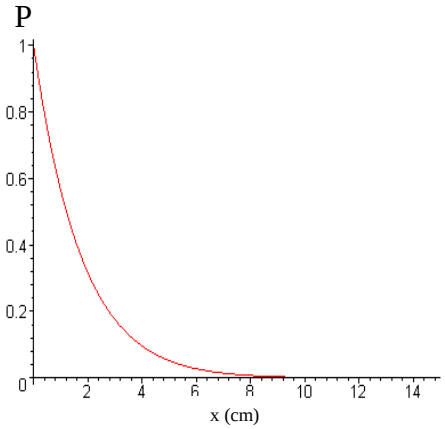

Fig: 8 AE wave amplitude verses distance in cm at 20^0C

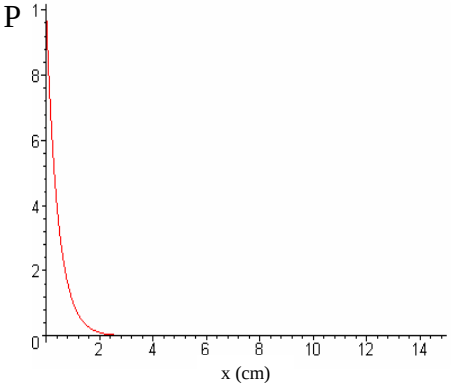

Fig: 9 AE wave amplitude verses distance in cm at 60^0C

P

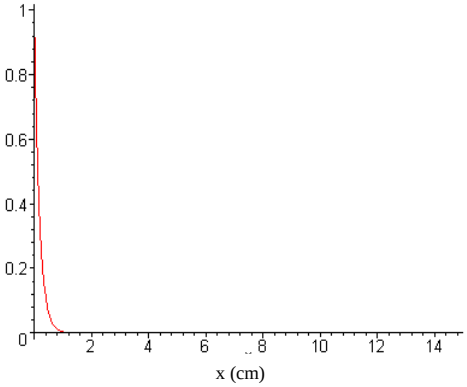

Fig: 10 AE wave Amplitude verses distance in cm at 100^0C

Figs. 8, 9 and 10 show that the acoustic wave amplitude decreases with both distance from the PD source and also increasing temperature. Clearly, there is a much faster attenuation in amplitude of the PD AE wave at higher temperatures. The result is in close agreement with [9]. With an increase in temperature the density and viscosity of the oil reduces and this helps to increase the pressure of AE wave front, so the radius of AE wave front increases which in turn decreases the amplitude of the AE wave (Amplitude of spherical wave is inversely proportional to the radius [3]). It is clear from the Fig. 8 and Fig. 9 that when the temperature increases three times the signal attenuates nearly four times. This result is very important, as it means that the detected AE signal strength will vary dependent on the temperature, even if the PD itself has not significantly changed in strength. This will assist practical AE engineer in more accurate interpretation of AE signals and phenomena within HV plant.

VI. CONCLUSIONS

FEMLAB, a Finite Element Analysis tool, has been used to simulate the propagation of the PD AE waves within oil. It is interesting to see that peak pressure amplitude decreases when the wave move further from the source. Faster attenuation at higher temperature has also been simulated. It is clear from the Fig. 8 and Fig. 9 that the temperature change from 20^0C to 60^0C results in an increased attenuation of 4. The outcome agrees with the laboratory results presented in [10]. Therefore it can be concluded that the attenuation of acoustic signal depends upon the location of the discharge and the temperature of the medium. Future work will involve simulating with complicated 3-D geometries in order to understand better the propagation of acoustic wave through real high voltage equipment.

ACKNOWLEDGEMENT

The authors wish to express their sincere thanks to Dr. Sameen A. Khan, R. R. Panda and Mr. Javeed A. Khan for their technical discussions.

REFERENCES

[1] British Standard BS EN 60270:2001, “High-Voltage Test Technique – Partial Discharge Measurement”, (IEC60270:2000), March 2001

[2] Lundgaard, L E,"Partial Discharge- Pt.XIV "Acoustic partial discharge detection – fundamental consideration", *IEEE Elect. Insul.Mag.*, Vol 8, No.4,pp. 25-31, Aug1992.

[3] Lundgaard,L E,"Partial Discharge- Pt.XV, "Acoustic partial discharge detection – practical consideration", *IEEE Elect. Insul.Mag.*, Vol 8, No.5,pp.34-43, December1992.

[4] T. Boczar, "Identification of a Specific Type of PD from Acoustic Emission Frequency Spectra" *IEEE Transactions on Dielectrics and Electrical Insulation*,Vol 8(4), pp.43-51, Aug 2001.

[5] Ashraf, S.A., Stewart B.G., Zhou,C., and Jahabar, J.M.," Modelling of Acoustic Signals from Partial Discharge activity,’’ *Proceedings of* 3rd International *IEEE-GCC conference*, Bahrain, pp116-119, March19-22, 2006.

[6] Ashraf, S.A., Stewart B.G., Zhou,C., and Jahabar, J.M.,"3-D Simulation and Modelling of Acoustic Signals from Partial Discharge activity," *Proceedings of IEEE Conference* on Electrical Insulation and Dielectric Phenomena, Kansas-USA, pp 619-622, October 15-18, 2006.

[7] Ashraf, S.A., Stewart B.G., D. Hepburn, and Zhou, C. " Simulation of Shock wave due to Partial Discharge using Finite Element Method," *Proceedings of IEEE Conference* on Electrical Insulation and Dielectric Phenomena, Vancouver-CANADA, pp 120-123, October 14-17, 2007.

[8] L. Tsang and D. Radar," Numerical evaluation of transient acoustic waveform due to a point source in a fluid filled bore hole," Geophysics, vol. 44, No.10, oct1979, pages1706-1720.

[9] Kundu, P., Kishore, N.K. , Sinha, A.K., "Simulation and Analysis of Acoustic Wave Propagation due to Partial Discharge Activity," *Proceedings of IEEE Conference* on Electrical Insulation and Dielectric Phenomena, Kansas-USA, pp 619-622, October 15-18, 2006.

[10]R. Meunier and G.H. Vaillancourt, “Propagation behaviot of acoustic partial discharge signals in oil-filled transformers”, Conference Record of the ICDL 96,12th International Conference on Conduction and Breakdown in Dielectric Liquid, Roma, Italy, July 15-19, 1996, pages 401-404.

CABLE DIAGNOSTICS IN HIGH VOLTAGE UNDERGROUND CABLES

A. S. Ayub*; W. H. Siew; J. J. Soraghan

Department Electronic and Electrical Engineering
University of Strathclyde, UK
* ahmad.ayub@eee.strath.ac.uk,

Keywords: partial discharge, denoising technique, online monitoring, underground cables

Abstract

The paper provides an overview of the current state of the art in partial discharge diagnostics and location and also suggests how some of the disadvantages of online detection and location might be overcome.

1 Introduction

Generally, partial discharges (PD) are small electrical sparks resulting from the electrical breakdown that is contained within a void or in a highly non uniform electric field and eventually cause the failure of the electrical insulation [1]. The partial discharges may be detected by using online and offline techniques. However, offline techniques have a significant disadvantage in that they require the cables to be taken out of circuit. Hence, electricity supply companies prefer the use of online techniques. The downside is that online techniques have their own disadvantages e.g. noise interference, ambiguity of partial discharge location, and sensor optimisation difficulties. As a result, the need of online condition-based monitoring is crucially important in order to sustain the power system. The key challenge in the area of monitoring and maintenance of power engineering systems is the operation reliability. Thus, one of the many options to overcome such problems are by using signal processing (denoising) techniques where extracting the original PD signal from an acquired signal has become much interest in this field.

2 Existing PD denoising and location techniques

Generally, conventional digital signal processing techniques are not capable of detecting low-level PD activity in environments where there are significant levels of noise [8]. Shim *et al.* [2] gave one of the earliest discussions of the application of wavelet-based de-noising techniques to PDs where they also presented the theoretical multi-resolution analysis and thresholding which are the main ingredients of the wavelet de-noising scheme. The major challenge of extracting the PD signals from the raw signal is especially when noise sources are less random. Shim et al. [3] uses pre processing and post processing approaches which cover signal averaging and spectral analysis. Their main conclusion was that the effectiveness of the denoising relied on the thresholding values and the number of decomposition levels. They concluded by suggesting that this scheme could improve by developing numerical methodologies for automatic threshold and wavelet selection. In a subsequent paper, Shim *et al.* [4] applied their methodology to denoise and locate PD injected in 11 kV and 33 kV cables online.

Ma *et al.* in their work has developed methodologies for automatic selection of the optimum threshold as well as the automatic classification of the different wavelets required for analysis. The data used were generated in the laboratory using discharge models [5]. In particular, they decomposed the PDs obtained from the detecting circuits using both Daubechies 2 and Daubechies 8 wavelets. They also decomposed the types of noise they considered, namely, white and narrow-band noise. They went on to utilize the information they extracted from these decompositions by devising a denoising scheme where the number of decomposition levels required is chosen by observing the levels in which the PD coefficients are mostly clustered. In another publication, MA *et al* [6] applied this methodology to different results.

Most of the measurements were made using the single ended method for PD location (as shown in Fig. 1)

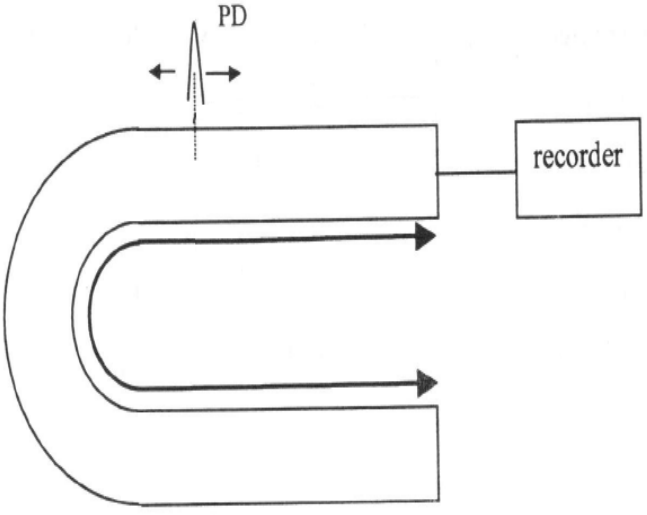

Fig. 1. Single ended method

However, when a cable length is too long, the PD signal may be attenuated below the detectable level. In such situations, it would be useful to be able to utilize the two ended PD location method on all types of voltage systems (as shown in Fig. 2). Two-ended location has the disadvantage of requiring the acquisition to be synchronized. In most cases, these were done using the injection of timing pulses.

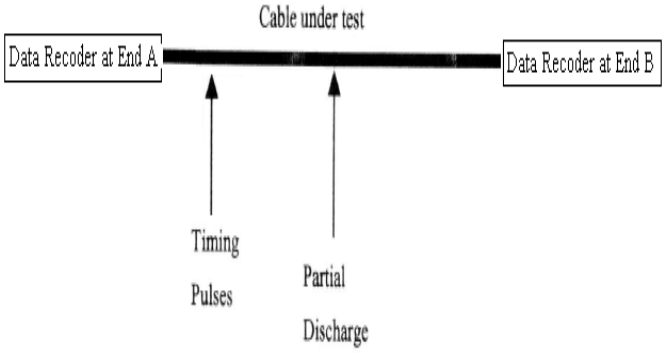

Fig. 2. Double ended method

In some measurement situations, reflections on the far end cable termination or on impedance transitions within the cable may be extractable at the near end. The difference in time of arrival (DTOA) between a PD signal and a corresponding reflection is bounded by some maximum time that can be determined from cable system identification measurements [7].

In some cases, the signal direction of arrival is also another factor of signal measurement accuracy. The measurement accuracy may be affected by other noise disturbances occurring along with the PD signals. In order to improve the measurement accuracy, compensation may be applied to the acquired signal (e.g. cable attenuation factor) to obtain a better signal dynamic range. The methods relied on the extraction of pulses that were reflected at impedance transitions within the cable system under test. Thus, it provided speediness of accessing data from measured model [8].

3. Discussion

Wavelet analysis has been used in other areas of partial discharge analysis such as in classification of multi source PD patterns [9] and in detecting electromagnetic [10] and acoustic [11] signals emitted due to PD occurrence. It has so far been demonstrated that PD denoising using wavelets is possible but this can be achieved only when prior knowledge of signal characteristics exist (this is due to the short time bandwidth of the real PDs). As a result, the above methodologies cannot denoise PDs that are well buried in noise, i.e. their peak values are much lower than the noise level, or when they are obtained from measurements on actual in service field cables.

In the attempts to alleviate the aforementioned problems, previous researchers have applied various signal processing techniques (i.e. algorithm development) for PD detection on power cables. In most cases, wavelet analyses were used by previous researchers. However, the main problem is that the interpretation of PD patterns and the prediction of remaining life of a cable system is still one of the continuing concerns for most researchers. Owing to this, the authors plan to investigate the effectiveness of alternative techniques, like Empirical Mode Decomposition and Prony Analysis, to address the problem highlighted.

In general, the Empirical Mode Decomposition method is used to analyse nonlinear and nonstationary signals [12]. This method has been used by some researchers to detect the power quality disturbances in noisy conditions [13, 14]. On the other hand, Prony Analysis is a method that can be successfully implemented with a short data window in the time domain but achieving high resolution in the frequency domain. In addition, this method has been used to detect a fault in an induction machine [15] and for flicker measurement [16] in which it can be adopted for wavelet analysis. However, those methods have not yet been investigated for PD detection in high voltage (HV) underground cables. Therefore, there is potential to investigate whether those methods are applicable to the problems of PD detection in cables.

4. Conclusion

Online partial discharge detection can identify local insulation imperfections, but has the problem of noise and measurement sensitivity. It is therefore the objective of the authors to further improve these online techniques and develop new and innovative algorithms which are more reliable and widely acceptable for cable condition assessment.

References

[1] IEC 60270, 'Partial discharge measurements', 3rd Edition, International Electrical Commission (IEC), Geneva, Switzerland, 2000

[2] I. Shim, J. Soraghan, W. H. Siew, 'Digital Signal Processing Applied to the Detection of Partial Discharge: An Overview', DEIS, IEEE Electrical Insulation Magazine, Vol 16, No. 3, May/ June 2000, pp. 6-12

[3] I. Shim, 'Signal processing techniques of partial discharge mapping in high voltage cables', PhD Thesis, University of Strathclyde, UK, 2000

[4] I. Shim, J. Soraghan, W. H. Siew, 'A noise reduction technique for online detection and location of partial discharges in high voltage cable networks', Meas. Sci. Technol. 11, 2000, pp. 1708-1713

[5] X. Ma, C. Zhou, I. J. Kemp, 'Automated wavelet selection and thresholding for PD detection, IEEE Electrical Insulation Magazine, Vol 17, 2002, pp. 37

[6] X. Ma, C. Zhou, I. J. Kemp, 'Interpretation of wavelet analysis and its application in partial discharge detection', IEEE Electrical Insulation Magazine, Vol 9, 2002, pp. 446

[7] Jeroene Veen, 'Online Signal Analysis of Partial Discharges in Medium Voltage Power Cables', PhD Thesis, Eindhoven University Press, 2005, ISBN 90 386 1693 7

[8] P.C.J.M van der Wielen, 'Online Detection and Location of Partial Discharges in Medium Voltages Power Cables', PhD Thesis, Eindhoven University Press, 2005, ISBN 90 386 1683 X

[9] E. M. Lalitha, L Satish, 'Wavelet analysis for classification of PD patterns', IEEE Trans. Dielectr. Electr. Insul. 7, 2000, pp. 40

[10] M. Kawada, M. Tungkawananich, Z. Kawasaki, 'Detection of wide band signals emitted from partial

discharge occurring in GIS using wavelet transform', IEEE Trans. Power Dielectr. 15, 2000, pp. 467

[11] T. Boczar, D Zmarzly, 'Application of wavelet analysis to acoustic emission pulses generated by partial discharges I', IEEE Trans. Dielectr. Electr. Insul. 11, 2004, pp. 433

[12] N. E. Huang et. al, ' Empirical Mode Decomposition and the Hilbert Spectrum for Nonlinear and Non Stationary Time Series Analysis', Proc. Of Royal Society of London Series A, Vol. 454, 1998, pp. 903-905

[13] V. Agarwal, L. H. Tsoukalas, 'Denoising Electrical Signal via Empirical Mode Decomposition', iREP Symp VII USA, August 2007

[14] Z.Lu. J. S. Smith, Q. H. Wu, J. Fitch, 'Empirical mode decomposition for power quality monitoring', IEEE PES 2005, pp. 1-5

[15] R. Zicanovic, S. Chen, 'Fault Diagnostic of Induction Machines using Prony Analysis', IEEE Powertech, Switzerland, 2007

[16] Y. Zhang et. al, 'A Novel Method Based On Wavelet Threshold Denoising Technology and Prony Analysis For Flicker Measurement', UPEC Conference, Padova, Italy, Sept 2008

Point-Plane Pulse Sequence Analysis Pattern Variation as a Function of Insulation Material and Supply Voltage

I. D. Bruce and B. G. Stewart

Glasgow Caledonian University, e-mail iain.d.bruce@btinternet.com

Keywords: Partial discharge, Pulse sequence analysis, scatter plot.

Abstract

This paper presents the results obtained using Pulse Sequence Analysis (PSA), on data from three partial discharge point plane test configurations, i.e. a needle and open plane, needle and mica covered plane and needle and polyethylene covered plane. An IEC 60270 based detection system is used to provide sequential data and a brief description of the capture system is presented. Marked differences in the conventional scatter plots obtained for each test configuration are then presented.

1 Introduction

Pulse Sequence Analysis, (PSA) is an increasingly used partial discharge (PD) analysis technique which uses streams of sequential partial discharge data captured over a number of consecutive supply voltage cycles. The main characteristics of interest are generally the supply peak voltage, the relative time of occurrence of the PD, from which can be obtained the supply cycle voltage at the time of occurrence and/or the phase of occurrence and the PD pulse amplitude. Using these parameters, a number of techniques, such as Phase Resolved Pulse Sequence analysis (PRPS) [1, 2], and voltage differential scatter plots [3] can be used to characterise and identify PD fault mechanisms.

Traditional analysis techniques [4] such as ϕqn plots present lumped discharge data parameters for pattern recognition and analysis in which the data sets need not be sequential. If an understanding of the physics involved in the discharge process is required, useful time related information is lost along with discharge pulse information for the PD pulses occurring between data captures. In capturing discharge pulse data over a number of consecutive cycles, the data afforded by PSA capture systems not only provides an opportunity to identify/characterise PD fault types, but also gives an opportunity to examine/determine the effect of the physical processes active at the discharge site and which will influence the occurrence of successive PD pulses. The advances in computing ability along with the increasing development of sophisticated PC based data capture systems has provided an opportunity to capture larger quantities of more detailed PD data.

2 Data Capture

2.1 Data Capture system

The data capture system used in these tests [5] utilises a custom designed IEC60270 detection circuit providing optically isolated outputs for the detected PD data and the supply voltage. A PC based NI5112 high speed digitiser card is used to capture and store the data for analysis. The capture card is configured using window triggering, with the upper and lower thresholds determined using sample data captures prior to the main data capture and based on the signal noise content. During these sample captures, the signal gains and offsets for both channels are also optimised using a number of cycles and a user selected allowance to accommodate changes in the characteristics of the PD signals over the period of the test. Capture rates can be selected up to 100MS/s and data records of 2ms duration are captured and stored for both channels on either positive or negative threshold triggers. The data capture, transfer and storage are all controlled using a suite of Labview programs.

Analysis of the captured data is undertaken using Matlab and the results are presented in the form of scatter plots utilising the previously described parameters shown below in figure 1. In this case, the supply voltage at the point of discharge is captured directly and not inferred using relative timestamps.

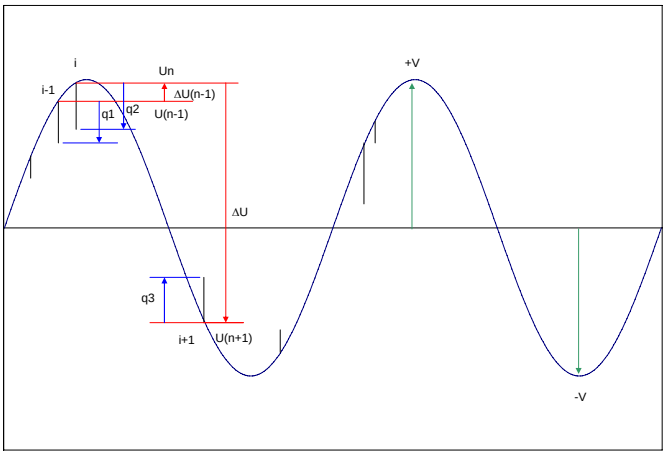

Figure 1. Characteristic parameters used during the Pulse Sequence Analysis of captured data.

2.2 Test Configuration

The tests detailed here used a point plane configuration in which a sharp steel needle mounted in a test jig formed the high voltage electrode. This electrode was suspended above an earthed plane, with the height adjusted using an adapted micrometer. The gap size in this case was set at 20mm. Three configurations of the above were used:
(i) the basic needle and open plane;
(ii) the configuration in (i) with a mica sheet covering the plane;
(iii) the configuration in (i) with a polyethylene sheet covering the plane.
In each case, the test voltage was increased and data captured at three supply voltage levels. At each test voltage, captures were undertaken at both 10MS/s and 100MS/s.

3 Results

Figure 2 shows typical data captured for each of the three test configurations described above. The results shown were all captured at a test voltage of approximately 12kV and a sample rate of 100MS/s. The 20ms records shown are some of the previously mentioned initial samples, used in setting up the thresholds, signal gain and signal offset.

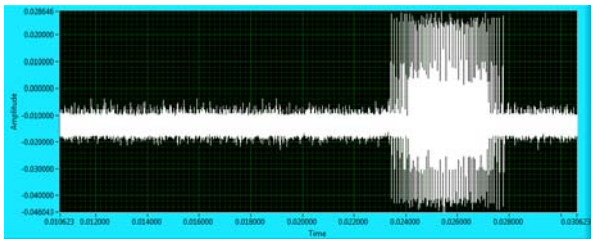

(i)

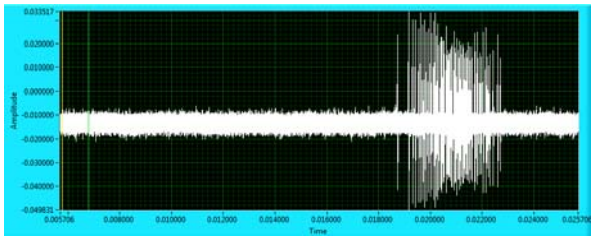

(ii)

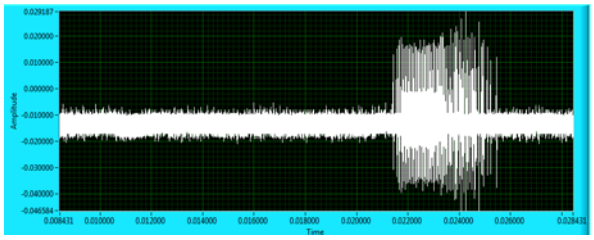

(iii)

Figure 2. Typical discharge data from, (i) needle and open plane, (ii) needle and mica covered plane and (iii) needle and polyethylene covered plane.

During testing, the number of records which can be captured at any particular sampling rate is dependant upon the size and spread of the pulse groups, characteristic of the fault type under test, with the rate at which data is transferred from the card into the main memory being the limiting factor. For the test configurations described here, the 10MS/s rate allowed over 1000, 2ms, records to be captured whereas the 100MS/s rate allowed only approximately 100 records. For the tests detailed, 100MS/s and 50 record captures are presented.

The scatter plots used here are generated using x-y plots in which the x co-ordinate represents the voltage differential between the pulse in question and the previous pulse, $\Delta U(n-1)$ in figure 1, and the y co-ordinate, the voltage differential to the following pulse, ΔUn in figure 1.

Figure 3 shows the scatter plot obtained for the open plane configuration at the test voltage used for the trace in figure 2(i). The right hand plot shows an exploded view of the central cluster shown in the left hand plot. The plots of figure 2 are typical of the continuous corona pulses obtained at the negative peak and which give relatively small ΔUn and $\Delta U(n-1)$ values hence the tight central cluster noted in figure 3.

The outer clusters, highlighted in figure 4, are the result of the voltage differences between the inception and extinction voltage levels for consecutive groups of pulses. The position of the group with respect to the peak will therefore determine where on the scatter plot these clusters lie in relation to the main central cluster. The interconnecting lines shown in the right hand plot of figure 4 are added to highlight the clockwise movement around the plot representing consecutive discharge pulse groups.

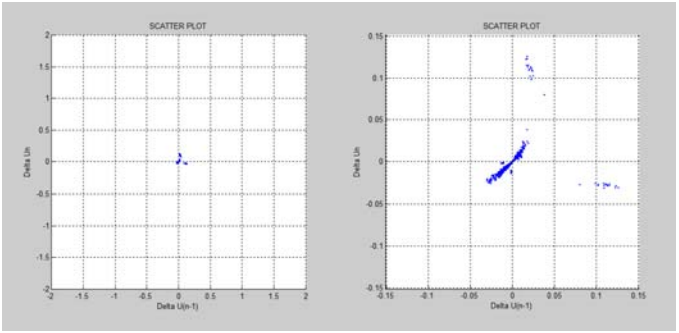

Figure 3. Typical scatter plot for needle and open plane configurations.

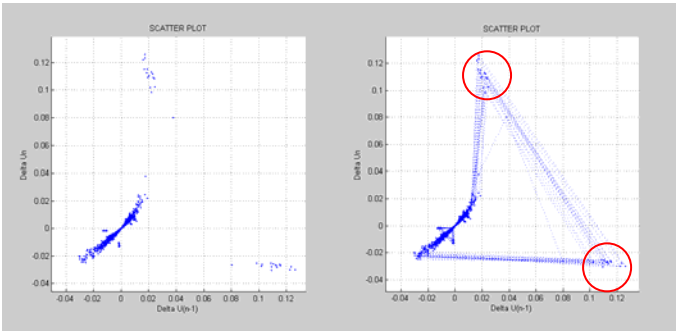

Figure 4. Cluster detail for the plot in figure 3.

The shape of the main cluster in figures 3 and 4 is typical of a point and open plane configuration. The elongated cluster at approximately 45^{o} is obtained as a result of the combination of time differences between consecutive pulses decreasing to a minimum at the supply voltage peak and then increasing to the point of extinction, and the supply voltage rate of change being at its lowest around the peak. The smaller clusters just discernable at the lead in to the main cluster indicate that the initial discharge pulses in each half cycle group follow similar patterns, with the variation in the inter pulse voltages limited. This is also evident in the thin structure of this cluster showing that the variation in voltage differentials through the group in each half cycle data is also limited. The direction of this cluster from bottom left to upper right is also characteristic of negative half cycle discharge pulses in which the ΔU values reduce up to the supply peak and then increase as the supply voltage increases. The shape of this cluster and its position relative to the origin will therefore describe the position of any large pulse group relative to the next voltage peak.

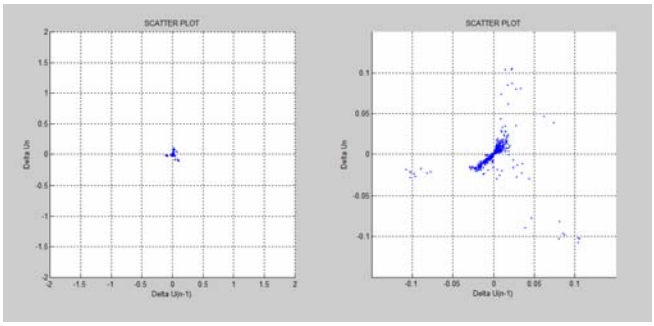

Figure 5. Typical scatter plots for needle and mica covered plane.

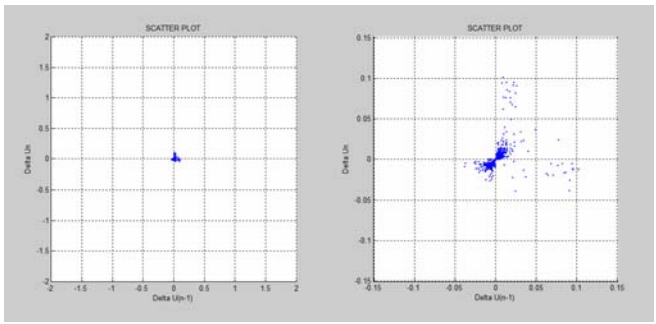

Figure 6. Typical scatter plots for needle and polyethylene covered plane.

The plot of figure 5, for the mica covered plane shows a slightly wider distribution on the outgoing end of the main cluster, indicating that the pulse patterns, and hence voltage differentials, at the end of each pulse group are more varied. This plot also shows outer clusters representing the voltage differential between consecutive group inception and extinction voltages, but the structure of these is less marked when compared with the open plane plot. There is also a distinct cluster at the lead in to the main cluster which is formed by the pulse/pulses which precede the main pulse group, evident in figure 2(ii).

The polyethylene covered plane scatter plot, shown in figure 6, shows wider distributions at both the lead in to and exit from the main cluster. The plot also has no distinguishable outer clusters, which indicates that the voltage differentials between the extinction and inception voltages for consecutive half cycles are not as regular as those for the other two test configurations.

Figure 7 shows the variation in scatter plot layout as a result of the increases in test supply voltage. It can be seen that the main cluster shape is similar for all the test voltages used, whereas the position of the outer clusters relative to the main cluster changes. The increasing relative position describes the way in which the PD group size alters with voltage. In this case the differential is positive indicating that the inception voltage is higher than the extinction and that the difference increases as the supply increases. This is confirmed in figure 8, which shows the supply voltage at the point of discharge occurrence for sample half cycles from the needle and open plane configuration results, at the test voltages used.

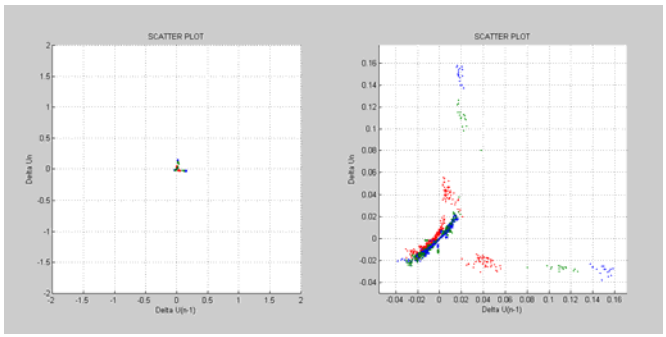

Figure 7. Cluster variation with increasing test supply voltage using the needle and open plane configuration. Red : 8800V, green : 12000V and blue : 14800V.

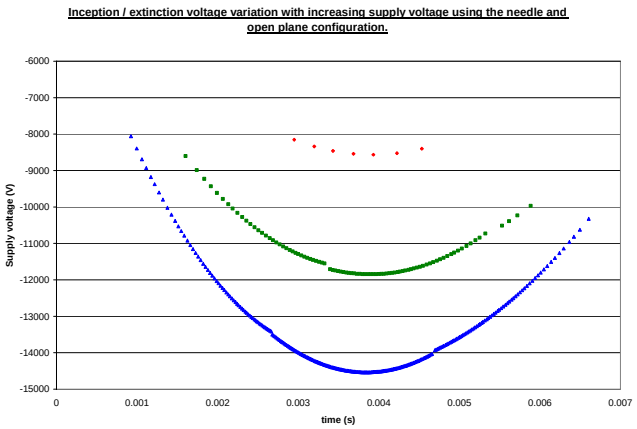

Figure 8. Sample half cycle discharge points for the needle and open plane configuration with increasing test voltage.

Figure 9 shows the variation in scatter plots with increasing supply voltage for the needle and mica covered plane, (left hand plot) and the needle and polyethylene covered plane, (right hand plot).

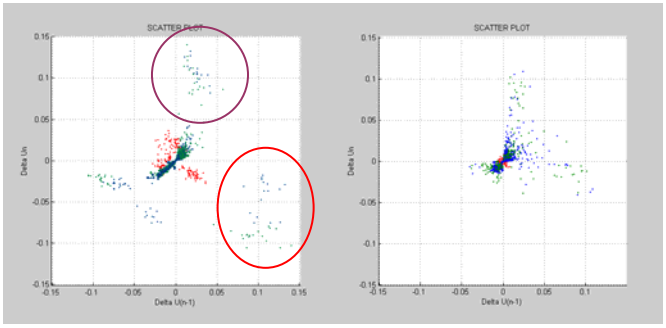

Figure 9 Cluster variation with increasing supply voltage using the needle/mica and needle/polyethylene covered planes. Red : 8800V, green : 12000V and blue : 14800V.

As can be seen from the plots in figure 9, there remains marked differences in the basic characteristics for each test configuration and the way in which these change with variations in the supply voltage. In the case of the polyethylene covered plane scatter plot, the lowest test voltage was at its point of inception with only one pulse per half cycle. The voltage differentials in this case were small, hence the small, tight red cluster around the origin in the right hand plot. The elongated cluster only forms at the higher test voltages where a larger number of discharge pulses are obtained in each half cycle. The variation in cluster position noted in figure 7 for the open plane configuration is not repeated in the plots of figure 9. The left hand plot shows the mica covered plane plots and from this it can be seen that the shape of the main cluster, once formed, remains consistent. The outer clusters highlighted in purple, show little variation with the increase in supply voltage, with only a slightly greater increase in the variation between the clusters highlighted in red. The difference between the two is the result of changes in the pulses which precede the main group. The number of preceding pulses increases with supply voltage and this change, rather than the main group inception/extinction differential gives the difference between the two outer clusters highlighted in red. This is highlighted by the number of clusters at the lead in to the main cluster increasing to two at the higher voltage (blue). The shape of the clusters obtained for the polyethylene covered plane (right hand plot), remain essentially unchanged with the increase in supply voltage.

Figure 10 shows plots of sample inception/extinction voltage differentials for consecutive discharge pulse groups for the mica and polyethylene covered plane tests. In both cases the characteristics noted in figure 9 are supported.

4 Conclusions

The results presented here have shown that the data available through utilising advances in data capture and computing technologies can provide detailed information on the nature of the discharge activity being observed. In the examples provided, marked changes in the characteristics of the discharge data and the corresponding differences in the scatter plots generated from these have shown that a limited form of fault classification could be applied, based upon cluster shape and position variation with supply voltage. The next stage of investigation is to interpret the scatter plots in terms of the physical properties of the insulation material and in particular the charge distribution properties.

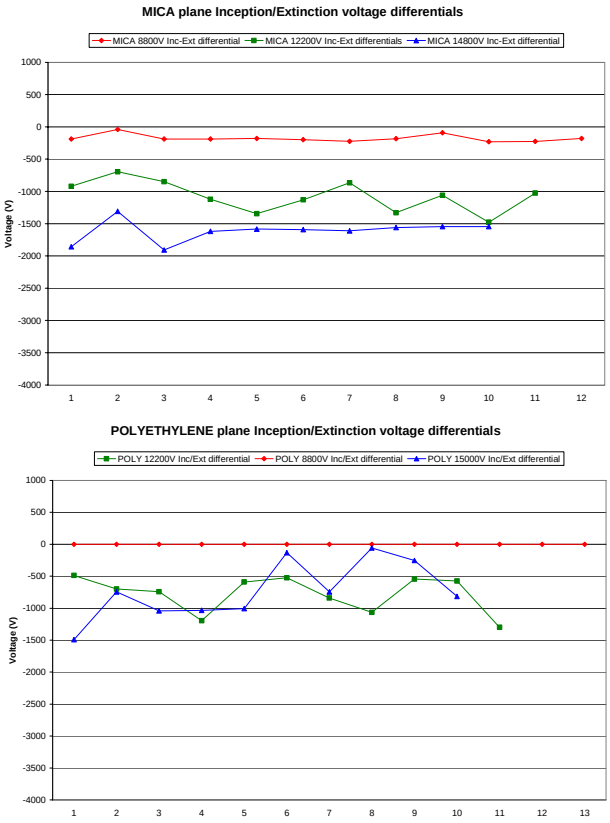

Figure 10. Voltage differentials between the extinction and inception voltages for consecutive pulse groups.

References

[1] H. G. Kranz, "PD Pulse Sequence Analysis and its Relevance for On-site PD Defect Identification and Evaluation.", IEEE Transactions on Dielectrics and Electrical Insulation, Volume 12, No. 12: April 2005

[2] S. Senthil Kumar, M.N. Narayanachar, R.S. Nema, "Pulse Sequence Studies on PD Data", 2002 Annual Report Conference on Electrical Insulation & Dielectric Phenomenaa

[3] F. Berton, R. Patsch, "Pulse Sequence Analysis – a diagnostic tool based on the physics behind partial discharges", Journal of Physics D: Applied Physics 35, 25-32, 2002.

[4] R. J. Van Brunt, "Stochastic Properties of Partial-discharge Phenomena", IEEE Transactions on Electrical Insulation, Volume 26, No 5: October 1991.

[5] I. Bruce, I. J. Kemp, B. G. Stewart, "Development of a Sequential Discharge Data Capture System", 39th International Universities Power Engineering Conference, Volume 1, 160-164, 6th – 8th September 2004.

LIGHTNING IMPULSE AGEING OF HDPE

N. L. Dao*, P. L. Lewin, S. G. Swingler

University of Southampton, Sothampton, Hampshire, SO17 1BJ, UK
*contact: nld06r@ecs.soton.ac.uk

Keywords: Lightning-Impulse, Ageing, Life-time, Breakdown.

Abstract

This work is concerned with the hypothesis that lightning impulses can lead to accelerated ageing of extruded polymeric cables. The behaviour of an insulation material when suffering lightning impulses is different from that for DC or power frequency over-voltages. Shaped HDPE material samples have been manufactured using a mould tool. The samples then may be electrically aged using one of the Tony Davies High Voltage Laboratory's impulse generators. A real-time software based monitoring tool has been designed to control the impulse wave-shape and process the measurement data. Sets of identical lightning impulses were applied to samples and this was then followed by ramped AC breakdown tests. The obtained results were analyzed using the Weibull distribution method to identify the difference in lifetime. These results will inform the further development of models describing the multifactor ageing mechanisms that in-service cables experience.

1 Introduction

Lightning strikes to overhead line power systems or overvoltage surges due to faults or switching actions are quite common. These surges may travel through the system as waves to underground cables and other equipment. Insulation quality of devices and cables will suffer from impulse over-voltages. These impulses can lead to accelerated ageing of extruded cables [1-4]. Lightning impulses are voltages with very high magnitudes and very short on times. Therefore the behaviour of a material when suffering lightning impulses is different from DC or power frequency over-voltage behaviour. In order to investigate the effect of lightning impulses on the ageing process of high voltage power cable insulation, pre-designed and shaped HDPE samples have been manufactured using a mould tool. The samples then can be electrically aged using one of impulse generators in the Tony Davies High Voltage Laboratory. A real-time software based monitoring tool has been designed to control the impulse wave-shape and process the measurement data. Sets of identical lightning impulses were applied to samples and then this was followed by ramped AC breakdown tests. The obtained results were analyzed using the Weibull distribution method to identify the difference, if any, in lifetime. These results will be used to improve our understanding of ageing mechanisms and facilitate lifetime prediction.

2 Lightning impulse definitions and parameters

A lightning impulse is a high voltage impulse that occurs over extremely short times (μs for lightning and ms for switching) with high magnitude. According to the IEC 60060-1[6] the smooth lightning impulse (Figure 1) is defined by a set of parameters:
Test voltage V_p: the peak value of the waveform.
Front time T_1: is measured as 1.67 times the interval T between the instants when the impulse is 30% and 90% of the peak value.
Tail time T_2: is measured as the time interval between the virtual origin O_1 and the instant when the voltage has decayed to half of peak value.

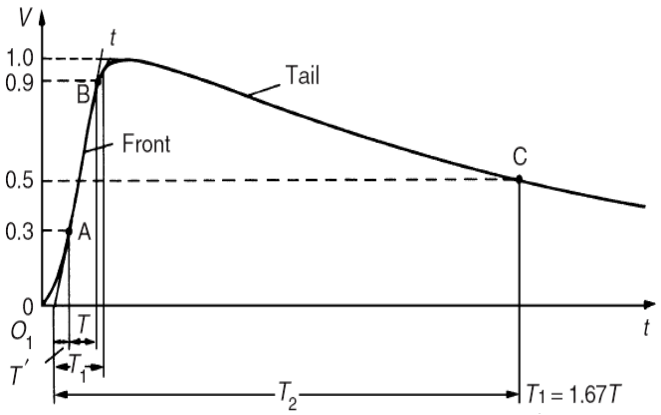

Figure 1: Lightning impulse [5]

The virtual origin is characterised by the value of t_0 where:

$$t_0 = \frac{t_{90}v_{30} - t_{30}v_{90}}{v_{30} - v_{90}} \quad (1)$$

Typically, the standard lightning impulse has the front time T_1=1.2μs±30% (0.84μs≤T_1≤1.56μs), the tail time T_2=50μs±20% (40μs ≤T_2≤60μs) and also the tolerance for peak value is ±3%. The time parameters for a switching impulse are much greater than the lightning case, they are in the order of milliseconds. A mathematical formula that represents the smooth impulse is:

$$f(t) = A\left(e^{\frac{-(t-t_0)}{\tau_2}} - e^{\frac{-(t-t_0)}{\tau_1}} \right) \qquad (2)$$

In order to measure the parameters of a lightning impulse that is generated in laboratory conditions where electromagnetic waves created by other equipment can superimpose into lightning waveform to create noise and overshoots, a programme was written to collect the data from oscilloscope, process it and produce a smooth curve and its parameters. The new IEC approach was used to process the waveform, raw measurement data was first taken, then the best fit curve found and subtracted from the raw data to create a residual. Applying the K-factor [7] to the residual and summing the result with the best fit curve provides a final curve for parameter calculation. The recommended K-factor filter has been developed at the University of Southampton. A new separated double exponential function (SDE) instead of normal double exponential (DE) [8] was used as the best fit curve.

$$f(t) = A_2 e^{\frac{-(t-t_0)}{\tau_2}} - A_1 e^{\frac{-(t-t_0)}{\tau_1}} \qquad (3)$$

This best fit curve approach has also been developed within the Tony Davies High Voltage Laboratory

3 Sample production process

Disc-shape (Figure 2) samples were produced by heat-press method using a 4 parts mould tool (Figure 3). HDPE pellets with melt flow index 2.2 were put inside the mould and heated to about 180^{o}C until all pellets were melted. After that, a pressure of 1 ton was applied to push all the residual material and air bubbles out. Cold water was used to quench cool the sample. When released from the mould, the sample has a thickness of approximately 180 μm and the inner surface of the sample has the Rogowski profile. The sample has inner/outer diameter: 25/30 mm, and a height of 5 mm. All samples were heat treated in a vacuum oven with temperature of 90^{o}C for half an hour before the top and bottom of the samples were gold sputter coated. Samples have electrodes that follow the profile thus reducing the edge effect and the likelihood of triple junctions. Mushroom electrodes were used instead of ball bearing electrodes to reduce the mechanical deformation.

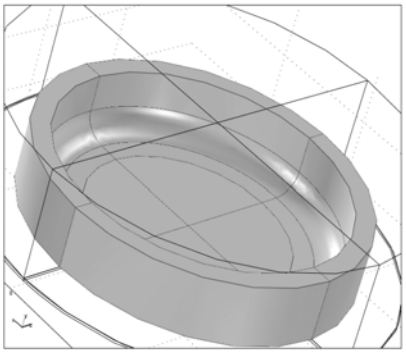

Figure 2: Disc sample

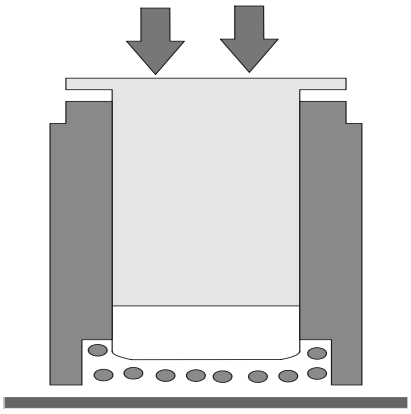

Figure 3: mould tool

4 Impulse ageing experiment

Figure 4 shows the lightning ageing experiment. The two-stage Marx impulse generator produced an impulse voltage that was applied to the samples. A multi-electrode system was made to age many samples at the same time. The impulse generator was controlled by a computer programme using signals from an oscilloscope. The impulse wave-shape from the scope is filtered and impulse parameters are returned using the new IEC 60060-1 standard. Signals were counted by the oscilloscope and Breakdown checking was done using a Labview program. After signal checking, if breakdown or flashover did not occur, the computer would send a command to the generator controller to generate the next impulse voltage, otherwise a signal would be sent to a relay circuit to shut the generator down.

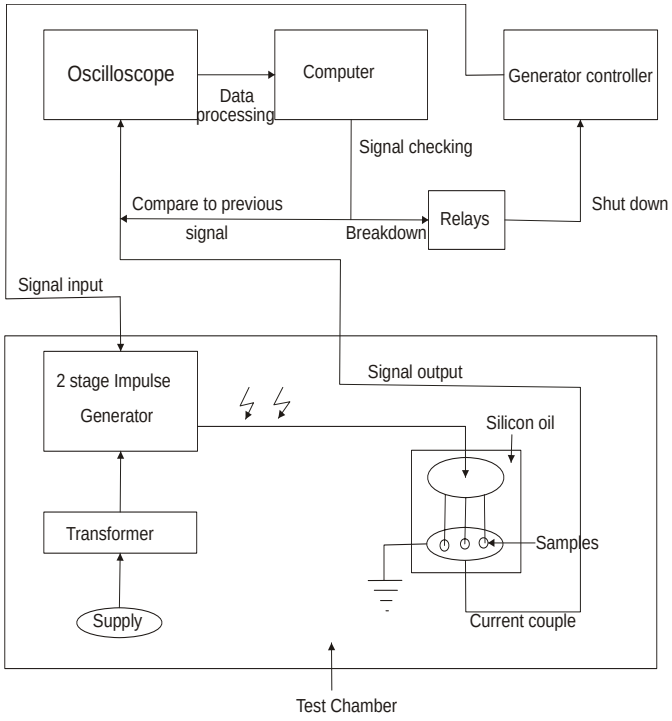

Figure 4: Ageing process

Approximately 3000 Impulses of front time 1.15us and tail time 42.6us were used to age samples for a duration of 75 minutes. These impulses generated a peak electric field of about 84kV/mm on the samples for both negative and positive polarity impulses.

5 AC ramp breakdown results

Aged samples and normal samples were subjected to an AC ramp breakdown test after the ageing process. Breakdown voltages were recorded and processed to obtain a Weibull probability distribution of breakdown strength [9-10], using

$$F_F(V) = 1 - \exp\left[-\left(\frac{V}{\eta}\right)^{\beta}\right] \qquad (4)$$

In order to estimate the cumulative probability the Bernard estimator was used [11].

$$F = \frac{i - 0.3}{n + 0.4} \qquad (5)$$

Where F is cumulative probability of i^{th} point, n is the number of data. 90% confidence limits were obtained using Weibull ++7 software.

6 Discussions

From Figure 5, the breakdown strength of unaged samples is higher than the aged samples as the confidence limits do not overlap for breakdown probabilities higher than 16%. Parameters of the Weibull distribution are reasonable and are shown in Table 1. Figure 6 shows that both positive and negative lightning impulses lead to a reduction in breakdown strength. However, there is no significant statistical difference between them except the breakdown voltages for positive impulse aged samples are little bit lower than the negative case. During AC ramp breakdown tests for aged samples, surface discharges were usually observed but not with the unaged samples. This may suggest that there are surface charges or space charge near the surface that has increased as a result of the impulse ageing process. As the on-time for each impulse is very short, space charge injected from the electrode may not be the dominant reason for ageing but the generation of hot electrons by the impulse voltage may cause damage to the molecular structure.

	β	η
Unaged samples	8.68	126.5
Negative impulse aged samples	10.6	102.8
Positive impulse aged samples	9	102.1

Table 1: Weibull parameters

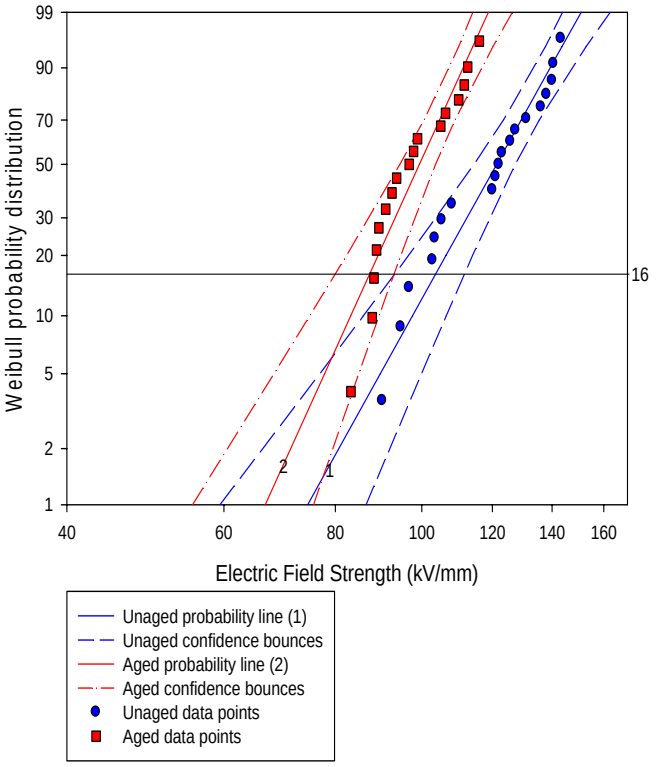

Figure 5: Aged and unaged HDPE

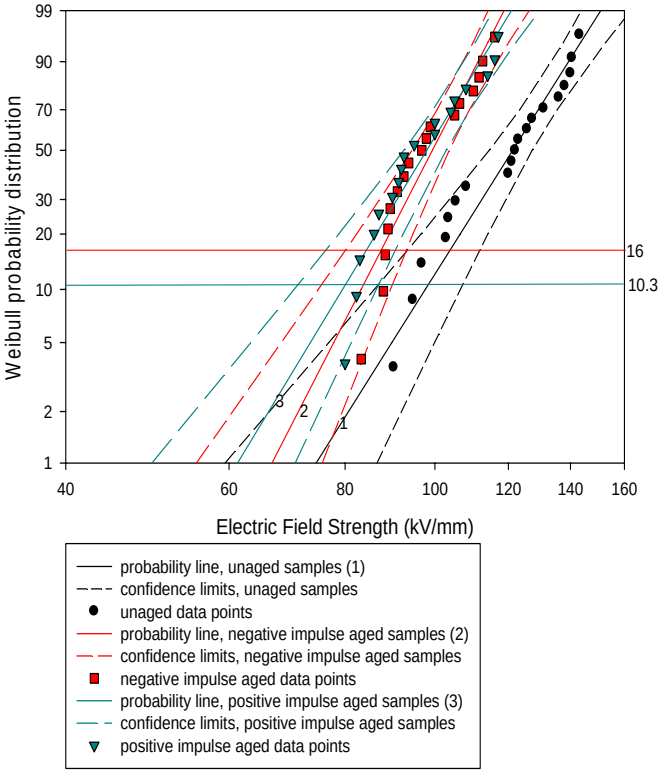

Figure 6: Positive and negative impulse ageing

7 Conclusions and Further Work

The results showed that a significant number of lightning impulse events accelerate the ageing process of HDPE. More comparison between the effects of lightning and switching impulses will be undertaken to identify the role of space charge on this ageing process. Front time variation of the impulse will also be altered as it will vary the gradient of the applied voltage. The relationship between level of electric field stress, number of impulses and the lifetime of materials will be considered.

References

[1] S. Boev "Electric aging of polyethylene in pulsed electric field" *12th IEEE International Pulsed Power Conference. (Cat. No.99CH36358) 1999*, p 1365-8 vol.2

[2] R.A Hartlein, V.S. Harper, Harry Ng **"**Effects of voltage surges on extruded dielectric cable life project update" *IEEE transactions on power delivery*, volume 9, issue 2, April 1994 Page(s):611 – 619

[3] S. Bahadoorsingh, S. Rowland "The Relationship between Insulation Ageing and Power Network Performance" *ICSD 07, IEEE international conference on solid dielectrics, 2007, 8-13 July 2007* Page(s):180 – 183

[4] G.C. Stone, R.G. Van Heeswijk, R. Bartnikas "Electrical aging and electroluminescence in epoxy under repetitive voltage surges" *IEEE transaction on electrical insulation*, volume 27, issue 2, April 1992 Page(s):233 – 244

[5] E. Kuffel, W.S. Zaengl, J. Kuffel, "High voltage engineering fundamental", *Newnes, second edition, July 17, 2000*

[6] IEC 60060-1: 1998, BRITISH STANDARD, "High voltage test techniques" – Part 1 "General definition and test require ment" *Published by the International Electrotechnical Commission*

[7] P.L.Lewin, member, IEEE, T.N.Tran, D.J.Swaffied and J.K.Hallstrom "Zero phase filtering for lightning impulse evaluation: A K-factor Filter for the revision of IEC60060-1 and -2" *IEEE Transactions on Power Delivery, 2008,* volume 23 (1). pp. 3-12. ISSN 0885-8977

[8] D.J.Swaffield, P.L.Lewin, N.L.Dao and J.K.Hallstrom "Lightning impulse wave-shapes: defining the true origin and its impact on parameter evaluation" *XVth International Symposium on High Voltage Engineering, University of LjublJana, Elektroinstitut Milan Vidmar, Ljubljana, Slovenia, August 27-31, 2007*

[9] G.C. Stone "The statistics of aging models and practical reality" *IEEE transaction on electrical insulation*, volume 28, issue 5, Oct 1993, page (s): 716-728

[10] L.A. Dissado, J.C. Fothrgill "Electrical degradation and breakdown in polymer" *IEE materials and devices series 9, Peter Peregrinus Ltd. On behalf of the Institution of Electrical engineers, 1992*

[11] J. C. Fothergill "Estimating the Cumulative Probability of Failure Data Points to be Plotted on Weibull and other Probability Paper" *IEEE Transactions on Electrical Insulation* Vol. 25 No. 3, June 1990 pp. 489-492

A VOLTAGE TRANSDUCER FOR HIGH VOLTAGE APPLICATIONS

M.F. Hussin, A. Haddad, N. Harid

High Voltage Energy System Group, School of Engineering, Cardiff University, United Kingdom

Abstract

An accurate measurement and monitoring technique is crucial to ensure health and safety of expensive high voltage power system equipment. Both conventional and non-conventional transducers are widely used for such purposes. However, the uses of conventional transducers are recognized to have several limitations compared with applications of non-conventional transducers. Hence, a novel exploitation of the electrical field distribution around the high voltage conductor is proposed using measurement principles similar to those developed for contacless conventional capacitive probes. This paper presents a new approach for contacless voltage measurement for HV applications, e.g. on substation equipment or overhead lines and cables. Numerical field computation is used to determine the electric field distribution around the high voltage terminal and the calibration of the proposed transducer. In addition, a simplified analytical method was developed which allows estimation of the capacitive probe parameters.

Keywords: capacitive probe, contacless voltage measurement

1 Introduction

Faults occurring on HV overhead lines are commonly caused by overvoltages and faulty equipment. The overvoltages originate from lightning strikes to the line and switching operations on the power system. The lightning overvoltage amplitudes are very high, usually exceeding 1000kV or more and each strike may inject lightning current up to 100kA[1]. The amplitudes of switching overvoltages are always interrelated to the operating voltage, and their shape is influenced by the impedances of the system including the switching condition [1]. The common factors that influence switching overvoltages include circuit configuration, circuit conditions between circuit breaker contacts and stray capacitances between the circuit breaker and shunt reactor [2]. Therefore, it is important that measurement and monitoring of the voltage that appears on HV conductors and terminals are assessed accurately to maintain safe and economic operation of HV substation and overhead equipment.

The conventional transducers used for voltage measurement and monitoring of HV power systems are usually voltage transformers. They can provide accurate and reliable voltage measurement. However, they are time-consuming both during installation and commissioning which requires sophisticated set-up procedures to minimize potential errors caused by proximity effects and asymmetric fields. In addition, these transducers tend to be bulky and heavy, and with the increasing system voltages, the insulation of these transformers becomes more difficult and expensive [3].

In this paper, a cylindrical-shape capacitive transducer is developed for measurement of voltages on HV distribution lines. This probe operates based on the principle of the contacless capacitive probe. According to this principle, the probe measures the displacement charge induced on the probe surface due to the electric flux density emanating from the energized conductor [4]. The advantages of capacitive probes are simple construction, low cost, easy to assemble and can be set up without a requirement for disconnecting the high voltage supply during installation [5]. More importantly, this type of transducer is of non-contact type.

A commercially available finite element software (SLIM) [6] is used to model and simulate the voltage and electric field distributions around the probe. This software has two modules; 2D and 3D modules. The advantage of the 2D analysis is that it is up to 10 times faster. However, the high accuracy of the 2D analysis is only limited to simple geometries such those presenting axial symmetry. However, 2D analysis may also yield a better simulation of complex phenomena-like nonlinear field or eddy current distributions in devices in which end effects are not important [6].

2 Analysis of Coaxial Probe Parameters

Figure 1 shows the configuration of the transducer developed in this work.

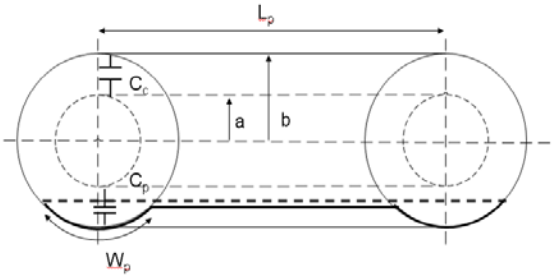

Figure 1: The representation of cylindrical capacitor transducer.

The parameters for the coaxial probe configuration are listed below:

- The radius of the inner cylinder or HV conductor, a, is 0.07m.
- The radius of the outer cylinder, b, is 0.15m.
- The length of cylinder, L_p, is 0.28m.
- The sensing probe width, W_p, is 0.20m.
- The capacitance, C_c, represents the capacitance for the entire cylinder.
- The capacitance, C_p, represents the capacitance for the sensing probe.

Simple cylindrical/ coaxial configuration.

The basic principle of this probe is governed by the induced charge generated by the electric flux collected on the sensor probe, and this can be quantified using Gauss law. Therefore, assuming a charge +Q on the inner cylinder and –Q on the outer cylinder, it can be shown that, at any radius, r, the electric field can be calculated using Equation (1) if the end effects are neglected.

$$E = \frac{V}{r \times \ln \frac{b}{a}} \quad \text{[V/m]} \qquad (1)$$

If the inner cylinder is at potential, V, above the earthed cylinder, the capacitance can be easily calculated [7]:

$$C = \frac{Q}{V} = \frac{2\pi\varepsilon_0}{\ln \frac{b}{a}} \quad \text{[F/m]} \qquad (2)$$

The capacitance, C, in Equation (2) is expressed in per unit length, $\varepsilon_0 = 8.854 \times 10^{-12}$ F/m is the permittivity of free space.

This yields easily the capacitance, C_c of the coaxial geometry including the sensor probe area,

$$C_c = C \,.\, L_p \qquad (3)$$

Equation (3) gives an approximation of the probe capacitance, C_p.

$$C_p = C \times L_p \frac{W_p}{2\pi b} \qquad (4)$$

with C_p expressed in Farads (F).

3 Numerical Modelling of Probe Geometry

In this investigation, two approaches were used within the FE software (SLIM) to model the capacitive probe in order to examine the field distribution and determine numerically the parameters of the probe. First, an axi-symmetric model is used in which the probe is a cylinder surrounding the high voltage conductor, and the second model is an x-y geometry which simulates a vertical section of the conductor above ground with the probe placed around it in close proximity. Figure 2(a) illustrates the axi-symmetric configuration and Figure 2(b) shows the 2D mesh used in this study for the axi-symmetric simulations. Figures 3(a) and (b) show the corresponding figures for the x-y model.

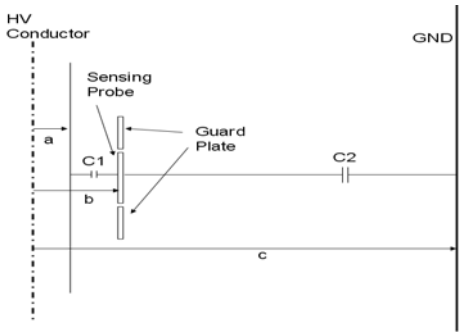

Figure 2(a): Transducer modeling based on axi-symmetric approach.

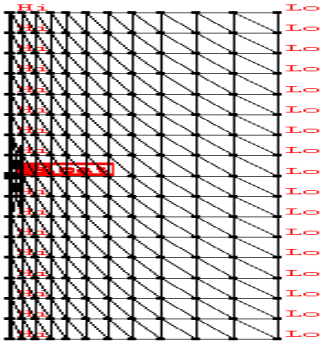

Figure 2(b): 2D mesh used in the axi-symmetric model.

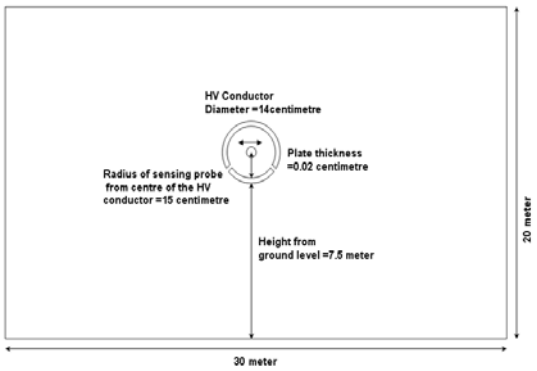

Figure 3(a): Transducer model used in x-y simulations.

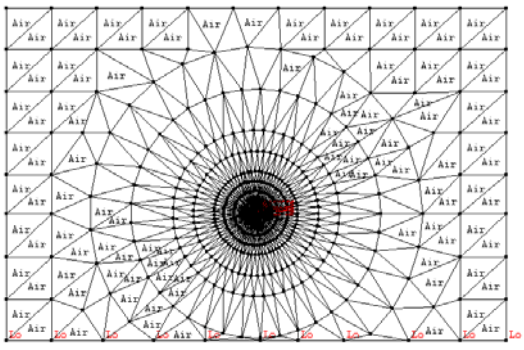

Figure 3(b): 2D mesh for x-y model.

This proposed transducer consists of a sensor-section surrounded by guard electrodes. The purpose of the guard electrodes is to reduce edge effects, and hence obtain a more uniform distribution of the field on the sensor and cause very little disturbance to the field lines compared to the case when the sensor was not in-circuit. In this case, the HV conductor is used as reference voltage and is connected to the integrating capacitor, C_1. Based on the capacitive divider principle, the capacitance C_2 is formed between the probe outer surface and the ground through the air, as shown in Figure 2(a).

Within the simulation software, the whole space is meshed except the HV conductor, the sensing probe and guard electrodes, as shown in Figures 2(b) and 3(b). The conductor and plate are subjected to a high potential, (Hi) while the ground is assigned a low potential, (Lo). The sensing probe is represented with a foil which simulates a floating electrode.

4 Computation of Probe Parameters

In this section, results of simplified analytical models and full numerical solutions are presented. The results are calculated for a conductor voltage of 6.35kVrms representing an 11 kV distribution line.

4.1 Analytical approach

Using Equation (1), the maximum electric field (E) obtained for the cylindrical geometry is 55.6kV/m. The cylinder capacitance in per unit length is 73pF/m, which is obtained using Equation (2). The resulting capacitance to the sensing probe, C_p is 4.33pF.

In addition, using Equation (1), the electric field strength range between the HV conductor and transducer can be calculated based on Figure 2(a). The electric field at the HV conductor of radius a = 0.07m is 119kV/m and at the probe surface located at radius b = 0.15 m is 55.6kV/m.

Moreover, the same approach was applied to obtain the electric field at ground level. In this case an approximation is used assuming that the ground is represented by a large cylinder around the conductor system. This yields an electric field strength at the probe surface, with the probe having a radius b = 0.15m, of 10.8kV/m and a field of 0.211kV/m at ground level is also calculated for a probe located at a distance c =7.65m above ground.

4.2 Numerical simulation results

Figures 4 and 5 show the electric field magnitudes at the probe's inner surface which were computed using the x-y and axi-symmetric 2D finite element models respectively. As can be seen on the figures, 3 components are shown: modulus, normal and tangential field quantities. As expected, the tangential component is zero since it is computed at the probe surface. Therefore, at the probe surface, the normal component is equal to the electric field modulus, and this component is used for the calibration of the probe.

It can be noted that the x-y model shows some end effects in the form of increasing field magnitudes towards the probe edges . The more realistic axi-symmetric model configuration shows less major changes of field towards the edges.

Figure 6 shows the computed equipotentials when the HV conductor and adjacent probe are placed above ground as described in section 4.1. The corresponding electric field profiles at the ground surface level are given in Figure 7.

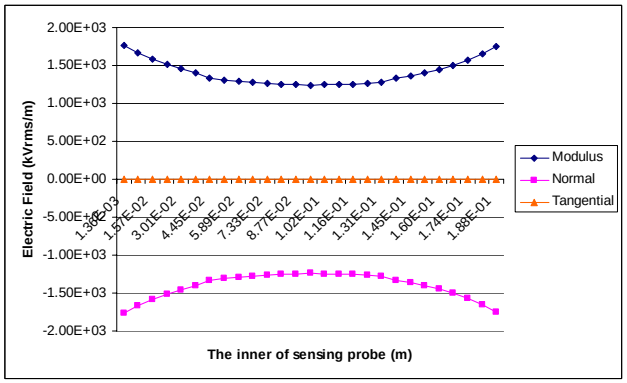

Figure 4: Numerically computed electric field components profiles at probe surface using the x-y model.

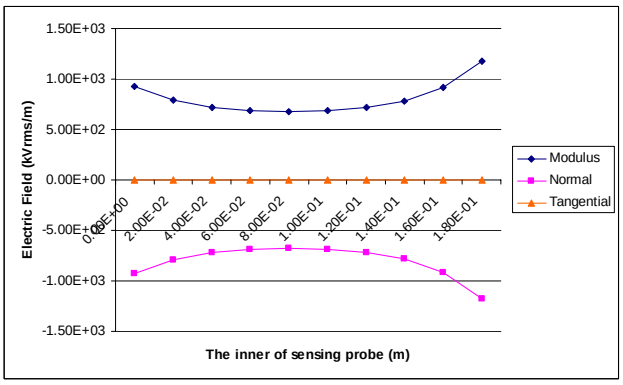

Figure 5: Numerically computed electric field components profiles at probe surface using the axi-symmetric model.

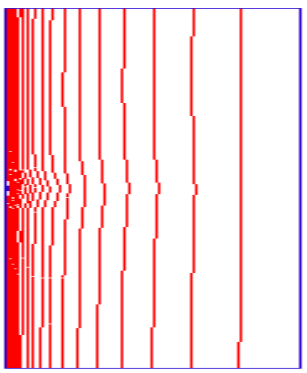

Figure 6: Equipotential contour at 5 % intervals for the axi-symmetric model configuration

As can be observed, the numerically computed values are in agreement with those calculated with the analytically derived approximate equations.

Similar results were obtained for the field at ground surface level when using the x-y model. Figure 8 shows the equivalent equipotential distribution. As can be seen, the equipotentials exhibit a diverging shape away from the space between the probe and the ground.

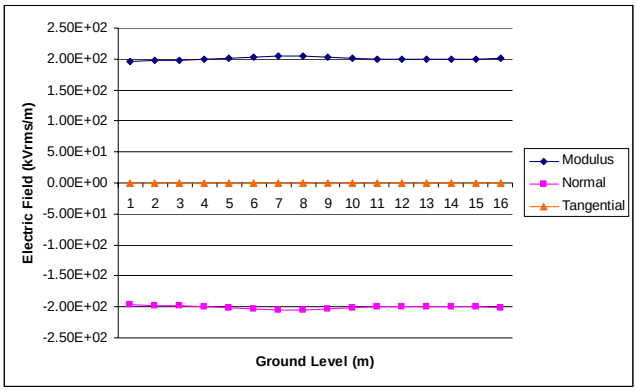

Figure 7: Electric field profile at ground surface level using the axi-symmetric model.

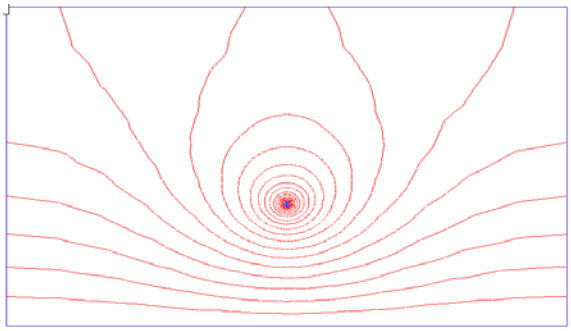

Figure 8: The equipotential contour at 5 % intervals for the x-y model configuration.

6 Conclusion

A new contactless capacitive probe is proposed to measure high voltages on the HV conductor/terminal. Initial design studies include determination of the probe's parameters including its capacitances and electric field magnitudes. A prototype is being constructed and will be tested both in the laboratory and the field.

A numerical field computation was used to model and simulate the voltage probe. Two models were developed and their simulation results were compared, these are 2D finite element models using an x-y – type configuration and an axi-symmetric model. Furthermore, a simplified analytical approach was developed and its results compared favorably with the numerical computations. However, in order to determine a more accurate field profile on the probe's surface, only the numerical method can make realistic predictions.

References

[1] E. Kuffel, J. Kuffel and W.S. Zaengl: "High Voltage Engineering Fundamentals", Newnes, ISBN: 0-7506-3634-3, pp.49, 460, 2001.

[2] G.W. Chang, H.M. Huang and J.H Lai: "Modelling SF6 Circuit Breaker for Shunt Reactor Switching Transient Analysis", International Conference on Power System Technology, Vol. 2,pp. 1315-1320, Singapore, 2004.

[3] Byoungho Lee: "Review of the Present Status of Optical Fibre Sensors", Optical Fibre Technology, Vol. 9, Issue 2, Invited Paper, Academic Press, pp. 57-79, 2003.

[4] M. Khalifa: "High-Voltage Engineering Theory and Practice", Marcel Dekker, Inc, ISBN: 0-8247-8128-7, pp.480-485, 1990.

[5] A. Haddad, C.A. Spellman, D.M. German and R.T. Waters: "Improved Three-Phase Voltage measurement using Capacitive Probe", Proceeding of the Universities Power Engineering Conference, Leicester, UK, Vol. 1, pp.352-355, 1999.

[6] SLIM Manual, "SLIM Electromagnetic Engineering for Microsoft Window NT40+, 2000, XP", software version 3.7.1, Copyright Areva T&D UK, 2004.

[7] M. Sibley, "Introduction to Electromagnetism", Essential Electronic Series, Arnold, ISBN: 0-340-64595- 4, pp.38-40, 1996.

Examining the Mathematic Approach for Calculation of Loss-of-Life: Physical Process and Statistical Representation

M.T. Ishak and Z.D. Wang

University of Manchester, Manchester M60 1QD
Email: zhongdong.wang@manchester.ac.uk

Keywords: loss-of-life, transformers, dual cooling mode, ambient temperature, hourly load and thermal model.

Abstract

Due to regulation of the electricity market, the power utilities are forced to increasingly operate aged power system networks unless a large amount of capital investment is injected to replace aged network infrastructure in the immediately near future. To estimate transformer thermal end-of-life, various strategies using statistical analysis have been developed in attempts to compensate the lack of sufficiently detailed loading data. This paper sets out to examine how estimation errors can be introduced by these statistical approaches, especially when dealing with dual cooling mode transformers. The accuracy of the estimated mean lifetime needs to be known by the asset managers, when used in replacement planning and decision making.

1 Introduction

Investment on power system network infrastructure has been low in the last twenty years due to the privatisation of the electric power industry, and this leads to the current situation that operating increasingly aged power system networks is becoming inevitable for most utilities in developed countries. Unless intense capital investment is injected in the electricity sector to replace the aged infrastructure in the immediately near future, this situation will be continued and could be worsened due to the increasing numbers of equipment approaching the transition point from ageing to degradation and to faults/failures.

Large power transformers represent a significant part of transmission network assets. Their replacement will involve a considerable amount of time and expense. Therefore it is necessary to understand the lifetime of a transformer population in order to minimize negative reliability impacts from the transformer failures. Another benefit is accurate lifetime estimation which would allow better planning for replacement. Consequently, many efforts have been devoted to find the best ways to estimate the end-of-life of power transformers in recent years[1-5].

It is well understood from past operating experience that transformers do not fail due to ageing only; in other words, thermal end-of life is not equal to transformer failure. When new a transformer is designed (and passed vigorous factory tests, being proved) to have sufficient dielectric and mechanical strength, with some spare margin, to withstand the maximum operation stresses. However design variations determine that the spare margin for each individual transformer would be different among a transformer population. Normal ageing processes, being represented as reduction of oil quality and paper mechanical strength, will degrade this spare margin until it no longer sustains the stress caused by external events (e.g. system short circuit and lightning/switching transients) and the transformer is prone to failure. Overall, transformer failure is a probability issue with three main controlling parameters: design, ageing and external trigging events.

In addition to normal ageing, a transformer may develop a fault which results in faster than normal ageing/degradation, with a higher consequent probability of failure. Occasions like this should be treated as an “abnormal” random event, which may need special care and treatment during constructing statistical end-of-life modelling approaches.

Fundamental quantitative relationships of extreme ageing conditions of transformer insulation and their intrinsic dielectric strength are still lacking, noting that most transformer failures are the symptoms of an eventual dielectric failure.

Nevertheless thermal end-of-life, represented as the operating years to lose the mechanical strength of conductor paper, is still important to determine, especially for a transformer population, from the perspective of effective asset management.

To predict the thermal end of life, assessing prediction errors is always needed and this leads us to give the end result of prediction as the mean lifetime and its scattering range (the standard deviation if it is represented as a normal distribution). Thermal loss-of-life calculation needs the operating history of the transformer (mainly loading) and the ambient temperature. The prediction uncertainties in the final determination of transformer loss of life may also come from the lack of the loading profiles and ambient temperature, the imprecision of the thermal model, and so on and so forth. The calculated loss-of-life must be accomplished with a certain range of associated errors identified.

The latest IEC 60076-7 revision 2005[6] thermal model, is the one we adopt in the simulation, where the improved hotspot temperature equations incorporate the new research findings by Pierce [7, 8]. The error caused by the transformer thermal model, especially the discrepancy between the assumed general hottest spot factor by the IEC standard and the real

hottest spot factor of the transformer under study, is beyond the scope of this paper, although we intend to report our sensitivity study on this matter in another paper.

This paper presents a sensitivity study on errors generated by the simulation approach proposed by [3]. In [3], to deal with variance of loading data and ambient temperature, it is proposed that data is processed as a set of data following a certain distribution and with certain random errors. This statistical approach is commonly used in pre-processing of raw data; however its suitability in dealing with loading profile of a transmission transformer is brought into question. In this paper the problem will be discussed in two parts, first for a transformer with only single cooling mode and second for a transformer with dual cooling mode.

2 The mathematical approach in calculating the loss-of-life of transformer

The rate of ageing of transformer insulation depends on its temperature. The hottest part (hottest-spot) inside the winding is considered since it will undergo the greatest deterioration. Experimental evidence indicates that the relationship of insulation deterioration to time and temperature follows the Arrhenius reaction rate theory. The equation for V, relative rate of loss is defined according to equation (1) for non-thermally upgraded paper.

$$V = 2^{(\theta_h - 98)/6} \tag{1}$$

where θ_h is the hotspot temperature in °C.

The loss of life L over a certain period of time is equal to

$$L = \int_{n=1}^{N} V_n \times t_n \tag{2}$$

where V_n is the relative rate during interval n, t_n is the nth time interval, n is the number of each time interval and N is the total number of intervals during the period considered.

The main factors affecting transformer insulation life are loading condition and ambient temperature. However moisture content and oxygen content of oil chemically age the paper insulation, and these two factors should also be considered.

2.1 Hourly load simulation

The methodology adopted by [3] is explained as follows. Load data was collected from a filed transformer at 30 min intervals and data for a particular day are summarized to get the daily mean load (μi) and standard deviation (σi). Next the average of daily mean load ($\mu_{overall}$) for a year and its standard deviation ($\sigma_{overall}$) are computed.

Daily mean load (μi^s , i=1,…..365) for a year is then simulated using a random generator assuming that they, as a data set, follow a normal distribution with mean as an overall average load ($\mu_{overall}$) and standard deviation ($\sigma_{overall}$) as calculated previously. The simulated hourly average load ($I^s_{i,k}$ $_{k=1,….24}$) is generated under the assumption that it also follows a normal distribution with simulated mean (μ_i^s) and σi as the standard deviation.

2.2 Ambient temperature simulation

The model for weather using historical daily average temperature has been proposed by [9], which was used to generate hourly ambient temperature by [3]. Daily average temperatures, daily minimum and daily maximum were used as inputs for simulating hourly ambient temperatures. The assumption has been made that hourly temperature in a day behaves in a sinusoidal pattern around the average temperature on that day with a small normally distributed uncertainty added to it.

An hourly factor is calculated by adding random normal variation to the estimated sinusoid. These 24 hourly factors are scaled to match the temperature range (the difference between the maximum temperature and the minimum temperature for that particular day). Lastly, these scale values are added to the average temperature of the day to provide the hourly ambient temperature simulations.

The other assumption made in [3], which can be of significant consequence, is that the loading profiles and ambient temperature were treated as two independent variables. No correlation between the distribution functions representing loading and ambient is assumed in [3].

3 Errors analysis in loss-of-life calculation

In this study, for illustrative purposes only, daily loss-of-life is calculated and the errors generated by the data processing proposed by [3] will be analyzed. The daily load profile, ambient temperature and transformer heat run test results were obtained from National Grid.

The daily mean and standard deviation were calculated from 48 data intervals. The real load and a simulated load profile for a typical summer day are shown in Fig. 1. To generate hourly load profile, we followed the method explained previously in session 2.1 that it follows a normal distribution with daily mean and standard deviation. The real ambient temperature profile and a simulated ambient temperature profile are shown in Fig. 2. The simulated ambient temperature data was generated following the method explained previously in session 2.2.

Several runs for generating simulation data have been done, and the simulated load and ambient profiles are used in transformer thermal loss of life calculation. The loss of life for the real load profile and ambient temperature acts as the baseline to compare the differences between the simulated loss of life values and the actual loss of life. Three case studies have been considered, i.e. the transformer with ONAN cooling mode only, the transformer with OFAF cooling mode only, and the transformer operating under dual cooling mode (ONAN/OFAF).

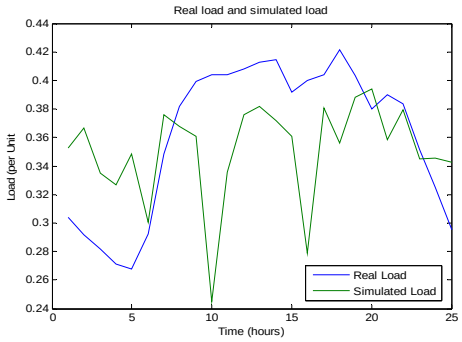

Fig.1: Real and simulated load profile

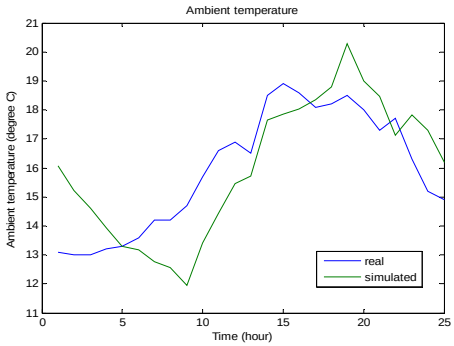

Fig.2: Real and simulated ambient temperature

A transformer with the following technical specification was considered for these case studies:

ONAN mode

Oil exponent, x =0.8, Winding exponent, y =1.3
Thermal model constant, k11=0.5
Thermal model constant, k21=3.0
Thermal model constant, k22=2.0
Toil oil time constant = 210 min
Winding time constant =10 min
Hotspot temperature rise =16.71K, Top oil rise=37K
Ratio of load losses to no load losses at rated =7.45

OFAF mode

Oil exponent, x =1.0 , Winding exponent, y =1.3
Thermal model constant, k11=1.0
Thermal model constant, k21=1.45
Thermal model constant, k22=1.0
Toil oil time constant = 90 min
Winding time constant = 7 min
Hotspot temperature rise =35.62K, Top oil rise=39.4 K
Ratio of load losses to no load losses at rated =26.8

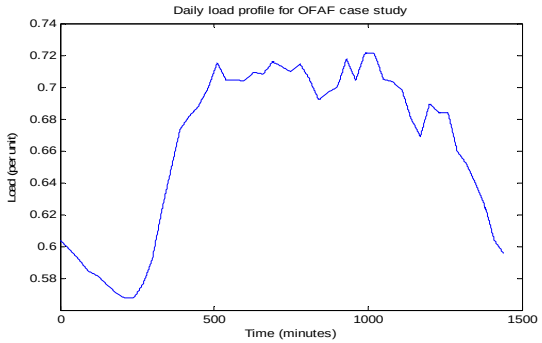

Fig.3: Load profile for OFAF study

Case 1: ONAN cooling mode

Table 1: Discrepancy between loss-of-life results calculated from real and simulated data for ONAN cooling mode

Loss of life (minutes in 24 hours)				Error	
Run	Hourly generated load	Minutely Generated load	Actual Load	Hourly generated load	Minutely Generated load
1	12.2999	11.7029	12.0431	+2.13%	-2.82%
2	12.0739	11.3867		+0.26%	-5.45%
3	11.6779	11.3079		-3.03%	-6.10%
4	12.512	11.6183		+3.89%	-3.53%
5	11.8395	11.4917		-1.69%	-4.58%
6	12.9498	11.4083		+7.53%	-5.27%
7	12.0933	11.8019		+0.42%	-2.00%
8	12.8219	11.064		+6.47%	-8.13%
9	12.4747	11.5971		+3.58%	-3.70%
10	14.2329	11.529		+18.18%	-4.27%
11	11.6234	11.2358		-3.48%	-6.70%
12	13.311	12.1385		+10.53%	+0.79%
13	11.3686	11.9369		-5.60%	-0.88%
14	10.2869	12.1006		-14.58%	+0.48%
15	14.2947	11.4338		+18.70%	-5.06%
16	14.8042	11.6471		+22.93%	-3.29%
17	13.7408	11.6517		+14.10%	-3.25%
18	13.4915	11.6949		+12.03%	-2.89%
19	11.0574	11.2006		-8.18%	-7.00%
20	14.823	11.2270		+23.08%	-6.78%

Case 2: OFAF cooling mode

In this case study, we used the following load profile as shown in Fig. 3. The ambient temperature is the same as the previous one.

Table 2: Discrepancy between loss-of-life results calculated from real and simulated data for OFAF cooling mode

Loss of life (minutes in 24 hours)				Error	
Run	Hourly generated load	Minutely Generated load	Actual Load	Hourly generated load	Minutely Generated load
1	13.1343	12.5401	14.0074	-6.23%	-10.48%
2	13.057	12.6513		-6.78%	-9.68%
3	11.8583	12.4441		-15.34%	-11.16%
4	14.4104	12.7067		+2.88%	-9.29%
5	13.8953	12.3198		-0.80%	-12.05%
6	12.6566	12.5359		-9.64%	-10.51%
7	12.4639	12.7631		-11.02%	-8.88%
8	13.3078	13.0178		-4.99%	-7.06%
9	11.0791	12.4656		-20.91%	-11.01%
10	10.5595	12.5039		-24.61%	-10.73%
11	14.7966	12.4405		+5.63%	-11.19%
12	12.5757	12.7850		-10.22%	-8.73%
13	12.563	12.9754		-10.31%	-7.37%
14	12.7832	12.2789		-8.74%	-12.34%
15	12.0147	12.9305		-14.23%	-7.69%
16	10.4967	12.5509		-25.06%	-10.40%
17	15.3865	13.0593		+9.85%	-6.77%
18	12.4001	12.7445		-11.47%	-9.02%
19	12.0385	12.4956		-14.06%	-10.79%
20	11.7098	12.8569		-16.40%	-8.21%

Case 3: Dual Cooling mode (ONAN/OFAF)

For the UK transmission transformers, they normally use dual cooling mode (ONAN/OFAF/ODAF) .The forced cooling of transformers is controlled automatically according to the winding temperature measured by a WTI (Winding Temperature Indicator). When the winding temperature

increases and exceeds a certain value of hotspot temperature, the pumps and fans will be switched on. For this study, the WTI is set to switch on the pumps and fans at 75°C and off at 50°C, as practiced in industry.

Table 3: Discrepancy between loss-of-life results calculated from real and simulated data for **Dual cooling mode**

Loss of life (minutes in 24 hours)				Error	
Run	Hourly generated load	Minutely Generated load	Actual Load	Hourly generated load	Minutely Generated load
1	15.8147	14.6955	24.444	-35.30%	-39.88%
2	14.8596	14.1341		-39.21%	-42.18%
3	16.712	13.8405		-31.63%	-43.38%
4	19.5661	15.9976		-19.96%	-34.56%
5	22.8985	15.2938		-6.32%	-37.43%
6	13.7096	13.7161		-43.92%	-43.89%
7	20.9785	16.0062		-14.18%	-34.52%
8	19.0131	15.1911		-22.22%	-37.85%
9	14.2111	15.3280		-41.86%	-37.29%
10	18.5200	13.6313		-24.24%	-44.24%
11	16.9532	14.7374		-30.65%	-39.71%
12	18.2041	14.3667		-25.53%	-41.23%
13	13.9661	15.3855		-42.87%	-37.06%
14	13.8696	13.8689		-43.26%	-43.26%
15	13.3908	13.9725		-45.22%	-42.84%
16	13.6519	14.6403		-44.15%	-40.11%
17	18.3339	14.3453		-25.00%	-41.31%
18	22.5334	14.3187		-7.82%	-41.42%
19	14.7959	16.2099		-39.47%	-33.69%
20	17.4065	13.2704		-28.79%	-45.71%

4 Discussion

In this study, a total of 20 simulation runs have been done using the data generation approaches proposed by [3] for ambient temperature and load data generation, together with the IEC thermal model to calculate the thermal loss-of-life of the transformer. From Table 1-3, it can be seen that the average errors generated from the simulation as compared to actual value of loss-of-life, are 11.5% and 11.6% for ONAN and OFAF cooling mode respectively, when hourly simulated load are used. However the errors become less for the minute simulated load situation as compared to the hourly simulated load, i.e. 4.1% and 9.67% for ONAN and OFAF respectively. The reason could be due to when more generated data is used, higher accuracy can be obtained since more data will be distributed at average value.

In the case of single and dual cooling modes, the errors generated have shown a significant increase in dual cooling mode as compared to the single cooling mode transformer. The dual cooling system produces an error of 30.58% for hourly simulated load and 40% for minute based simulated load. Most importantly, the calculations using the simulated data tend to underestimate the loss-of-life. The 20 data set is severely skewed to the left. Although following a normal distribution, the randomly generated load data, do not follow the physical process of the loading change, causing the hotspot temperatures to behave intermittently and as a result of this, the on/off switch of the pumps and the fans will operate intermittently. From the error calculations in Table 1-3, the simulation method proposed by [3] might be suitable for single cooling mode transformers (transformers below 90MVA rating), although detailed statistical analysis on the data listed in table 1-2 is still needed to understand why the simulations most often underestimate the loss-of-life. However, this method seems not suitable for transformers which are operated with dual cooling mode. For the loading data, although their overall distribution is correctly modelled, the individual load at a time is generated randomly without any correlation with its previous load at a previous time – this may not be a correct assumption.

The errors can be expected to be much bigger if a daily loss-of-life calculation is extended to yearly loss-of-life calculation, since two distribution functions, loading and ambient temperature, would be used in yearly loss-of-life calculation. A further factor is that the correlation between ambient temperature and loading profile is considered independent of each other.

5 Conclusion

The statistical methods proposed by [3] to generate loading and ambient temperature data are examined in this paper. While it might work for ONAN and OFAF single cooling mode transformers, in terms of acceptable error in estimated loss-of-life calculation; it seems that it generates significant errors when used for loss-of-life estimation of dual cooling mode (ONAN/OFAF) transformers. There is a significant underestimation of loss-of-life for the transformer calculation used as an example in this paper.

Acknowledgements

The authors would like to thank Paul Jarman from National grid UK for his technical contribution towards this PhD research. The first author is grateful toward his PhD scholarship provided by Malaysian government.

References

[1] Li, W., *Evaluating Mean Life of Power System Equipment with Limited End-of-Life Failure Data.* IEEE transactions On Power System, 2004. **Vol.19**(1): p. 236-242.

[2] Kurtz, C., et al., *Managing Aged Transformer.* Transmission & Distribution World www.tdworld.com/July 2005,

[3] Muthanna, K.T., A. Sarkar, and K. Waldner, *Transformer Insulation Life Assessment.* IEEE Transactions On Power Delivery, 2006. **Vol.21**(1): p. 150-156.

[4] Schijndel, A.v., J.M. wetzer, and P.A.A.F. Wouters, *Forecasting Transformer Reliability.* Conference on Electrical Insulation and Dielectric Phenomena, 2006.

[5] Chen, Q. and D.M. Egan, *Predicting transformer service life using simplified Perks' equation and Iowa curves.* IEEE Power Engineering Society General Meeting, 2006. **18-22 June 2006**.

[6] 60076-7, I., *Power Transformer-Part 7: Loading guide for oil-immersed power transformers.* 2005.

[7] Pierce, L.W., *Predicting Liquid Filled Trasnformer Loading Capability.* IEEE Transactions On Industry Applications, 1994. **Vol.30** (1): p. 170-178.

[8] Pierce, L.W., *An Investigation of The Thermal Performance of An Oil Filled Transformer winding.* IEEE Transactions On Power Delivery, 1992. **Vol.7** (3): p. 1347-1358.

[9] Blanco, C., J. Gray, and M.Hazzard, *Weather Contigent Load Simulation:Financial Engineering Associates. Inc.* 2003.

PARTIAL DISCHARGE LOCATION SYSTEM FOR POWER TRANSFORMERS

P Kakeeto[1]*, M Judd [1], D Templeton[2], J Pearson[2]

[1]Institute for Energy and Environment, University of Strathclyde, Royal College, Glasgow, G1 1XW, UK
[2]Diagnostic Monitoring Systems Ltd, 39 St Vincent Place, Glasgow, G1 2QQ, UK

***Corresponding author. Email: peter.kakeeto@eee.strath.ac.uk**
Tel: +44 (0) 141 548 2120 Fax: +44 (0) 141 552 2487

Keywords: Partial discharge location, power transformers, partial discharge (PD), UHF couplers.

Abstract

UHF methods for locating partial discharge in power transformers have be under development for the past years. Because the cost involved in repairing a PD-faulty transformer is high – it is important that PD sources can be located as accurately as possible. A PD location system is being developed that can locate PD in a transformer to within 20 cm. The system, which applies ultra high frequency techniques, has been tested on power transformers and an experimental tank in the laboratory producing accurate results.

1 Introduction

Determining whether power transformers are suffering from dangerous levels of partial discharge (PD) is very important because failure without warning can result in damage to the equipment, cause economic disruption and lead to imposition of regulatory fines for power utility companies [1]. However, PD detection alone will only solve part of the problem if the source of the PD is not located. In addition, the cost and the long lead time for new transformers have forced many companies to consider repairing PD-faulty transformers rather than replacing them. This has led to an increase in the demand for PD location capability and expertise for power transformers.

Various methods (such as Dissolved Gas Analysis [2]) of detecting PD in transformers already exist - thanks to the development and research carried out over the last twenty years. The acoustic and UHF are currently the main techniques used in industry for locating PD in power transformers. A partnership between the University of Strathclyde and Diagnostic Monitoring Systems Ltd (DMS Ltd), has led to the development of a PD location system (PD Locator) for transformers that is based on the UHF technique.

This paper describes how the system works, its capabilities, the accuracy of the located PD source and its future developments. Figure 1 shows a snapshot of a software model of a five-limb transformer created by the PD Location system described in this paper.

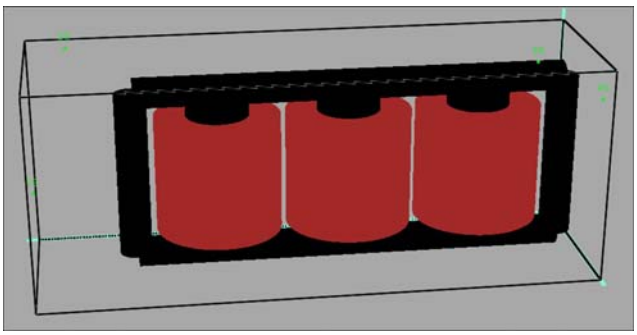

Figure 1: Internal model of a five-limb transformer

2 UHF couplers for power transformers

The main three types of UHF couplers that are used on transformers are: internal, external and oil-drain valve couplers. Figure 2 shows the three types of UHF couplers.

a) b) c)

Figure 2: Types of UHF couplers. a) Internal coupler. b) External coupler. c) Oil-drain valve coupler.

Internal couplers are mounted in the transformer during its assembly or maybe refitted later during refurbishment. These are fitted to flanges specifically installed for this purpose on the transformer tank. Internal couplers are best suited to long-term monitoring and are increasingly being included in new transformers at the manufacturing stage. External (window) couplers are designed to fit over a dielectric aperture that is usually manufactured on a replacement inspection hatch

cover. An outage is still required for installation, as the oil level must be dropped below the top of the tank. Usually, window couplers are only mounted on top of the tank so that the windings can remain immersed in oil when the tank is opened briefly during installation. On the other hand, oil drain valve couplers can be installed by inserting the coupler probe through an oil valve. Provided the correct procedures are followed, this can be carried out when the transformer is in service. However, it is unlikely that four oil valve sensors could be installed at suitable positions for PD location purposes.

3 UHF PD signals

In order to locate PD in transformers using UHF techniques; the power transformer is fitted with UHF sensors which respond to UHF PD signals inside it. Cables of equal length are used to connect the sensors to the oscilloscope - this is to ensure that any difference in *arrival time* between the signals can only be caused by different path lengths inside the tank [3]. Signals from all sensors are acquired simultaneously using high-speed sampling equipment, typically operating at greater than 1GSamples/s. Figure 3 shows four UHF signals of a record length of 100 ns.

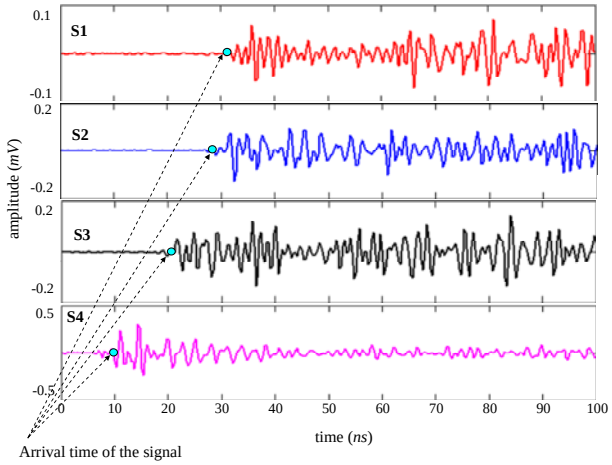

Figure 3: Recorded UHF PD signals at 5GSamples/s. The signal on S4 arrived at 10 ns, while the signals on S3, S2, and S1 arrived at 21.5 ns, 27.9 ns and 31.5 ns respectively.

Accurate determination of arrival time is one of the keys to effective PD location. While UHF systems have been in the development phase, experts have tended to employ several different methods to help them come to a decision. For example, if the leading edges of the waveforms are very clear, taking measurements "by eye" can be very effective. However, for systems that are to be more widely deployed and used by non-experts, an automated approach is needed that will be both accurate and consistent. Over recent years, different methods and algorithms for determining the *arrival time* of signals have been investigated. However, more work needs to be done to improve the accuracy and ensure consistency in the method used. The *arrival times* of UHF signals used in this report were determined using a simple 'threshold' method [4].

4 PD Location System

The PD Location System incorporates a user interface software targeted for use on the Windows Operating System platform. The user interface comprises of lists for displaying data; buttons, check boxes and sliders. These provide the user with a means of interacting with the interface. The user interface is capable of creating a three-dimensional model of a transformer and its internal structure (transformer coil windings, cores and yokes) and displaying them in a window on the interface. Sensor positions are shown on the transformer outline and PD locations are plotted once a search has been performed. The user can rotate and zoom the view as desired.

4.1 Transformer modelling

For each transformer to be monitored using the PD Location system, the necessary plant model is first created using a separate software tool. This takes as its input the dimensions and internal structure of the transformer, locations of the sensors fitted on the tank and propagation velocity of the signal in dielectric materials such as oil. The internal structure information is used to define volumes in the tank where UHF signals will or will not propagate depending on the dielectric constant of the object occupying that volume. The resulting transformer model is at the heart of the PD location system, allowing quick identification of PD positions once the time-of-flight measurements become available.

4.2 Three-dimensional user interface

The PD Location System models the transformer magnetic circuit using horizontal cylinders to represent yokes and vertical cylinders to represent cores and windings**.** However, the way the transformer's internal structure is represented and modelled is specified to each type of transformer. In general, the system is capable of modelling transformer windings, yokes, cores and objects with rectangular cross-sections. Figure 4 shows how the software models the internal and external structure of a *3-phase 3-limb core* transformer.

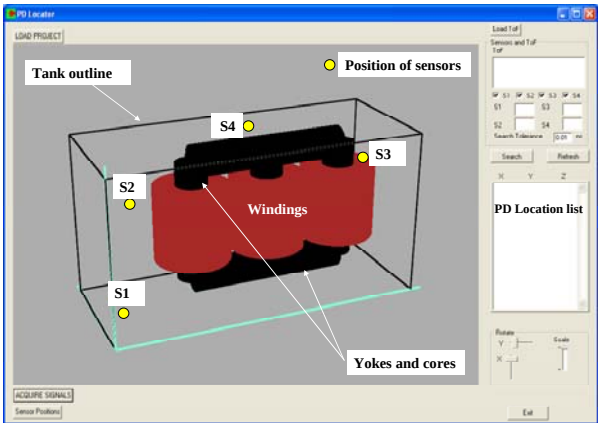

Figure 4: Rendered 3-D structure of the transformer within the software interface

Sensor positions are represented as points in space relative to what is chosen as the origin of the transformer. The transformer tank outline is rendered as a box. The transformer modelled in Figure 4 is of dimensions 5.42 x 2.25 x 2.9 m and is fitted with four UHF sensors.

4.3 Partial discharge location

When the *arrival time* of each signal has been estimated - then the PD Location System can be used to determine the location of the PD source. The software interrogates the transformer model to find the optimum point(s) that best match the observed time differences. It populates the *PD locations* list with the coordinates (*x, y, z* m) of any found points. Then it plots these points onto the scene containing the modelled 3-D structure of the transformer. This provides an indication of the location of the PD source in the transformer (see Figure 5).

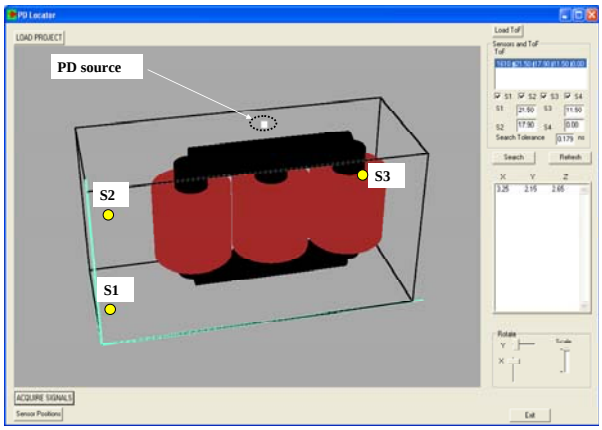

Figure 5: Three-dimensional plot of the PD source location onto the 3-D scene of a transformer.

The system can be used to search for possible PD location sources using at least two, three or four UHF sensors. If two sensors are used, and the system finds points – a plot of these points will form a surface inside the modelled transformer space. In contrast, searching using three sensors - the plotted points identify a region which is used to determine a more accurate PD source. However, searching with four sensors will return a single point (or cluster of points) which indicates the location of the PD source. For example, the PD source is located at 3.25 x 2.15 x 2.65 m for the transformer in Figure 5. This example corresponds to a pulse injection test using a 4th sensor S4 whose actual coordinates were 3.26 x 2.25 x 2.61 m.

The software informs the user if no matching PD source location can be found. For the software not to find any point may be due to a number of reasons. First, the *arrival time* used may be in-accurate (this may depend on the method used to determine the *arrival time*). Secondly, the arrival time may be of signals that are not coming from inside the transformer tank (non PD signals).

On completion of each search, the software displays the *search tolerance* value in nanoseconds (ns). One nanosecond is equivalent to 30 cm in air and 20 cm in mineral oil (taking the velocity of the signal to be 0.2 m/ns in oil [5]). This value indicates the accuracy of the found PD source location. A low value indicates that the returned PD locations are relatively accurate, while a high *search tolerance* indicates less accuracy. The value of the *search tolerance* will increase with the number of sensors used. Typically, a *search tolerance* of at most 0.1 ns is expected when searching with only two sensors. This value tends to increase with a search using more than two sensors.

5 PD location accuracy

The accuracy of the located PD source is dependent on the accuracy of the *arrival time* used. There are several factors that affect the process of estimating the *arrival time* of UHF signals, including:

- the method used to determine the onset time of the signal
- the way the signals propagate inside the transformer tank to the UHF sensor
- calibration of UHF sensors
- noisy UHF PD signals
- Bandwidth of the acquisition hardware

The choice of the digitising hardware for capturing the UHF signals should be governed by the aim of achieving timing accuracy of better than ± 1 ns, which corresponds to ± 20 cm in mineral oil. Over several industrial projects where the PD location system has been used, results have confirmed that accuracy of the PD source location using the system is typically better than 20 cm.

6 Model transformer tank

In order to support the investigation and development of the accuracy of the PD location system - the University of Strathclyde has installed a steel tank (of dimensions 3 x 2.44 x 2 m) in the high voltage laboratory (see Figure 6). The tank is used to replicate the electromagnetic characteristics of a power transformer tank.

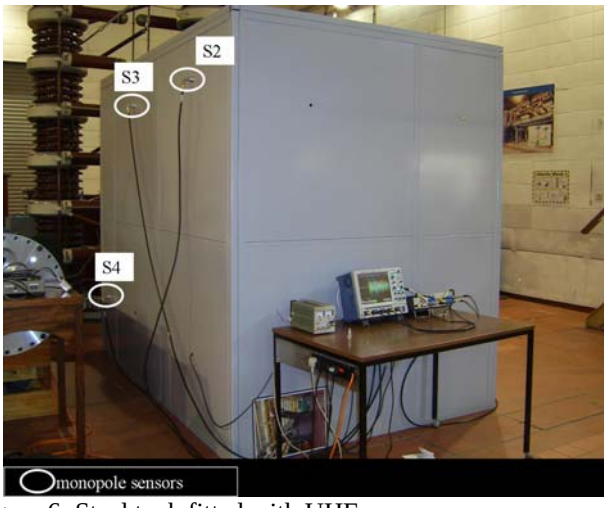

Figure 6: Steel tank fitted with UHF sensors.

Initially the tank has been fitted with four UHF monopole sensors which respond to the component of UHF electric field that is perpendicular to the inner surface of the tank. In the near future, the tank will be fitted with different types of UHF sensors (e.g. those shown in Figure 2) so that the PD location system can be tested with signals from these sensors. An avalanche pulser is used as a PD source which can be moved to different positions in the tank. In order to more accurately replicate the electromagnetic characteristics of a power transformer, the next step will be to fabricate the internal structure of a power transformer. High Voltage PD test cells will then be used in comprehensive experiments on PD location.

7 Conclusions and future work

A PD location system for power transformers has been described. The types of sensors and the different ways in which they can be installed have been described. The system will plot PD locations on a 3D model of the transformer. PD location accuracy to within 20 cm is possible when the PD location system is used.

The aim of this project is to develop a fully integrated system that can acquire, log, analyse UHF PD data and locate PD automatically. Once all of this functionality has been achieved, the PD location algorithms will be optimised further through their application to data recorded in the field. For example, different algorithms for determining the arrival time could run in parallel to determine the most effective long-term solution.

Acknowledgements

This project is funded by Knowledge Transfer Partnership Number 6231.

References

[1] M Wang, A J Vandermaar and K D Srivastava, “Review of condition assessment of power transformers in service,” *IEEE Elect. Insul. Mag*, vol. 18, no. 6, pp. 12-25, Nov./Dec. 2002

[2] M Duval and J Dukarm, “Improving the reliability of transformer gas-in-oil diagnosis”, *IEEE Electrical Insulation Magazine*, Vol. 21, No. 4, pp. 21-27, July/August 2005

[3] M D Judd, L Yang and I B B Hunter, “ Partial discharge monitoring for power transformers using UHF sensors part 1: Sensors and signal interpretation,” *IEEE Electrical Insulation Magazine*, vol. 21, no. 2, pp.5-14, March/April 2005

[4] P Kakeeto, “Experimental investigation of positional accuracy for UHF partial discharge location”, Condition Monitoring and Diagnosis conference, vol 2, pp.1070-1073, April 2008

[5] A Convery and M D Judd, “Measurement of propagation characteristics for UHF signals in transformer insulation materials”, *Proc. 13th Int. Symp. on High Voltage Engineering (Delft)*, August 2003

Distributed Wireless Transient Measurement System

K.Y. Liu, W.H. Siew, R.W. Stewart

Affiliation: Department of Electronic and Electrical Engineering, University of Strathclyde, Glasgow, UK;

ABSTRACT

This paper presents a distributed wireless system to measure transient electromagnetic field in power substations. The system enables cooperative multi-node measurement, flexible data acquisition, powerful data transmission capability, and easy interface to computer control system. In particular, through incorporating a wireless trigger function this system could help evaluate the transient field's effect on other control signals by simultaneously measuring these signals' conditions and the transient electromagnetic field.

Index Terms—Transient Measurement, Wireless Trigger, Time Synchronization

1.0 INTRODUCTION

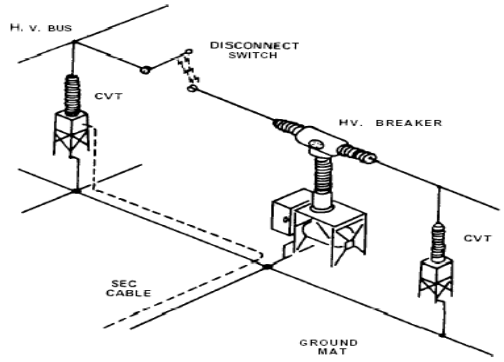

Fig.1: Example of switching operation in power substations [1]

In power substations, electric and magnetic emissions are generated during all operational conditions. In particular, switching operations of primary plant components such as disconnect switches and circuit breakers generate significant transient electromagnetic fields (Fig.1).

The transients generated in power substations have two significant characteristics: short duration and high amplitude.

As we all knows that short durance or fast rising time means high frequency contents. These unwanted high amplitude and high frequency emissions constitute potential electromagnetic interference (EMI) to sensitive electronic equipments within the substations. They may couple into the control circuits and electronic equipments and constitute serious threat to their normal function.

Therefore electronic equipments in substations must be suitably designed and protected to survive in the harsh EM environment. In fact some standards have been issued to deal with this situation, such as IEEE 1613 - IEEE Standard Environmental and Testing Requirements for Communications Networking Devices in Electric Power Substations and IEC 61850-3 Communications Systems and Networks in Substations (Section 5.7). As a result, a measurement system is needed to ensure the electromagnetic environment in substations comply with EMC standards, and evaluate the transient fields' impact on substations control signals or other important electronic parameters.

This paper describes the design and implementation of such a distributed data acquisition system that uses wireless technique and programmable device technique to implement flexible trigger function, accurate synchronization and interactive multi-node network management, which permit comprehensive measurement of the amplitude, frequency and relative time information of transient electromagnetic fields in power substations and help to evaluate their impact on other control signals

2.0 TRIGGER OPERATION

In most measurement devices, it is desirable to integrate a trigger function to capture useful information and make more effective use of the usually limited data storage space. For example, digital sampling oscilloscopes usually periodically save data before getting triggered.

Inside this system, we adopt a more flexible trigger strategy. There are two trigger options inside one measurement device: internal trigger and external trigger.

2.1 EXTERNAL WIRELESS TRIGGER

Conventional methods of electromagnetic emission measurement are based on the measurement of amplitude and frequency of the transient. While these methods are generally sufficient to check if the emissions satisfy some specifications, they provide little useful information about how the transient electromagnetic emissions would affect the control wires. To correctly relate the cause and effect of any transient disturbance, we need to record the coupled emission on control wires when the transients occur. In other words, we need to simultaneously measure both the transient field and the signals on the control wires and it is important to ensure that the events detected on the control wires are time-synchronised to the corresponding transient events detected by the transient field sensors. In order to ensure this, the control wire measurement nodes must start

to record at the same time that the transient data acquisition node find a transient, so that no effective delay is observed between them.

In addition, to measure transient electromagnetic field's distribution, the data from all the measurement nodes have to be correlated in time, since the transient field basically is a kind of time-varying field.

Fig.2 shows an example, Node B is used for measuring transient emission, Nodes A and C are used to record the events of control wires. From the left part of Fig.2 it is difficult to find the time correlation of measured data from these nodes since they start at different times whilst from the right part of Fig.2 it is easy to realize accurate time correlation, from which we can derive some useful information about cause and effect.

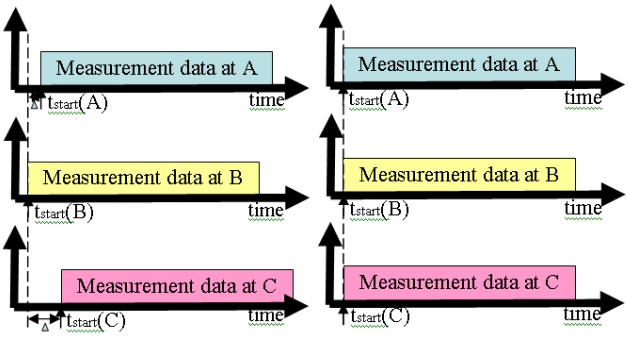

Fig.2: Example of simultaneous measurement

Since the ability to discern the time delay between data acquisition nodes is determined by the sampling frequency, the best achievable resolution would be one sampling period. The low limitation of resolution will be the worst time from which we can differentiate the correlation. Since usually there exists no determined period of transient, a reserved assumption of the low limitation would be one transient duration to get acceptable correlation.

In this developed system, the simultaneous saving of data is achieved by a function called wireless trigger. When one measurement node detects the transient signal, namely when the local input surpasses some pre-defined threshold, it will send out a trigger signal as shown on Fig.3. After receiving the trigger signal, the measurement nodes will keep the corresponding sampled data according to trigger signal's time information and stop sampling and data saving.

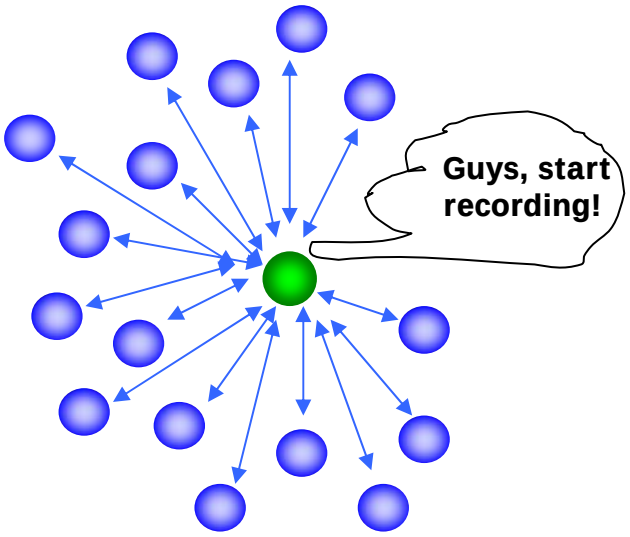

Fig.3: The concept of wireless trigger

2.2 INTERNAL TRIGGER

The internal trigger works like the normal amplitude or edge trigger function that could be found in most digital sampling oscilloscopes. But, besides the possibility of a trigger using the time domain trigger information, it could also be triggered using the frequency domain information, which is realized by real-time spectrum conversion through the imbedded FPGA chip.

3.0 TIME SYNCHRONIZATION

The incorporation of time synchronization scheme in this system has two advantages. The first one is that it makes wireless trigger more reliable and more accurate. Under some conditions, the trigger signal could be missed or not effectively received by some nodes. This happens when the receiver nodes are affected by some interference or the trigger signal has to pass some other nodes to arrive at the destination nodes, which will add some delay to the trigger signal. The first condition would be improved by resending the trigger signal. But this also will add time delay. Therefore, judging the trigger time by the arrival of trigger signal is not accurate and reliable. A solution to this issue would be making all the nodes time synchronized and incorporating the trigger time information into the trigger signal, which is unchanged during resending. The destination receiver nodes judge the trigger time based on the time information incorporated, by which the receiver measurement nodes would not be affected by any form of the trigger signal's delay.

The second advantage is increased power efficiency. With time synchronization, communication between different nodes including external trigger can work in TDMA way. Therefore the measurement nodes stay in doze or idle mode and enter receiver mode periodically to wait for possible trigger signal or other information. Through this, power

consumption will be decreased.

There are two strategies available: one is pre-synchronization that keeps system synchronized all the time; the other one is achieving time synchronization only when necessary, known as post-facto synchronization [3]. Post-facto synchronization is more power efficient, while pre-synchronization is more reliable and accurate.

So which time synchronization scheme and strategy to choose depends on the practical requirements on power consumption and resolution.

Fig.4 show the measured result of time synchronization of the system, from which we can see the accuracy is less than 1 microsecond.

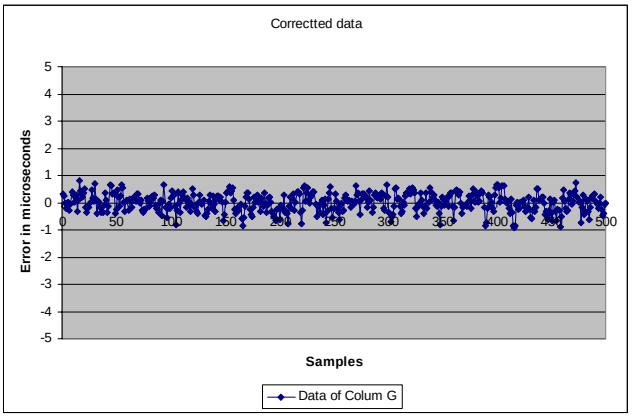

Fig.4 Measured time synchronization accuracy

4.0 INTERACTIVE MULTI-NODE MEASUREMENT

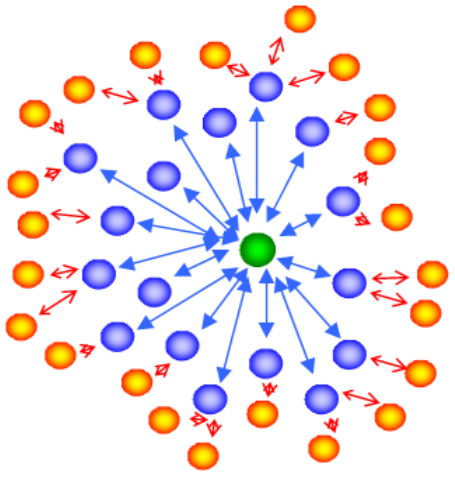

Fig.5: System topology

As we said before, instead of consisting of just one or several stand alone measurement devices used in conventional measurement setup the system is designed as an interactive multi-node network, in which up to thousands of measurement devices could be distributed and managed through some simple flexible wireless networking protocol.

Transient measurement is usually conducted in a determined environment, namely we usually have the knowledge of node locations, so there is no need to implement complicated auto-organizing networking topology like mesh, which need more software overhead and possibly less reliable. Instead, we adopt an easy to use tree topology, even though it could be adapted to other topologies (Fig.5).

5.0 OTHER CHARACTERISTICS

Besides the trigger function, time synchronization and networking, the system has some other characteristics:

1) It supports 100MSPS sampling rate
2) It integrates an 802.11b/g module therefore has very powerful data transmission capability and could be easily controlled by a laptop.

6.0 CONCLUIONS

The system described in this paper is more like an interactive wireless distributed network with high data acquisition capability, the nodes of which could work cooperatively to get amplitude, frequency and time information, rather than a static amplitude-only measurement device. Therefore it could be used not only as a system to evaluate the electromagnetic environment in power substations but also a useful tool for transients induced power system fault diagnosis and verification of transient field distribution modelling.

7. ACKNOWLEDGEMENT

The authors wish to acknowledge the funding provided by ScottishPower through the grant of a Dorothy Hodgkin Postgraduate Award.

8.0 REFERENCES

[1] W. C. Kotheimer, “Substation Transients and Solid State Controls”, Northwest Electric Light and Power Association, April 1974.

[2] Thomas, D.E. Wiggins, E.M. Salas, T.M. Nickle, F.S. Wright, S.E. “Induced transients in substation cable: measurements and models”, IEEE Trans on Power Delivery, vol.9, no.4, pp.1861-1867, October1994.

[3] J. Elson, D. Estrin, “Time Synchronization for Wireless Sensor Networks,” Proceedings of the 2001 International Parallel and Distributed Processing Symposium (IPDPS), Workshop on Parallel and Distributed Computing Issues in Wireless and Mobile

Computing, San Francisco, California, USA, April 2001.

[4] Yu Wang, thesis “Design and Implementation of Wireless Data Acquisition System for Measurements in High Voltage Substations”, University of Strathclyde.

[5] connectBlue AB, datasheet “The OWSPA Electrical & Mechanical Datasheet”.

ELECTRICAL TESTING OF DECOMMISSIONED 25kV RAIL SUPPLY INSULATORS

R. Mason, A. J. Reid, M. J. Given, M. D. Judd

University of Strathclyde, Glasgow, G1 1XW, contact: r.mason@eee.strath.ac.uk

Keywords: Partial discharge, RF measurement, ceramic insulators.

Abstract

Partial Discharge measurements were carried out on 101 Ceramic Insulators removed from service from three different locations on a 25 kV rail supply network. Measurements were taken using a combined IEC 60270 apparent charge and RF measurement system to assess the condition of the insulators. Low level (25 – 35 pC) PD activity was observed in 15 of the samples, and was thought to be the result of voids at the terminal surfaces where delamination of the porcelain could have taken place through mechanical stress or environmental conditions. The RF and apparent charge measurement systems were comparable in their ability to detect PD activity, which indicates that it might be possible to develop a non-contact RF condition monitoring system for use with rail supply insulators.

1 Introduction

Partial discharges (PDs) are a sign of localised electrical breakdown within an insulator, often involving quite small amounts of electrical charge. Left unchecked, PD tends to erode and degrade insulation over time, and can lead to electrical failure if the discharges involved succeed in bridging the insulation gap between conductors. Should PD damage become extensive it can also lead to mechanical failure.

PD can be monitored to assess the condition of the insulator, and is traditionally achieved by measurement of apparent charge magnitude according to IEC 60270 [1]. Another method which is used to monitor insulation is the radio frequency (RF) technique, where the energy radiated from the discharges can be observed via an RF sensor. This method has an advantage over the standard method, in that the technique is non-contact and can be performed in-service when the insulator is under normal load and environmental conditions. Recent research [2] using a combined measurement system has shown that, due to the different responses of the two systems, simultaneous PD measurement can give an insight into the underlying shape of the PD current pulse and therefore the type and number of defects present within the test object.

The insulators supplied for testing were removed from three different locations on the rail network. Two types of insulator were supplied, with an obvious mechanical difference in the end caps, relating to the position in which they are used, either strut or upper, as can be seen in Figure 1.

New insulators of this construction would not be expected show any PD at normal operating voltages. This is because their test requirements include a wet power withstand voltage of 95 kV (peak) and a dry lightning impulse withstand voltage of +200 kV peak (as indicated in Table 1). In order to meet these requirements, the electric fields at 25 kV should be comparatively small with respect to the insulation capabilities of a (pristine) device.

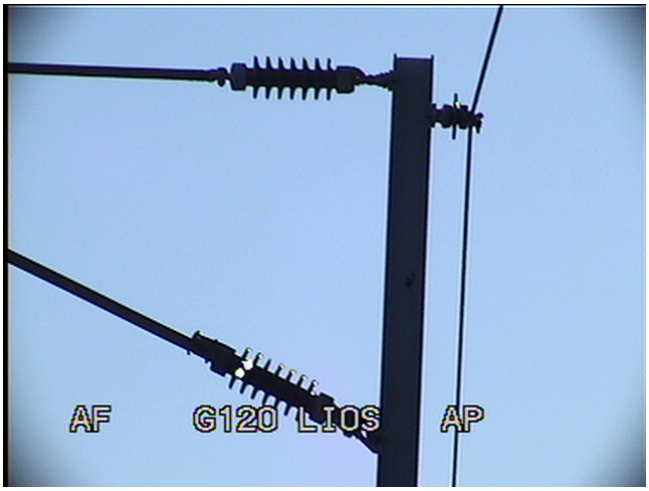

Figure 1: Example of insulator location and orientation – the top insulator is referred to as *'upper,'* and the lower insulator as *'strut'*.

Table 1: Rated insulation voltages and clearances.

Parameter	Value (line to earth)
Wet Power Withstand Voltage (Vertical and Horizontal)	95kVp
Dry Lightning Impulse Withstand Voltage (+ve)	200kVp
Minimum Creepage Path (Non Polluted Area)	790mm
Minimum Creepage Path (Polluted Area)	1070mm

2 Electrical specification for new insulators

The specification document on overhead line equipment outlines the requirements which new insulators must meet, in terms of many different stresses (electrical, mechanical, environmental etc.), and describes the conditions under which

the insulators must operate in normal and abnormal circumstances. A list of relevant standards relating to electrical tests includes:

- BS 137 – Insulators of ceramic material or glass for overhead lines with a nominal voltage greater than 1000V
- BS 60383, IEC 383 – Tests on insulators of ceramic material or glass for overhead lines with a nominal voltage greater than 1000V
- IEC 1109 (composite insulators)
- BS 60168, IEC 168 – Tests indoor and outdoor post insulators of ceramic material or glass for overhead lines with a nominal voltage greater than 1000V

Insulators have to be subjected to the following tests prior to delivery by the supplier:

- Design, type, sample and routine tests in accordance with relevant standards
- Performance tests
- Any additional tests defined in the procurement document
- It is further required that insulators must be free from defects, voids, cracks, contamination, etc., tested using ultrasonic methods.
- Wet Power Withstand Voltage (IEC 1109 clause 6.1, BS 60383 clause 14)
- Dry Lightning Impulse Withstand Voltage (IEC 1109 clause 6.2, BS 60383 clause 13)
- Salt Fog Pollution Test (BS EN 60507 section 3)
- Electromechanical failing load test (Power frequency voltage and tensile force applied simultaneously) (BS 60383)
- Ultrasonic flaw detection test

After these tests have been completed each insulator is considered ready for service. No further electrical testing is carried out prior to installation on the network or while in service to monitor reliability. Maintenance can therefore either be time based, which may result in unnecessary effort, or the use of inspections or diagnostic tools that allow maintenance effort to be focussed only on insulators that actually show some signs of deterioration. Researchers at the University of Strathclyde have successfully used non-contact RF methods to monitor and locate PD in other HV equipment, hence the interest in carrying out these experiments.

3 Experimental Work

In total, 101 25kV insulators were removed from service from three different locations on the rail supply network. Among these were units originally supplied by three different manufacturers. Insulators are about 400 mm long - a typical sample is shown in Figure 2. They were not cleaned prior to testing, however, following removal from service the insulators had been stored in warn dry conditions for several weeks.

Each sample was initially tested using a Megger (model BM100) for insulation resistance at an applied voltage of 500 V dc. Each sample was then PD tested according to IEC60270 [1] at 25kV AC, with simultaneous measurement of any RF PD signals. If no PD was measured at normal operating voltage, each device was then tested at up to 29 or 30 kV, representing the highest voltages that might be seen in service.

Figure 2: Typical example of insulator as supplied.

The IEC measurements were conducted using the LDIC LDS-6 while simultaneous RF measurements were recorded with an RF sensor connected to a 3 GHz bandwidth oscilloscope via a 25dB amplifier. A variable 0.38/100 kV step-up transformer provided high voltage to the test object. The HV supply was connected to the lower terminal of the insulator through an HV resistor connected in series (included in order to limit the current in the unlikely event of a flashover), while the upper terminal was earthed.

Due to the presence of the series current-limiting resistor, there was potential for a discrepancy between the HV supply voltage and the voltage across the insulator under test. The significance of this difference would depend on the unknown capacitance of the insulator. Therefore, an HV probe was used to measure the actual voltage *V* across the insulator in the circuit of Figure 3. Results, shown in Table 2, indicate that the voltage difference is negligible and the applied voltage was considered equal to the HV supply voltage for the purpose of these tests.

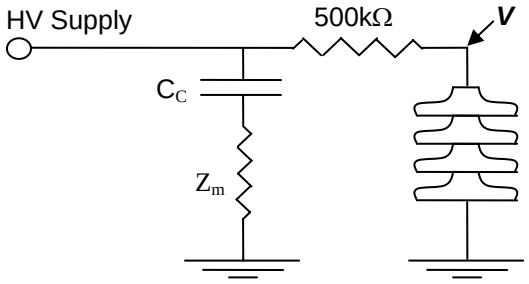

Figure 3: Test circuit used to energise the insulators. An HV probe was used to measure *V*. C_C is the PD coupling capacitance and Z_m is the impedance for the IEC apparent charge measurement.

Table 2: Supplied and measured voltages across test object

Supply voltage (kV)	Measured voltage across insulator (kV)
4.9	4.8
10.0	9.8
15.0	14.8
20.1	19.9
25.3	25.1

The supply voltage was increased from 0 to 29 or 30 kV in steps of 5 kV (the normal operational voltage of the insulators is 25 kV, while the maximum voltage in service may reach 29 kV). In the cases where PD was found, both the average apparent charge level and the phase-resolved partial discharge (PRPD) pattern were recorded.

4 Results and Discussion

The initial (Megger) insulation resistance test showed, as expected, that each insulator was open circuit up to 500 V dc. This is unsurprising given the relatively small electric field and the scale of any expected defects.

Of the 101 insulators tested, PD was observed in 15 samples. Figure 4 shows PRPD patterns for 3 typical samples exhibiting PD designated D_1, D_2 and D_3 (each unit is described in Table 3). Discharge levels can be seen in the region of 25 – 35 pC (in one extreme case, a discharge level of ~70pC was observed below normal operating voltage), a comparatively low level considering power transformers are said to be *'defect-free'* if PD is observed in the region of 10 – 50 pC [3].

Of the 15 samples exhibiting PD, all except 4 produced measurable RF signals. However, these four samples had exhibited very low level PD, only marginally above the noise threshold. Additionally, in one case among the other 11 samples, RF signals were observed when the corresponding apparent charge levels were comparable to noise levels. It must be remembered, however, that PD levels and RF signals are likely to be significantly higher under the damper outdoor conditions to which the insulators are normally exposed.

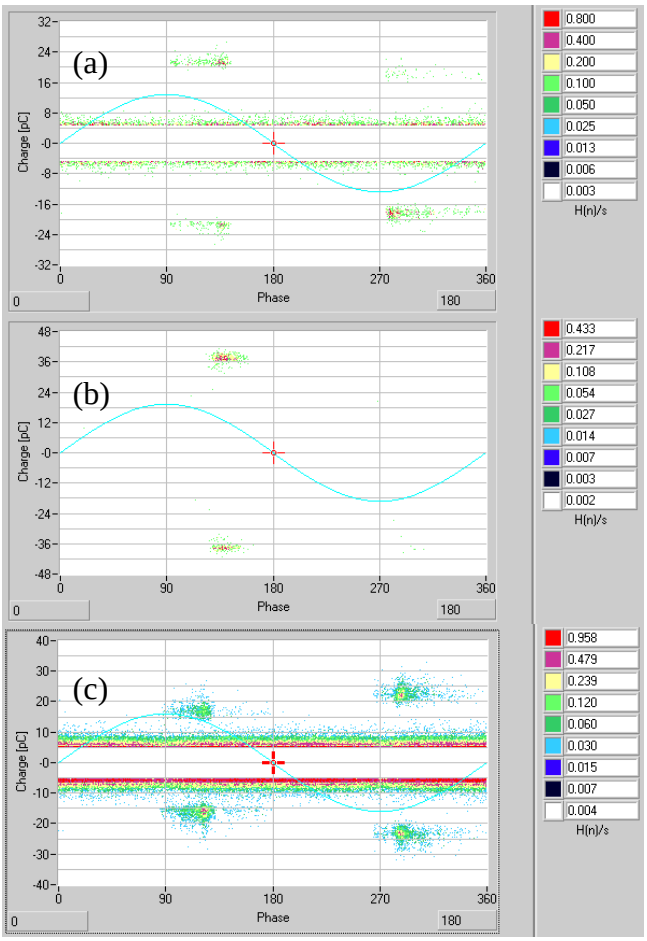

Figure 4: Phase resolved PD patterns for (a) Insulator D_1 at 30 kV; (b) D_2 at 35 kV and (c) D_3 at 20 kV.

Table 3: Description of 3 typical sample experiencing PD

Sample	Orientation	Manufacturer	Location
D_1	Strut	B	1
D_2	Strut	C	1
D_3	Strut	B	2

As previously mentioned, the combined measurement method can reveal information about the discharge events that may not be found using either technique independently. The correlation plots in Figure 5 show the relationship between apparent charge levels and radiated energy for the 3 typical samples discussed previously. Patterns within these correlation plots relate to the underlying physics which cause variation in the PD current pulse shape. Different clusters within the patterns correspond either to different discharge sites, or different discharge mechanisms as a defect progresses. As the period over which results were gathered is so short and the electric fields the samples were exposed to were relatively low, it is assumed that the clusters are due to multiple discharge sites.

Statistical evaluation of the results was conducted to identify relationships between the insulators presenting with PD (displayed in Figure 6). It was found that there was a higher occurrence of PD in insulators from Manufacturer B, insulators in the strut orientation, and those removed from Location 1.

These statistics need to be evaluated carefully to avoid misinterpretation, as there may have been a greater percentage of insulators from Manufacturer B in Location 1. In fact, Manufacturer C actually accounted for 51% of the insulators in that location while Manufacturer B made up the remaining 49%, the lowest proportion from this manufacturer among all three locations (manufacturer B accounts for 59% of insulators from location 2 and 58% from location 3), indicating that there is propensity for PD in that location.

5 Conclusions

Although the PD events may not have been likely themselves to lead to failure – as the discharge levels would not be regarded as severe in this insulation type – it is likely that the PD observed is related to the degradation mechanism. That is to say, the PD events may be a result of another form of damage, and that PD observed in insulators could indicate the potential for eventual failure. However, this would need to be

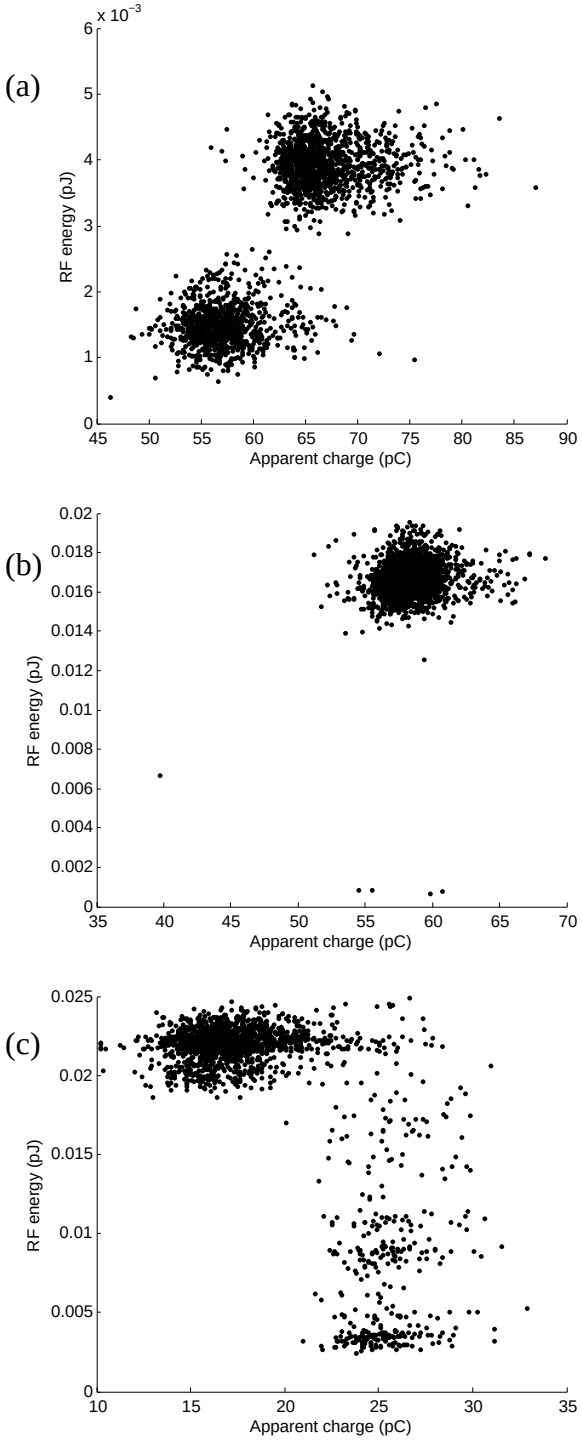

Figure 5: Correlation plots showing relationship between apparent charge levels and radiated energy for (a) Insulator D_1 at 30 kV; (b) D_2 at 35 kV and (c) D_3 at 20 kV.

verified through further PD testing of out of service and in-service insulators measured against the propensity for failure of insulators in terms of manufacturer, location, etc.

It was concluded that the most likely source of PD was the presence of internal voids in high field regions. Since even quite severe physical damage, such as broken sheds, did not

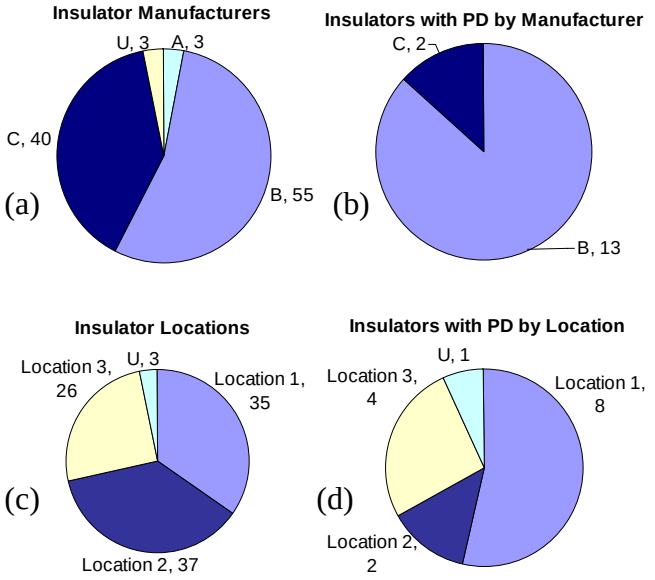

Figure 6 (a): Total number of insulators by manufacturer
(b): Number of insulators showing partial discharge by manufacturer
(c): Total number of insulators by location.
(d) Number of insulators showing partial discharge by location on the network

result in PD, it is thought likely that the PD occurs at the terminal interface, where delamination of the porcelain surface could have taken place. Under these conditions the PD activity would be a *result* of mechanical deterioration, as opposed to being the *cause* of the degradation.

RF methods have been shown to have similar capability to apparent charge measurements in terms of observing low levels of PD in these ceramic insulators. Further research will be required to discover whether RF monitoring of in-service insulators is viable. If so, it might become possible to survey insulators from a moving vehicle because of the fast response of the RF measurement system. When conducting such tests it would be necessary to take into account increased levels of RF noise and interference, but this might be counteracted to some extent by the increased discharge levels expected during outdoor operation.

6 Acknowledgement

The authors are grateful to Network Rail for permission to publish this study.

7 References

[1] IEC International Standard 60270, *High Voltage Test Techniques – Partial Discharge Measurements*, International Electrotechnical Commission (IEC), 3rd Edition, 2000

[2] A. J. Reid, M. D. Judd, B. G. Stewart and R. A. Fouracre, *Correlation between RF and IEC 60270 apparent charge for selected partial discharge source geometries*, 15th International Symposium on High Voltage Engineering – ISH2007 (Ljubljana, Slovenia), August 2007

[3] CIGRE Working Group A2.18, *Life management techniques for power transformers*, CIGRE Brochure No. 227, June 2003

On-line Partial Discharge detection in Medium voltage cables using Protection/Instrument Current Transformers

F. P. Mohamed, W. H. Siew, J. J. Soraghan

University of Strathclyde, Glasgow, Scotland, United Kingdom

Email: pfaisalbe@eee.strath.ac.uk

Keywords: Partial discharges, Current transformers

Abstract: This paper investigates the performance of protection/instrument current transformers in detecting partial discharge signals from medium voltage cables. This research work involves developing an appropriate high frequency model of the CT, simulation parameter calculation followed by experimental analysis.

1. Introduction

Power transmission and distribution is achieved using networks of overhead lines and underground cables. Underground cable designs vary with the age, voltage and capacity of the particular circuit. The majority of the existing medium voltage (11kV to 33kV) cables in the UK are of a paper insulated, mass impregnated, lead sheathed design which was used, for more than 100 years, since the latter part of the 19th century up to the present day. Partial discharges within the insulation result in degradation of these cables and this degradation due to partial discharges is the main cause of cable failures that are not due to mechanical damage. Deregulation of the electricity market focuses network operators on pro-active management of network reliability. A condition based maintenance strategy can prevent forced outages and improve supply reliability and availability for customers. The detection and location of partial discharge sites offers an important tool when building a maintenance strategy for these underground cable networks.

Partial discharges are localized electrical discharges which form a partial bridge between the electrodes. This partial breakdown generates high frequency pulses which is useful for the PD quantifications and PD mapping. They are the early symptoms of insulation degradation, prolonged activity leads to complete breakdown of the cable. PD signals which originate from the discharge source have two propagation paths namely phase-phase and shield-phase. In normal case inductive couplers are inserted into the earth strap of the cable. PD data obtained from such configuration has information from all three phases. From the Signal processing point of view this data is not preferred for PD mapping. As a result Phase-Phase measurement is normally used. Sensor positioning in live phase conductors is always not possible. Since PD is an early symptom of cable breakdown, it is often not necessary to monitor the insulation condition continuously. This means there is no need for permanent installation of sensors in the cable. This paper is investigating the robustness of preinstalled protection/measurement CT for PD detection by conducting frequency response modelling and experimental analysis. These CTs often deal with power frequencies and the bandwidth of these CTs are often not available. Once PD signal acquisition equipment is connected to these preinstalled CTs, it should not increase the burden since this will have impact on measurement protection and control circuitry connected to the power system.

2. High Frequency Equivalent circuit model

Frequency response modelling of CT is not a new area. Many high frequency models are available. Most of the models are developed for the behaviours of CT in substation switching. Energy of the high frequency signals in those models is very high. As far as PD is concerned energy content is very low. This is the major difference between the existing models and this work.

Protection CTs are normally air gapped. Air gap avoids the magnetic core to be saturated by a dc component in the primary current. Furthermore, it increases the linearity of the magnetic curve [3]. High frequency model of the protection CT differ from measurement CT in terms of inductance of air gap. Measurement CTs are designed in the linear portion of the magnetization curve for metering accuracy while protection CTs are designed in the lower portion of the magnetization curve so that higher fault current does not push those CTs into saturation. Factors which influence the high frequency limitations of the CT are

i. Inter winding capacitance.
ii. Capacitance between primary winding and core
iii. Secondary winding turn to turn
iv. Secondary winding turn-core
v. Core material permeability
vi. Core loss
vii. Winding resistance variation due to skin effect

Based on the above parameters high frequency model of the transformer is as shown in Figure 1. Stray capacitance parameter for modelling can be calculated by finite element methods or analytical methods. Finite element analysis (FEA) needs 3D FEA simulation software. Analytical method is

preferred in this paper. Stray capacitance can be determined experimentally by using impedance-phase analysers. Jiles Atherton model can be used to model the core losses at various frequencies. Jiles Atherton parameters can be determined by experimental analysis.

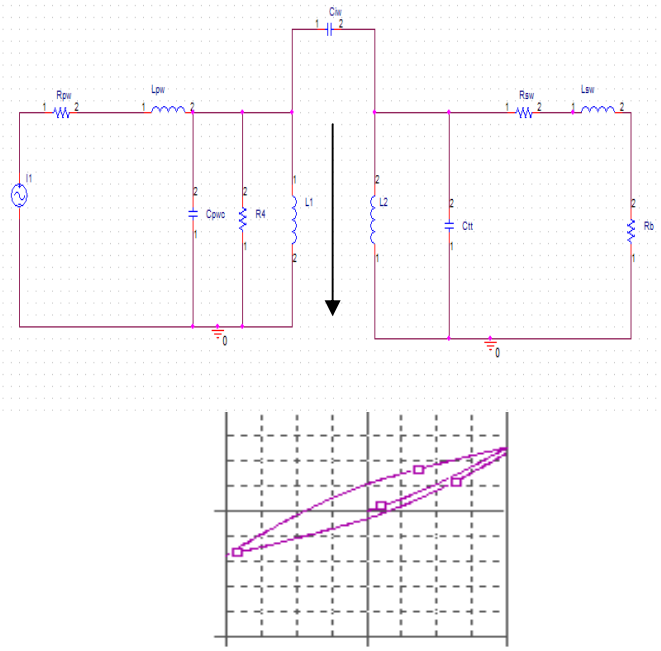

Figure 1. High frequency Equivalent Circuit

3. Secondary winding capacitance

Secondary winding capacitance has two components namely between turns and between turn to core. Antonio Massarini et al [1] used an analytical approach to predetermine the capacitance of winding from the winding geometry. This method is discussed briefly in this section. Figure 2 shows cross sectional view of CT winding.

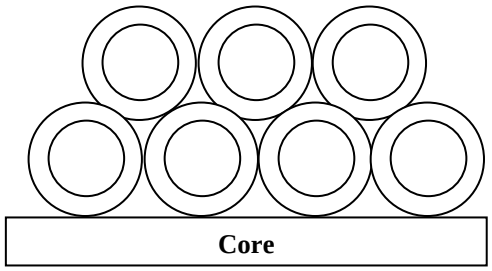

Figure 2. Cross sectional view of coil

Figure 2 can be viewed as a combination of many numbers of basic cells as shown in Figure 3. Each basic cell is a combination of two winding turns separated by two insulation coatings and an air column between them. This arrangement forms a series connection of three capacitors as shown in Figure 4. Capacitance between two turns can be calculated by choosing an elementary curved surface area followed by integration. Turn-turn capacitance (C_{eq}) is given by the equation (1)

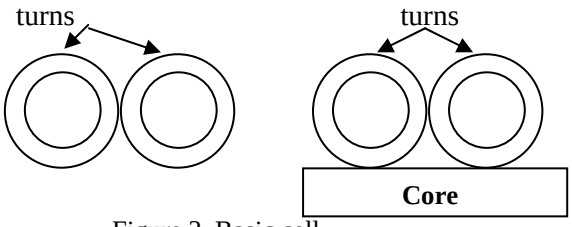

Figure 3. Basic cell

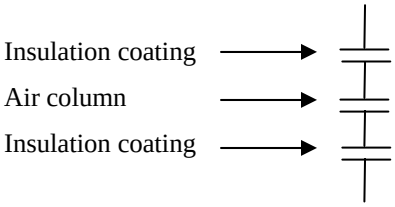

Figure 4. Equivalent Capacitance

$$c_{eq} = \frac{2\varepsilon_r \arctan\left(-1+\sqrt{3}\right)\left(2\varepsilon_r \ln\left[D_o/D_c\right]\right)}{\varepsilon_o l_t \left(1+\sqrt{3}\right)\sqrt{\ln\left[D_o/D_c\right]\left(2\varepsilon_r + \ln\left[D_o/D_c\right]\right)}\sqrt{\left(2\varepsilon_r \ln\left[D_o/D_c\right]\right)+\left(\ln\left[D_o/D_c\right]\right)^2}}$$

------(1)

€$_r$: Relative Permittivity of insulation

l_t : Mean length of turn (from data sheet)

Same basic cell structure is used to calculate the turn to core capacitance. Here the capacitance will be two times the capacitance in previous case since E field propagates only half distance of the turn to turn path. So turn to core capacitance will be 2*C_{eq}. Figure 5 shows the basic structure for odd and even turns of transformer winding.

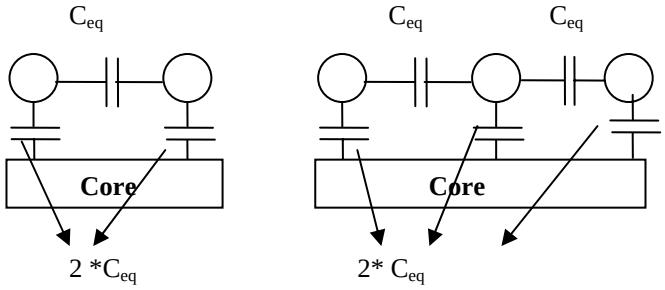

Figure 5. Even and odd turns

By applying basic network reductions to Figure 5 equivalent capacitance of odd or even turns can be computed. There by total capacitance can be calculated by using equation (2)

$$C_{tot} = C_{eq} * C_s(n-2)/(2C_s(n-2) + C_{eq}) + C_{eq} \quad \text{-------- (2)}$$

Example Iteration of the above equation is shown below.

$$C_{s(5)} = [C_{eq} * C_{s(3)}]/[2 * C_{s(3)}] + C_{eq}$$
$$C_{s(7)} = [C_{eq} * C_{s(5)}]/[2 * C_{s(5)}] + C_{eq}$$
$$C_{s(9)} = [C_{eq} * C_{s(7)}]/[2 * C_{s(7)}] + C_{eq}$$
$$C_{s(11)} = [C_{eq} * C_{s(9)}]/[2 * C_{s(9)}] + C_{eq}$$

$$C_{s(4)} = [C_{eq} * C_{s(2)}]/[2 * C_{s(2)} + C_{eq}] + C_{eq}$$
$$C_{s(6)} = [C_{eq} * C_{s(4)}]/[2 * C_{s(4)} + C_{eq}] + C_{eq}$$
$$C_{s(8)} = [C_{eq} * C_{s(6)}]/[2 * C_{s(6)} + C_{eq}] + C_{eq}$$
$$C_{s(10)} = [C_{eq} * C_{s(8)}]/[2 * C_{s(8)} + C_{eq}] + C_{eq}$$

4. Primary winding capacitance

Size of the primary conductor influences the capacitance between primary cable phase conductor and the winding. Primary conductor dimension is predetermined from air breakdown fields and corona inception field [4]. CT and the cable is treated as coaxial cylinder geometry as shown in Figure 6.

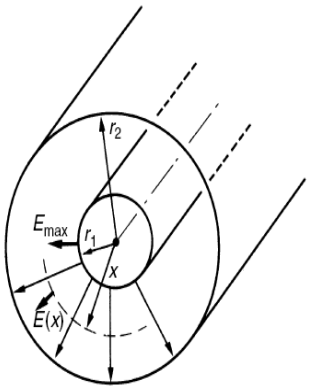

Figure 6. Coaxial geometry

Uniform Electrical field equation is given by equation (3) and corona inception field is given Peek's expression, equation (4)

$$E(x) = [V] / \ln(r_2 / r_1) * x \quad \text{---------- (3)}$$

$$E_i = E_0 * m_0 * \delta \left[1 + 0.308 / \left(\sqrt{\delta * r_w}\right)\right] \quad \text{---------(4)}$$

Solution of equations (3) and (4) will give the optimum diameter of the primary conductor which should not cause air breakdown and corona.

Primary winding capacitance can be calculated by a numerical approximation is explained with reference to Figure 7. Primary conductor treated as bundled cylindrical conductors and primary conductor is treated as an equipotential surface. Part of the Secondary winding turn above the primary conductor is assumed as cylindrical conductor coated with insulation. Capacitance exists between each turn of secondary and cylindrical segment of primary conductor (C_{iw}). Capacitance also exists between inter turn space of secondary and cylindrical segment of primary conductor (C_{pwc}).

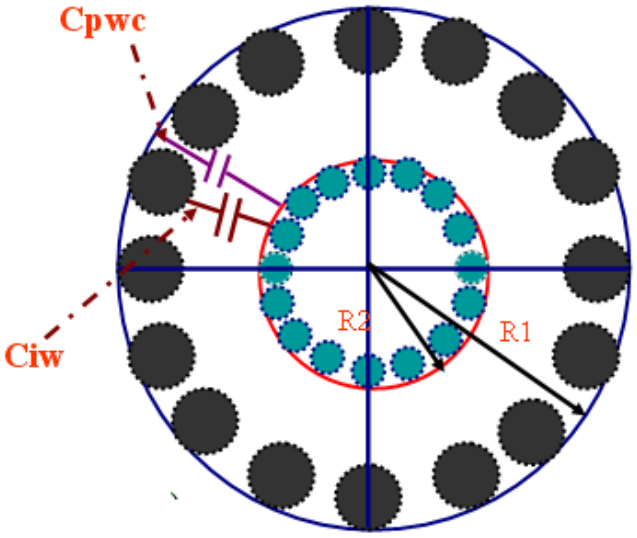

Figure 7. Coaxial geometry

R_1-Inner radius of the CT
R_2-Radius of the Primary Conductor
r_1-Radius of the black circle
r_2-Distance between the black circles
r_3-Radius of the blue circle
r_4-Distance between the blue circles
N-Number of turns in secondary
M-Number of inter turn spaces
H-Height of the core
$r_3 < r_1$

C_{pwc} can be calculated by parallel plate approximation, as in equation (5). Hence,

$C_{pwc} = \varepsilon_o \varepsilon_r A / d$ ----------(5)

A -Area of the plate = r_2*height of the core
d-distance between the plates = R1-R2
ε_o - 8.854 x E-12 Farad/meter
ε_r - 1 for air

C_{iw} can be approximated as the capacitance of cylindrical conductors of different radii with different radial thickness of dielectric (air and turn insulation), see Das et al. [2] method of capacitance calculation of cylindrical conductors of different radii with different radial thickness of dielectric.

5. Core loss

Saturation, hysteresis, and eddy currents effects are not considered in linear transformer model. However, these nonlinearities significantly influence the behaviour of transformer during abnormal conditions [5]. Effect of saturation is not considered in PD aspect. Hysterisis loss can be calculated by the product of area under the curve of hysterisis loop and the operating frequency and is given by the equation (6). BH loop can be determined by using Epstein frame. By using a variable frequency source, frequency effects on BH loop can also be found. As the frequency of primary current is high, material will have wide BH loop due to the increase in coercivity. Figure 8 shows the effect of frequency on the hysterisis loop. As the frequency increases eddy current loss dominates over hysterisis loss. Eddy current effects can also be included in the BH loop, see Figure 9.

$$p = f \oint b.dh \quad \text{----------} \quad (6)$$

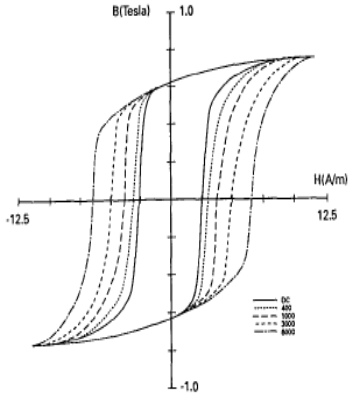

Figure 8. Hysteresis curve of Permalloy for frequency Hz [3].

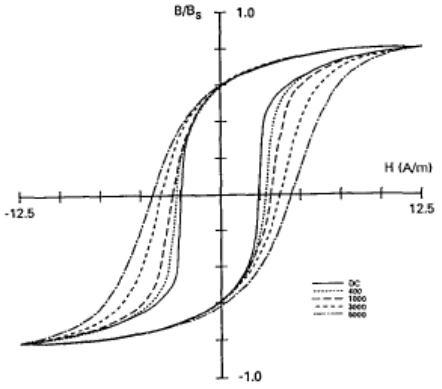

Figure 9. Hysteresis curves with eddy current effect included [3].

6.Conclusions and Future work

Phase - Phase measurement of PD favours signal processing for finding the discharge location. Installation of inductive coupler in a live phase-conductor is not preferable. Hence pre-installed CT may be used for PD detection. These CTs are designed to operate at power frequencies and thus the bandwidth characteristics of these devices are not available. Frequency response analysis of conventional CT was investigated for this purpose. High frequency modelling parameter calculation of conventional CT is in progress. Denoising PD signals, PD mapping is our ongoing research.

7. Acknowledgements

The authors wish to acknowledge the funding support provided by ScottishPower through the ScottishPower Advanced Research Centre and by the University of Strathclyde through the award of a University Studentship. Thanks are also due to Paul Cunningham of ScottishPower for his comments on this paper.

8. References

1. A. Massarini and M. K. Kazimierczu "Self Capacitance of Inductors", *IEEE TRANSACTIONS ON POWER ELECTRONICS, VOL. 12, NO. 4, JULY 1997*

2. B. N. Das, S. Das, and D. Parida, "Capacitance of Transmission Line of Parallel Cylinders with Variable Radial Width", *IEEE TRANSACTIONS ON ELECTROMAGNETIC COMPATIBILITY, VOL. 40, NO. 4, NOVEMBER 1998*

3. D. C. Jiles, "Modelling of eddy current losses on frequency dependant hysterisis in electrically conducting media", *IEEE TRANSACTIONS ON MAGNETICS, VOL. 30. NO. 6, NOVEMBER 1994.*

4. F. P. Mohamed, W. H. Siew and Q. M. Li ,"On-Line Partial Discharge detection in high voltage cables using conventional current transformers", *International Conference on Condition Monitoring and Diagnosis, Beijing, China, April 21-24, 2008*

5. H. Akçay and D. G. Ece ,"Modelling of hysterisis and power loss in transformer lamination", *IEEE TRANSACTIONS ON POWER DELIVERY, VOL. 18, NO. 2, APRIL 2003*

6. P. Poulichet, F. Costa, and E Laboure, "High-Frequency Modeling of a Current Transformer by Finite-Element Simulation", *IEEE TRANSACTIONS ON MAGNETICS, VOLUME 39, ISSUE 2, PART 2, MARCH 2003.*

TIME DOMAIN ANALYSIS OF SWITCHING TRANSIENTS FIELDS IN HIGH VOLTAGE SUBSTATIONS

B.U. Musa, W.H. Siew and M. Judd

Department of Electronic and Electrical Engineering, University of Strathclyde-mail: musa@eee.strath.ac.uk

Keywords: Electromagnetic fields, switching transients, disconnect switch, Finite Difference Time Domain (FDTD), air-insulated substations.

Abstract

Switching operations of circuit breakers and disconnect switches generate transient currents propagating along the substation busbars. At the moment of switching, the busbars temporarily acts as antennae radiating transient electromagnetic fields within the substations. The radiated fields may interfere and disrupt normal operations of electronic equipment used within the substation for measurement, control and communication purposes. Hence there is the need to fully characterise the substation electromagnetic environment as early as the design stage of substation planning and operation to ensure safe operations of the electronic equipment. This paper deals with the computation of transient electromagnetic fields due to switching within a high voltage air-insulated substation (AIS) using the finite difference time domain (FDTD) method

1 Introduction

Substation emissions can be characterised by measurements or computations. Measurements involve complex and expensive equipments. The alternative is to develop models to predict the emissions. Substation models can be developed to aid in understanding the measurements and to provide means for estimating electromagnetic interference levels beyond measurement limitations [3]. Once the models have been demonstrated to be robust and accurate they have the potential to greatly simplify the analysis process.

Initially, the emphases of the transient field analysis are mainly focused on control rooms within the substations. Also, the equipments are mainly electromechanical in design and construction, thus not seriously affected by electromagnetic emissions. However, equipment used in the substations has greatly changed today. Moreover and most importantly some new electronics equipments that have been introduced into the substation are not necessarily housed in the control rooms anymore; they may be located close to the switching devices. This is referred to as “distributed electronics” in the switchyards [2]. For the successful introduction and operation of this new equipment into the substations, they must be immune to the disturbance in this harsh environment. There is therefore the need to consider the electromagnetic compatibility of such equipment in this environment.

The FDTD method can be used to simulate the above scenario and predict the electromagnetic fields effectively. For the computation of the transient fields in a substation, the transient current propagating along the bus-bars is needed. Instead of using the actual bus currents, a damped sinusoidal current and a differentiated Gaussian pulse which are good representations for transient currents in substations have been used to calculate the radiated fields in this research. Once the capability of the method for the field calculation is established using the assumed current, the next level in the research is to consider the development of a suitable method to compute the actual transient current on the bus-bars. The calculation of the transient current will include the physics of the switching elements. The current thus obtained can be used to calculate the transient fields, thus predicting the electromagnetic emissions due to switching operations in the switchyard. First the results obtained with FDTD code for a simple electromagnetic field transient model will be compared with analytical method in a similar environment to demonstrate the capability of the method. Secondly, simulation results for a section of high voltage substation will be presented.

2 Computation of transient fields

(a) Analytical method

The computation of transient electromagnetic fields in substations is effectively a two step procedure [4]; (i) calculation of the transient currents on the conductors due to switching and (ii) calculation of the resulting radiated fields in the vicinity of the conductors due to the travelling current. The electromagnetic fields can be calculated by analytical or numerical methods.

The analytical or the hertzian dipole [6] method assumes the conductor to be of cylindrical shape. The radius is assumed to be small in comparison with the minimum wavelength of the transient current so that it can be regarded as a filament. With reference to fig.1 below ,assuming the line is of length L lying along the z axis, $p(x,y,z)$ is the coordinate of point of observation, the transient fields can be calculated as follows[7].

With the orientation of the conductor as above, the x and y component of the magnetic vector potential A can be neglected. E and H are computed using A.

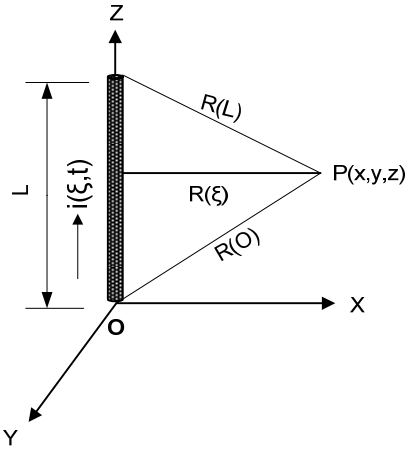

Fig. 1: Vertical filament of line

For example E_x and H_y are given by:

$$E_x(t) = \frac{-x}{4\pi\varepsilon_o c}\left\{\frac{F_o(t)}{R^2(o)} - \frac{F_L(t)}{R^2(L)} - \frac{z}{R(o)}I_o(t) + \frac{L-z}{R(o)}I_L(t)\right\} \quad (1)$$

$$H_y(t) = \frac{x}{4\pi}\{I_o(t) + I_L(t)\} \quad (2)$$

$$F_o(t) = c\int_0^\tau i\left(0, \tau - \frac{R(o)}{c}\right)d\tau \quad (3)$$

$$F_L(t) = c\int_0^\tau i\left(L, \tau - \frac{R(L)}{c}\right)d\tau \quad (4)$$

I_o: Current at the lower end of the conductor
I_L: Current at the upper end of the conductor
$R(0)$: Distance from the lower end of the conductor which is also the origin to the observation point P
$R(L)$: Distance from the upper end of the conductor to the observation point P
c : Speed of light in vacuum
$i\left(0, \tau - \frac{R(o)}{c}\right)$: Current at the time $[\tau - \frac{R(o)}{c}]$ and at the position $z = 0$ on the line
$i\left(L, \tau - \frac{R(o)}{c}\right)$: Current at the time $[\tau - \frac{R(L)}{c}]$ and at the position $z = L$ on the line
$R(\xi)$: Distance from an arbitrary point ξ on the conductor to the observation point P
L : The length of the conductor

From the equations above it can be seen that the fields are functions of the currents at the ends of the conductor.

The model considered is that of fig.1, a single conductor, 30m long, vertically oriented as shown. The travelling current wave assumed is of the form

$i(t) = I_m e^{-\alpha t} sin\omega t$

With

$I_m = 20$ A.

$\alpha = 500000$

$\omega = 2\pi f$

$f = 0.315$ MHz

With this current, equations (3) and (4) can be solved by the following approximation:

$$\int_{-\infty}^{+\infty} e^{\alpha\tau} sin\omega t d\tau = \frac{e^{\alpha\tau}(\alpha sin\omega t - \omega cos\omega t)}{\alpha^2 + \omega^2}$$

$$F_o(t) \approx cI_m\int_0^\tau e^{-\alpha\tau} sin\omega t d\tau \quad (5)$$

$$\approx -\frac{cI_m e^{-\alpha\tau}(\alpha sin\omega t_o + \omega cos\omega t_o)}{\alpha^2 + \omega^2}$$

$$F_L(t) \approx cI_m\int_0^\tau e^{-\alpha\tau} sin\omega t d\tau \quad (6)$$

$$\approx -\frac{cI_m e^{-\alpha\tau}(\alpha sin\omega t_L + \omega cos\omega t_L)}{\alpha^2 + \omega^2}$$

$$t_o = \tau - \frac{R(o)}{c}, t_L = \tau - \frac{R(L)}{c}$$

Equation(1) can be solved by substituting equations (5) and (6). The ground is assumed to have constant constitutive parameters that are frequency-independent and considered to have relative permittivity and permeability of one. This model will be simulated using both the analytical and FDTD methods to validate the developed method.

(b) FDTD Method

The FDTD method is a numerical technique which models transient electromagnetic signal scattering or radiation from objects of arbitrary shapes. The method relies on solving Maxwell's time domain curl equations (7-8) in discrete space and time, where all derivatives are approximated by a central difference equation (9-10).

$$\nabla \times \vec{E} = -\mu\frac{\partial}{\partial t}\vec{H} \quad (7)$$

$$\nabla \times \vec{H} = \sigma\vec{E} + \varepsilon\frac{\partial}{\partial t}\vec{E} \quad (8)$$

$$\frac{\partial F^n(i,j,k)}{\partial x} \approx \frac{F^n\left(i+\frac{1}{2},j,k\right) - F^n\left(i-\frac{1}{2},j,k\right)}{\Delta x} + o(\Delta x^2) \quad (9)$$

$$\frac{\partial F(i,j,k)}{\partial t} \approx \frac{F^{n+1/2}(i,j,k) - F^{n-1/2}(i,j,k)}{\Delta t} + o(\Delta t^2) \quad (10)$$

The computational region of interest is divided into cells with the corresponding electric and magnetic fields being located on the edges and the faces. It may be assumed that all fields in the entire solution region are initially zero. The scattering or radiating objects of interest are defined by specifying the dielectric and magnetic material parameters at the electric and magnetic fields' locations in the FDTD environment. The computational region must be large enough to enclose the objects to be analyzed. Also, suitable boundary conditions on the artificial boundary must be imposed to absorb outgoing waves to simulate the extension of the computational region to infinity [1]. Finally, to ensure the stability of the finite-

difference scheme, the time increment Δt must satisfy the Courant condition [1],

$$\Delta t \leq \frac{1}{v\sqrt{\frac{1}{\Delta x}+\frac{1}{\Delta y}+\frac{1}{\Delta z}}}$$

$v = \sqrt{\mu\varepsilon}$ is the maximum phase velocity in the model; μ and ε are the permeability and permittivity of the medium respectively. Δx ,Δy and Δz are the spatial increments in the x ,y and z directions respectively.
Equations (7-8) can be solved using the approximation in (9-10), for example E_x and H_x components of the field vectors can be obtained as:

$$E_x^{n+1/2}(i, j+1/2, k+1/2) = K_1 E_x^{n-1/2}(i, j+1/2, k+1/2)$$

$$+K_2\left\{\begin{matrix} H_z^n(i, j+1, k+1/2) - H_z^n(i, j, k+1/2) \\ -H_y^n(i, j+1/2, k+1) - H_y^n(i, j+1/2, k)\end{matrix}\right\} \quad (11)$$

$$H_x^{n+1}(i-1/2, j+1, k+1) = H_x^n(i-1/2, j+1, k+1) \quad (12)$$

$$+K_3\left\{\begin{matrix} E_y^{n+1/2}(i-1/2, j+1, k+3/2) - E_y^{n+1/2}(i-1/2, j+1, k+1/2) \\ -E_z^{n+1/2}(i-1/2, j+3/2, k+1) - E_z^{n+1/2}(i-1/2, j+1/2, k+1)\end{matrix}\right\}$$

$$K_1 = \left(\frac{1-\frac{\sigma\Delta t}{2\varepsilon}}{1+\frac{\sigma\Delta t}{2\varepsilon}}\right), \quad K_2 = \frac{\Delta t}{\varepsilon\Delta s}\left(\frac{1}{1+\frac{\sigma\Delta t}{2\varepsilon}}\right), \quad K_3 = \frac{\Delta t}{\mu\Delta s}$$

To model the structure in fig.1, the spatial increments are set as $\Delta x = \Delta y = \Delta z = 0.5m$ and the discrete time step was set at 95% of the courant condition giving $\Delta t = 9.141 \times 10^{-10}$. The perfectly matched layer (PML) absorbing boundary condition [5] is applied to the artificial boundaries to absorb outgoing waves. The method of thin wire representation proposed by Noda [8] was adopted in this paper to model the conductor. The wire radius was set to be 0.025 meters.

(c) Simulation and results

Having specified all the parameters, the model in fig.1 was set up in the FDTD space and simulated. The current is applied at the lower end of the wire as shown. The transient field calculation assumes matching at both ends. Fig. 2 shows the y component of the magnetic fields at a point 10m from the centre of the conductor computed by the FDTD as well as the analytical methods.

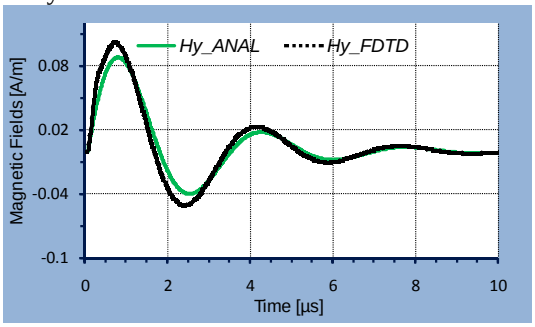

Fig. 2: H_y component of electric field at a point 10m from the centre of 30m long antenna produced by damped sinusoidal wave

Comparing the above result it can be seen that there is a good agreement between the two methods. The difference has been that absorptions at the boundaries are not perfect.

3 Modelling a section of high voltage air-insulated (AIS) substation

High voltage bus-bars in a substation can be modelled by simply specifying their constitutive parameters within the FDTD grid if the length, radius and position above ground are known. The source location representing the current due to switching can then be specified. To model a complete high voltage substation for transient fields simulation using FDTD method however requires specification of all materials with their respective constitutive properties within the computational grid, including joints and bends. Hence as the complexity of the substation increases the programming and computation resources also increase. This may even require a mesh generation algorithm to be employed. For the meantime a simple substation model is considered here for simulation. Typical bus lengths are 20m to 80m long and located 5m to 10m above ground.

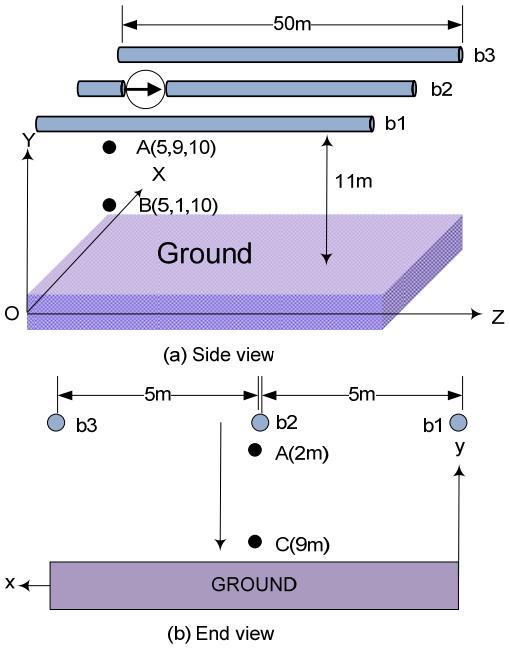

Fig. 3: Simple typical bus section in high voltage substation model

Thus a typical bus section in a substation consisting of three parallel bus-bars; 50 meters long located 11 meters above ground as shown in fig.3.was considered.

Two different ground conditions are considered for this simulation: imperfect ground and a perfectly conducting ground, the conductor radius assumed is 0.05m in both cases. The imperfect ground properties are chosen as follows: relative permittivity of 10, conductivity of 0.01S/m and relative permeability of unity. In both cases a differentiated Gaussian current pulse was used.
The equation of the pulse is:

$I_m \frac{t}{\beta} e^{-\left(\frac{t}{\beta}\right)^2}$

$I_m = 1000$A, the peak magnitude of the current
$\beta = 5 \times 10^{-7}$

The pulse was applied at 10m from one end of the middle conductor as shown fig. 3 and travels in positive z directions thus simulating a typical bus section acting as antenna.

The peak magnitude of the current was chosen as 1000A to emulate a typical high voltage bus current transient due to switching. The spatial increments are chosen as $\Delta x = \Delta y = \Delta z = 0.5m$ and at 95% of the Courant criteria gives $\Delta t = 9.141 \times 10^{-10}$.The computational domain was set as $50 \times 50 \times 130$ cells. The perfectly matched layer absorbing boundary condition was applied as before.
Figures 4 and 5 show the E_x, E_y and E_z components of the electric fields at two locations within the substation: points A 2m below the bus conductors (9m above the ground) and B 10m below the bus conductors (1m above the ground) respectively for imperfect ground conditions. Comparison of these figures reveals that for imperfect ground conditions, electric fields are higher at points close to the switching equipment as expected. It can also be seen that 10m below the bus conductors, E_y fields have reduced by a factor of 0.07 and E_z by a factor of 0.02. E_x is negligible in both cases.

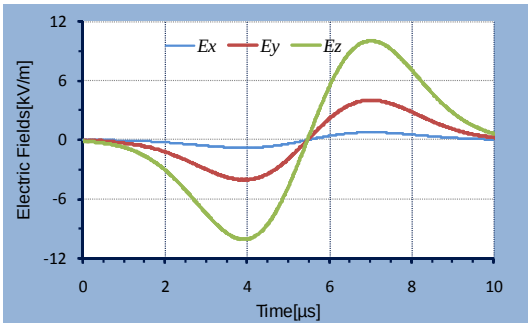

Fig. 4: Electric at point A for imperfect ground conditions

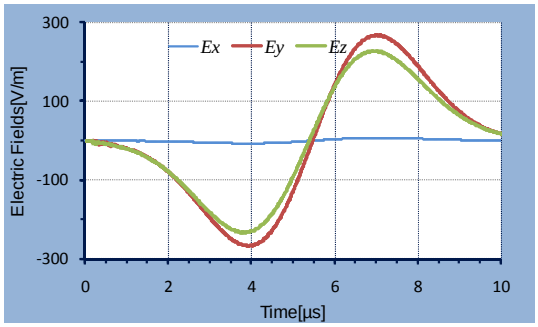

Fig. 5: Electric field at point B for imperfect ground conditions

Fig. 6 shows the electric field components at point B, 10 meters below the bus conductors for perfect ground conditions. Examination of the fig. 7 and fig. 8 shows that at points close to the ground the electric fields are higher with perfect ground than with true ground conditions. Thus perfect ground enhances the fields due to higher reflections as expected.

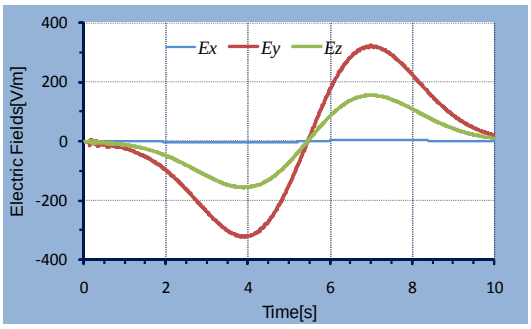

Fig. 6: Electric fields at point B for perfect ground conditions

4 Conclusion

The results presented indicate that within the limit of computer resources, the FDTD method can be used to model and simulate bus-bar structures in high voltage air-insulated substation to predict electromagnetic emissions. The ability of the code to model the effect of imperfect ground conditions has also been presented. Although the model used to test the ability of the developed code is a section of a substation, it has been demonstrated that with additional resources, it would be possible to model a complete high voltage air-insulated substation and predict transient electromagnetic fields emissions.

References

[1] A. Taflove, S. C. Hagness, "Computational Electrodynamics the Finite Difference Time Domain Method" Artech House, 2000
[2] C. Imposimato, J. Hoeffel man, A. Eriksson, W. H. Siew, P. H. Pretorius and P. S. Wong, "EMI characterization of HVAC substations-updated data and influence on immunity assessment", *CIGRE Working Group 36.04(EMC and EMF, General aspects).2002*
[3] C. M. Wiggins, D. E. Thomas, F. S. Nickel, T. M. Salas, and S. E. Wright, "Transient electromagnetic interference in substations," *IEEE Trans. Power Del.*, vol.9, no.4, pp.1869-1878, Oct 1994.
[4] D. E. Thomas, C. M. Wiggins, F. S. Nickel, C. D. Ko and S. E. Wright, "Prediction of electromagnetic field and current transients in power transmission and distribution systems", *IEEE Trans. Power Del*, vol. 4, no.1, Pp 744-754 April 1989.
[5] J. P. Berenger, "A perfectly matched layer *Journ. Comp. Phy.*, vol. 114, no.2, pp 185-200, Oct. 1994.
[6] M. A. Uman, D. K. McLain and E. P. Krider, "The electromagnetic radiation from a finite antenna", *Am. Journ. Phys.*, vol. 43, pp. 33-38, 1975
[7] R. S. Shi, J. C. Sabonadare and D. A. Dacherif "Computation of transient electromagnetic fields radiated by a transmission line: An exact model", *IEEE Trans. Magn.* vol.31, no.4, pp 2423-2431, July 1995.
[8] T. Noda, S. Yokoyama, "Thin wire representation in finite difference time domain surge simulation," *IEEE Trans. Power Del.*, vol.17, no.3, pp. 840-847, Jul.

IMPROVED TECHNIQUE FOR LOCATING INSULATION DEFECTS IN HIGH VOLTAGE EQUIPMENT

T. Pinpart*, M.D. Judd

Institute for Energy and Environment, Department of Electronic and Electrical Engineering
University of Strathclyde, Royal College, Glasgow, G1 1XW, UK
*Corresponding author. Email: tanya.pinpart@eee.strath.ac.uk

Keywords: Ultra high frequency (UHF), Partial discharge, Arrival time, Relative increase in energy

Abstract

Accurately locating insulation defects of high voltage equipment is valuable for maintenance and repair purposes. A triangulation method is used based on arrival times of signal outputs from four UHF sensors installed at different positions on the tank. In this work, an improved technique for accurately determining arrival times obtained from the ultra high frequency (UHF) technique is investigated. Determining arrival times accurately depends on waveform characteristic, which is influenced by three factors, i.e., shape of the PD current pulse, internal propagation path, and background noise. Two methods (i.e., knee point of cumulative energy curve and threshold-crossing of signal power waveform) have been applied with reasonable success for partial discharge (PD) location. The first method deals with signal and background noise energies, while the second method deals with signal and noise powers. The improved technique combines cumulative energies, background noise energies and threshold crossing. It considers the relative increase in energy between successive samples of the digitised signal. The result from this method is more promising than ones from the others and may be suitable for an automated system. Moreover, this method has a potential for applying to other PD detection systems that detect transient signals such as acoustic system.

1 Introduction

High voltage equipment is always distributed among any parts of power systems. For example, power transformers and high voltage cables can be commonly found in substations. They are very important for energy transferred. If only one component has a failure, both utilities and their customers can encounter major problems such as outages, high-cost maintenance and repair.

One measure of maintenance procedures, which is to prevent the eventual breakdown of high voltage equipment, is the PD measurement. PD can be a warning sign of insulation defects, which might lead to final breakdown of the equipment. Many PD detection systems have now been implemented in practical fields such as UHF, acoustic, electrical methods, etc. In addition, analysis techniques are available such as a triangulation method for locating insulation defects, wavelet transform for signal de-noising, phase resolved measurement, etc.

In this work, determining the onset of PD signal, called the arrival time (T), is investigated because insulation defect positions are located based on arrival times of signal outputs from four UHF sensors installed at different positions on the tank. Determining arrival times accurately depends on waveform characteristics, which are influenced by three key factors, i.e., shape of the PD current pulse, internal propagation path, and background noise. Two methods are now available for determining arrival times of PD signals obtained from the UHF detection, which are a knee point of cumulative energy curve and a threshold crossing of signal power waveform [1]-[2]. The first method deals with signal and background noise energies and arrival times are judged by the observation. The second method deals with signal and noise powers and arrival times are determined by certain amount of the signal power waveform such as 2 %, which is selected based on practical experiences.

Although these two methods provide reasonable successes, they are ambiguous in that how knee point can be determined and what power percentage should be selected, for the first and second methods respectively. Therefore, an improved technique is introduced, which combines cumulative energies, background noise energies and threshold crossing. It considers the relative increase in energy between successive samples of the digitised signal. By using four sets of signals obtained from pulse injection tests for a power transformer, the results (arrival times) from the improved technique are more promising than ones from the others. This could be highly beneficial to accurately determining insulation defect locations in high voltage equipment.

2 Pulse injection tests for PD location

A typical UHF monitoring system for PD locations is composed of at least three UHF sensors installed on the tank in different positions as seen one example in Figure 1 [2].

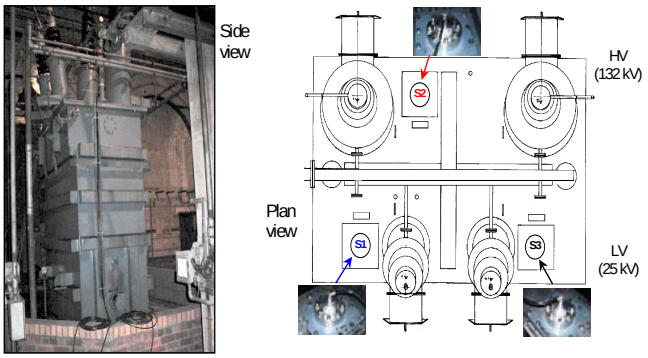

Figure 1 UHF sensors installation at the top of an 18 MVA single phase transformer.

In this work, signals to be analysed were obtained from pulse injection tests on a 252 power transformer (5.9x2.7x4.0 m.), which a PD source position was known. Experimental set up was made up of four UHF sensors (S1, S2, S3, and S4) installed and a digital oscilloscope, a sampling rate of 5 GS/s. Table 1 illustrates positions of four UHF sensors in 3D Cartesian system. Figure 2 also illustrates UHF waveforms, where a 100V impulse was injected into S4 and no amplifiers were used on the detected UHF signals.

Items	Coordinate x,y,z (m)
S1	5.9,1.9,0.5
S2	5.8,0.0,3.5
S3	0.0,0.2,3.6
S4	2.8,2.6,3.5

Table 1 Coordinates of UHF sensors.

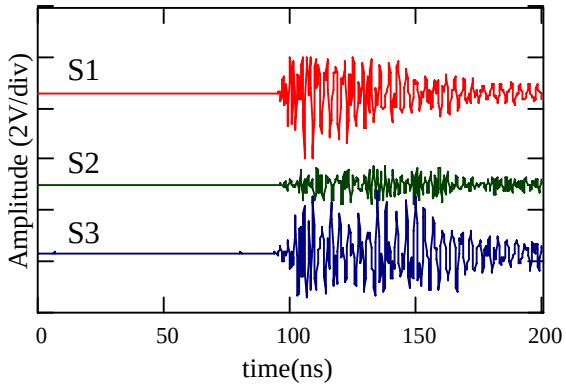

Figure 2 UHF waveforms obtained from the pulse injection test, the impulse injected into S4.

An advanced mathematical model [2] was created from internal components of the power transformer, such as main components inside the tank (i.e., windings, cores, yokes), material properties, coordinates of sensor and PD source positions, and combined with a theory of electrometric wave. It was used to simulate and determine time differences (ΔT_{ij}) between three pairs of signal outputs, such as ΔT_{12}, ΔT_{23}, ΔT_{31} for signals displayed in Figure 2.

Time differences obtained from this model provide high accuracy enough to be references because they are calculated based on propagation theory for one known source location. Based on the mathematical model described above, three internal propagation paths, when the impulse was injected into S4 while S1, S2 and S3 captured radiated signals, can be demonstrated in Figure 3. In addition, all time differences are shown in Table 2.

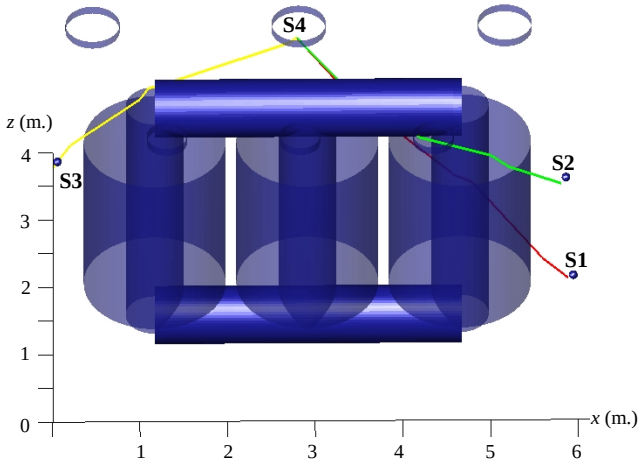

Figure 3 Internal propagation paths when the impulse was injected into S4.

Impulse injected into	Time differences ΔT_{ij} (ns)		
	ΔT_{12}	ΔT_{23}	ΔT_{31}
S4	1.5	1.7	-3.2
	ΔT_{12}	ΔT_{24}	ΔT_{41}
S3	7.3	10.3	-17.6
	ΔT_{13}	ΔT_{34}	ΔT_{41}
S2	-11.3	8.6	2.7
	ΔT_{23}	ΔT_{34}	ΔT_{42}
S1	-18.6	14.4	4.2

Table 2 Time differences when the impulse was injected into each of the four sensors.

3 Factors affect measured PD waveform

To locate insulation defects using the triangulation method, it is necessary to accurately determine the arrival times of the signals at two or more sensors and calculate time differences between them for determining defect positions. Accurately determining the arrival time depends on the PD waveform, which is influenced by various factors, i.e., shape of the PD current pulse, internal propagation path, background noise, measurement bandwidth, and sensor response time [3]. They can cause some difficulties for determining the exact arrival times. Only the first three factors are considered in this work because the last two can be controlled by the measurement system.

(i) Shape of the PD current pulse
Rise time of the PD current pulse has the significance on the radiated electric field, which is proportional to the rate of change of current. When the rise time is slow, this will make a difficulty to determine the arrival time.

(ii) Internal propagation path
The radiated electric field is distorted when travels along a tank because of material properties installed inside the tank such as insulators, windings, iron cores, etc. This tends to disperse the wavefront of the measured PD signal.

(iii) Background noise
This factor occurs because noise can contribute into the system such as communication noise interference, operation of switching devices, etc.

4 Improved technique for locating insulation defects

Presently, two methods for determining arrival times are (i) knee point of cumulative energy curve and (ii) threshold-crossing of signal power waveform. Both provide reasonable success in many practical applications

An improved technique for accurately determining arrival times will now be described. It combines cumulative and background noise energies. The concept is composed of two main equations. The first equation is defined as:

$$e_i = e_{i-1} + \frac{\Delta t}{R} \cdot V_i^2 \qquad (1)$$

where the initial energy level e_0 is set to zero,

- e_i = the energy accumulated up to the i-th sample
- V_i = sampled UHF voltage waveform at i-th sample
- Δt = 1/sampling rate
- R = input impedance of the measurement system (50Ω)

$$R_{iEj} = \left(\frac{e_j}{e_{j-1}} - 1 \right) \qquad (2)$$

Where

- R_{iEj} = relative increase in energy between successive samples of the digitised signal
- j starts from τ, where τ is time delay (e.g. 10% of sample number N, therefore $\tau = 0.1N$)

j starts from τN because e_i values at the beginning of the PD waveform are very small, causing numerical instability. Therefore, to avoid the uncertainty of this kind of behaviour, equation (2) would start calculating after a certain time delay.

By using equation (1) and (2), it is easy to identify time interval containing the arrival time. The arrival time is the point when the first obvious peak from R_{iEj} appears.

5 Results and discussion

After applying equation (1) and (2), e_i and R_{iEj} of each signal can be displayed as one set shown in Figure 4. This figure shows R_{iEj}(solid lines) and e_i(dotted lines) resulted from one set that the impulse was injected into S4. Three arrival times can be sorted out based on the first obvious peaks of each sensor output, which are 95.8,95.4 and 94.0ns, for S1, S2 and S3, respectively. The results yielded so far are based on a clear arrival time interval. Compared with knee points of cumulative energy curves, the arrival times located from the improved technique can be easily seen.

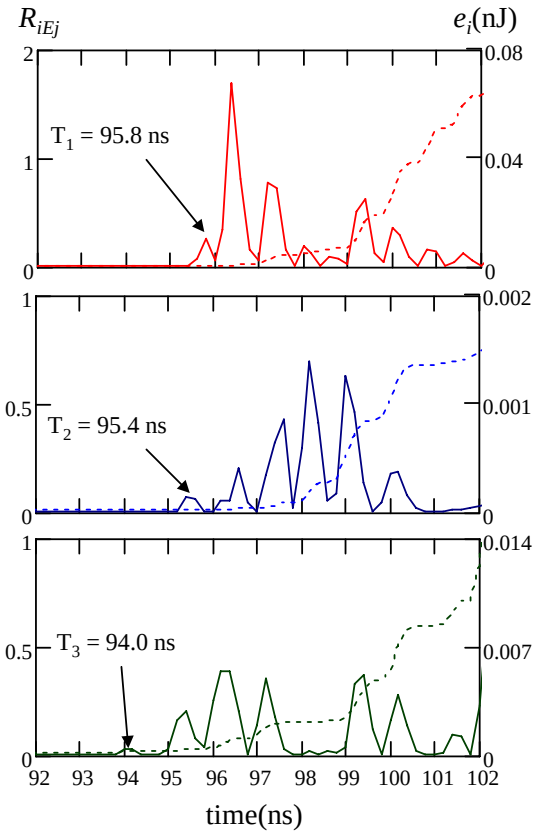

Figure 4 Arrival times determined by R_{iEj}(solid lines) and cumulative energy curves (e_i) are dotted lines, the impulse injected into S4.

Locating PD sources in power transformers by using the triangulation method is ideally based on arrival times of four UHF sensors installed at the different position in the tank. Therefore, in order to evaluate the ability of the improved technique, time differences obtained from the two-percent threshold crossing (2% TH) of signal power waveforms were used to compare based on time differences shown in Table 2, which were used as references. Table 3 illustrates time differences obtained from the reference, improved, and 2% threshold crossing methods. Table 4 summarises error comparisons.

Impulse injected at		Time differences ΔT_{ij} (ns)		
S4		ΔT_{12}	ΔT_{23}	ΔT_{31}
	Reference	1.5	1.7	-3.2
	Improved	0.4	1.4	-1.8
	2% TH	-1.0	-1.0	2.0
S3		ΔT_{12}	ΔT_{24}	ΔT_{41}
	Reference	7.3	10.3	-17.6
	Improved	6.2	10.8	-17.0
	2% TH	16.8	7.2	-24.0
S2		ΔT_{13}	ΔT_{34}	ΔT_{41}
	Reference	-11.3	8.6	2.7
	Improved	-9.2	7.2	2.0
	2% TH	-11.2	6.2	5.0
S1		ΔT_{23}	ΔT_{34}	ΔT_{42}
	Reference	-18.6	14.4	4.2
	Improved	-19.6	14.8	4.8
	2% TH	-27.2	24.8	2.4

Table 3 Time differences calculated from 3 methods

Impulse injected at		Error (ns)			±Mean(ns)
S4		ΔT_{12}	ΔT_{23}	ΔT_{31}	
	Improved	1.1	0.3	-1.4	0.9
	2% TH	2.5	2.7	-5.2	3.5
S3		ΔT_{12}	ΔT_{24}	ΔT_{41}	
	Improved	1.1	-0.5	-0.6	0.7
	2% TH	-9.5	3.1	6.4	6.3
S2		ΔT_{13}	ΔT_{34}	ΔT_{41}	
	Improved	-2.1	1.4	0.7	1.4
	2% TH	-0.1	2.4	-2.3	1.6
S1		ΔT_{23}	ΔT_{34}	ΔT_{42}	
	Improved	1.0	-0.4	-0.6	0.7
	2% TH	8.6	-10.4	1.8	6.9
Average mean error of Improved (ns)					0.93
Average mean error of 2% TH (ns)					4.58

Table 4 Error comparisons

Results show that all values of mean error obtained from the improved technique are less than ones obtained from the two-percent threshold crossing method. The average value of mean error from the improved method is less than one from the threshold method significantly, which are 0.93 and 4.58 ns, respectively. These can trace back to mean error of distances for PD location, that is, 0.19 and 0.92 m, for the improved and threshold crossing methods, respectively. These are based on a propagation velocity of $2x10^8 ms^{-1}$ for UHF signals in transformer oil.

6 Conclusions and future work

The improved concept for determining arrival times accurately, which affects PD locations in high voltage equipments, is introduced and investigated using four sets of signals obtained from pulse injection tests on a full-scale power transformer. Although these promising results were based on a single experiment, its ability for accurately determining the arrival times seems better than the two-percent threshold crossing method, which has been normally applied to practical applications and provides reasonable success. The improved technique could also apply windowing and thresholding for automated systems of UHF PD locations.

Moreover, by using the improved technique, it could be beneficial to time offset compensation when a large quantity of PD signals is measured, before these signals will be analysed by traditional methods such as phase resolved measurement, etc. In addition, not only the improved technique can apply for determining the arrival times of UHF PD signals, but may also be useful for other PD detection systems that detect transient signals such as acoustic.

Future work will focus on three possibilities, which are (i) the validity of the improved technique based on both experimental and high voltage practical tests, (ii) the development of automated system for determining arrival times, and (iii) time offset compensation.

References

[1] M. D. Judd, L. Yang and I. B. B. Hunter., "Partial discharge monitoring for power transformers using UHF sensors Part 1: Sensors and Signal Interpretation", IEEE Electr. Insul. Mag., **21**, 2, pp 5-14, (2005)

[2] M. D. Judd, L. Yang and I. B. B. Hunter. "Partial discharge monitoring for power transformers using UHF sensors Part 2: Field experience", IEEE Electr. Insul. Mag., **21**, 3, pp. 5-13 (2005)

[3] P. J.G. Orr, A.J. Reid, and M.D. Judd. "Sensor response characteristics for UHF location of PD sources", International Conference on Condition Monitoring and Diagnosis (CMD 2008), pp. 1119-1122, (2008)

Dispersion, rheology and electrical properties of Poly(ethylene oxide) / Montmorillonite nanocomposites

M.D. Reading*†, A.S. Vaughan*

* School of Electronics and Computer Science, University of Southampton, Highfield, Southampton, SO17 1BJ, UK
† Author for correspondence: mdr06r@ecs.soton.ac.uk

Keywords: Rheology, poly(ethylene oxide), montmorillonite, dispersion, dielectric.

Abstract

The rheological behaviour of a range of systems containing various levels of MMT have been studied to produce materials with different shear histories and different degrees of MMT dispersion and to explore rheological response as a practical means of determining the dispersion state of a nanofiller in a liquid. This would have great practical utility as a quality control device in, for example, the production of epoxy-based nanodielectrics. The AC ramp electrical breakdown strength and dielectric response of the resulting samples were analysed. This paper investigates the effect of MMT loading and shear history on structural evolution, dielectric response and breakdown beahaviour in PEO.

1 Introduction

The topic of nanodielectrics is one that has grown enormously in importance since Lewis first introduced the concept of a nanodielectric in 1994. In the modern day, nanodielectrics are still very much of interest in both research and industry. In such composite systems, properties are strongly influenced by the dispersion of the nanophase within the matrix, and therefore it is imperative that reliable methods are available for the cost-effective determination of the dispersion state of the nanofiller in the host polymeric matrix.

Polyethylene oxide (PEO) is a water-soluble polymer that is technologically used as an electrolyte solvent in lithium polymer cells, but is more widely used as a model system to observe filler effects. This paper details an investigation into the dispersion, rheology and electrical properties of polyethylene oxide / montmorillonite composites. Three different molecular weight PEOs were used - 100,000 g mol^{-1}, 400,000 g mol^{-1} and 1,000,000 g mol^{-1}, and aluminium pillared montmorillonite (MMT) was chosen as the filler. This non-functionalised MMT is a polar material and is therefore relatively compatible with aqueous systems.

With the general properties of polyethylene being far superior to those of poly(ethylene oxide) it possibly seems an odd choice to perform these experiments on a PEO system. However when creating a polyethylene-MMT composite, due to its hydrophobic properties, requires a compatibiliser, as shown in Figure 1 below. Our aim to create a system with the maximum possible dispersion state would be far easier and less complicated without a compatibiliser. By using PEO and MMT, which are hydrophobic, no compatibiliser is needed and a high level of dispersion should be achieveable.

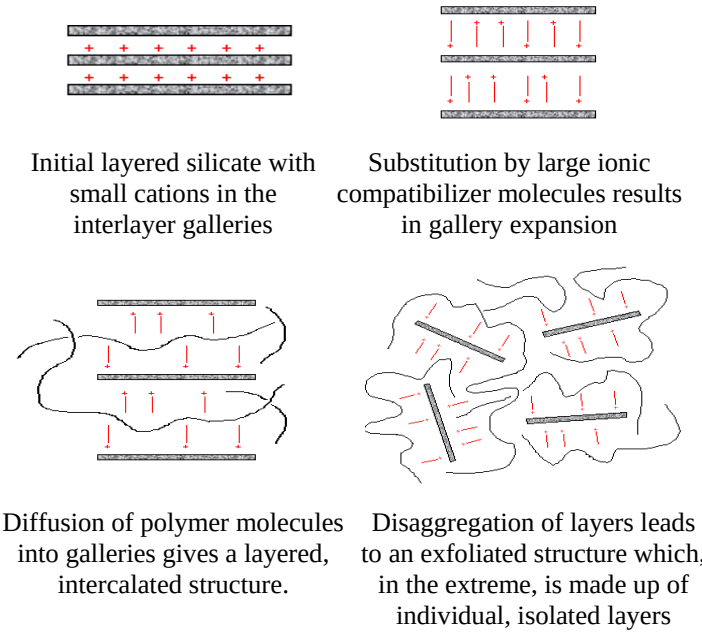

Figure 1: PE-MMT requires a compatibiliser to disperse into an exfoliated structure, unlike PEO-MMT. [2]

2 Experimental

The main aim of rheometry is to characterise fluid or solid properties when dealing with a system containing a number of components. However it has also been known to aid in mixing as well as providing the afore-mentioned data [4,5]. The rheometer used here was a RHEOLAB MC1 Paar Physica. The PEO was supplied by Sigma-Aldrich, as was the MMT, both in granular form. Samples were mixed in glass flasks with 20 ml of distilled water added. PEO was added by a weight-weight ratio in accordance with Table 1. For some samples, MMT was then weighed and added in a weight-weight ratio relative to the PEO present. Initial hand mixing provided basic dispersion.

For higher molecular weight solutions a longer mixing time was required before the solution was visually dispersed. To counter any water lost through evaporation, the flask's total weight was recorded and checked, with addition of distilled water when necessary.

Sample Name	Molecular Weight PEO / g mol^{-1}	X% PEO to DW		% MMT Filler to PEO and Weight	
100k "X" pc 400k "X" pc 1M "X" pc	100,000 400,000 1,000,000	1% 2% 5% 10%	0.2g 0.4g 1.0g 2.0g	-	
A "X" 5 B "X" 5 C "X" 5	100,000 400,000 1,000,000	1% 2% 5% 10%	0.2g 0.4g 1.0g 2.0g	5%	0.01g 0.02g 0.05g 0.1g
A "X" 10 B "X" 10 C "X" 10	100,000 400,000 1,000,000	1% 2% 5% 10%	0.2g 0.4g 1.0g 2.0g	10%	0.02g 0.04g 0.1g 0.2g

Table 1: Samples generated and tested

In addition to providing rheological data, the rheometer should help to break up any agglomeration within the solution and provide good dispersion of the final system. The rheometer used in this investigation is based on a spinning cylinder and a rheometer cup, designed to measure the torque acting on the cylinder as a result of the viscosity of the solution in the cup. The solution is poured into the cup around the centre pillar, then the cylinder is lowered into the mixture and the complete assembly is attached to the rheometer prior to testing. The Physica Rheologic RS 100 software package was used and allows for instrument control, data collection and analysis.

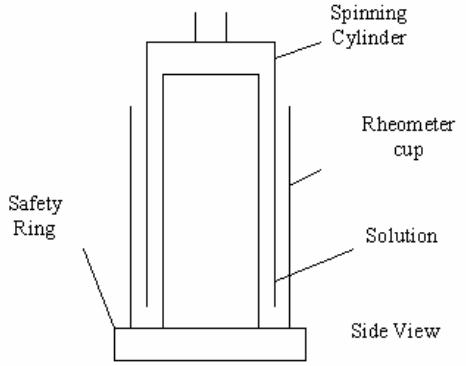

Figure 2 : Diagram of Rheolab Paar Physica cup-bob rheometer

A four process system was defined to provide data on each sample; initial hand mixing followed by the three processes outlined in Figure 3. Process 0 - hand mixing. Process 1 - shear stress as a linear ramp rate, 30 points taken from 0.1-60 Pa. Process 2 - shear stress held at a constant 60 Pa, 30 points recorded. Process 3 - shear stress as a linear ramp rate, 30 points taken from 60-0.1 Pa. Samples were tested three times each, subsequently providing 3 ramp up, ramp down and holding data sets.

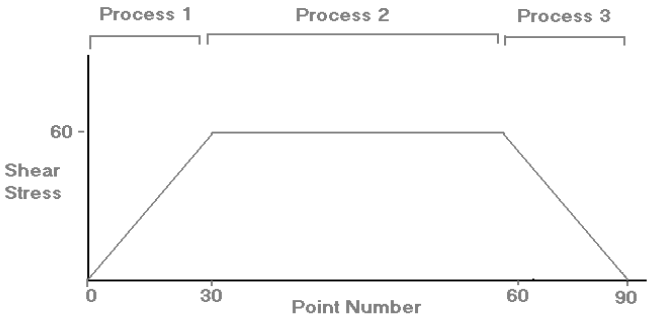

Figure 3 : After hand mixing, each run is comprised of the above three processes

Process one provides rheological characterisation of the initial dispersed system. Process two then holds the system at a fixed shear stress and should achieve further dispersion followed by a ramp down as process three. If any additional dispersion has been achieved by the rheometer it should be apparent during process three.

For AC breakdown strength tests, thin air-free discs were required, therefore all samples were de-gassed in a vacuum oven held at 80 ^{0}C. This process worked well for the 1,000,000 g mol^{-1} and 400,000 g mol^{-1} PEO systems, the 100,000 g mol^{-1} samples appeared to undergo a thermal aging process before the air was successfully removed. The behaviour of this aged PEO will be reported elsewhere. A Grazeby Spec-ac press was then used to press samples to a thickness of around 100 μm. For most polymers this process simply involves melting the sample within a press, pressing the sample to the desired thickness, followed by quenching the sample in cold water. However the solubility of PEO meant that this quenching method could not be used. Instead, quenching was achieved using a separate chilled press that the sample was placed into straight from the hot press. After initial tests this proved quite effective.

8-12 discs were produced for each sample, with 5 breakdown sites designated for each, providing a healthy population for analysis. In the test cell silicone oil was used to cover the sample and lower electrode. The two electrodes were 6.3 mm steel ball bearings and were changed after every other sample. The equipment was calibrated to ensure the AC ramp rate was linear. A 2 parameter weibull equation with likelihood confidence bounds was used to analyse the data.

For dielectric spectroscopy tests thicker discs were produced, using the same method as above, of around 400 μm. These samples were gold coated to provide a better contact for the electrodes using a gold sputter coater. Both sides of the samples were coated, leaving a ring of uncoated sample at the edge to avoid pure conduction across the electrodes. The data obtained was used to generate graphs of relative real permittivity and loss tan delta against frequency. Cole-Cole plots were also generated. For permittivity values a background scan was subtracted from the raw data to remove any contributions from the cables or the measurement cell itself.

3 Results

Data collected show expected shear rate-shear stress curves. Lower percentages of PEO to distilled water start by showing a linear dependence, before shear thinning occurs. However, data from the lowest percentage solutions have emphasised the limitations of the rheometry system. Guidelines for the Rheolab equipment state that the maximum shear rate for high accuracy data is around 4000 s^{-1}, while the data collected here suggests the limitation is around 5000 s^{-1} before data collection fails. The reliability of data between 4000 s^{-1} and 5000 s^{-1} may therefore not be as high. Guidelines for the Rheolab apparatus express an accuracy of 1% maximum values with shear rates between 1 and 4000 s^{-1} and shear stresses equally accurate at 0-67 Pa. For accuracy, samples with large portions of the data falling outside the recommended region were discounted (A15/A25/A110/A210/ B110).

After the first set of three processes described previously, plotting shear stress against shear rate demonstrated the repeatability of the data. Sequential testing, with and without delays, suggested good precision with majority of variations not exceeding 5%. This repeatability suggests that any history effects that may alter the rheometry data are either very small or only take effect after excessive previous testing. Nevertheless, on the first experiment for each set of data the ramp up and ramp down did not overlap. Ramp down shear stress values were around 8% higher than ramp up values. Similar effects have previously been reported by Daga et al. [1] when testing laponite filled PEO solutions and they deemed the variation to be due to shear re-dispersion. For this investigation the variation only occurs in the first set of data and is thus not assumed to be repeating re-arrangement, but instead, a single re-distribution with the achievement of further dispersion during processes one and two leading to a maximum level of dispersion for following tests.

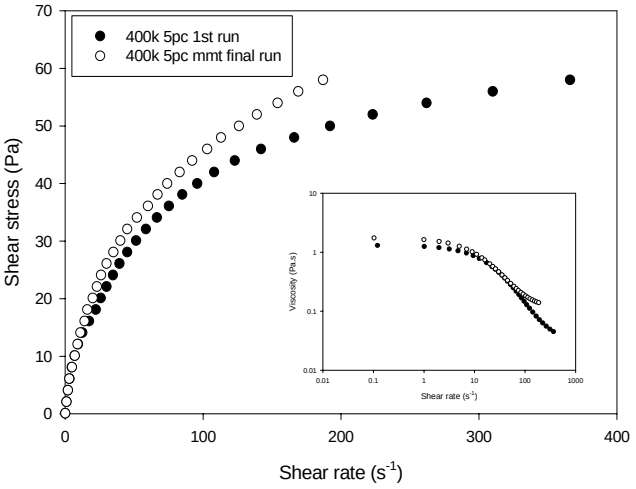

Figure 4 : Example of shear stress – shear rate curve with achievement of further dispersion after rheology

Several models were fitted to the shear rate- shear stress data obtained, the Ostwald-de Waele model (equation 1) and a simple 3 parameter hyperbolic (equation 2).

$$\tau = K \times \dot{\gamma}^{n_o} \qquad (1)$$

Here, τ represents shear stress, γ represents shear rate, K is a parameter related to viscosity (larger K represents higher viscosity) and n_o is a parameter defining the measure of distortion from a Newtonian fluid. Although previous work by Lewandowska [3] showed that data on polyacrylamide followed the power law, results from this investigation, along with calculated residuals, showed the Ostwald-de Waele equation to be a poor fit to data.

$$\tau = \frac{a\dot{\gamma}}{b + \dot{\gamma}} + c\dot{\gamma} \qquad (2)$$

The above 3 parameter hyperbolic function provided a much better fit for all samples, as shown in Figure 5, with much smaller residuals. This function was therefore differentiated to calculate viscosity data for samples

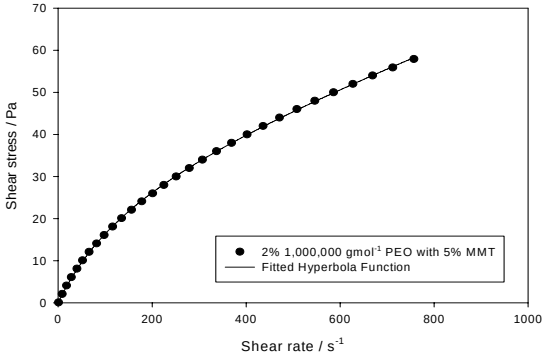

Figure 5 : The 3 parameter hyperbolic provided a very good fit to data

Comparing calculated viscosity data with increasing MMT loading showed little to no apparent change. The MMT is therefore deemed to be dispersed enough to not affect the mobility within the system.

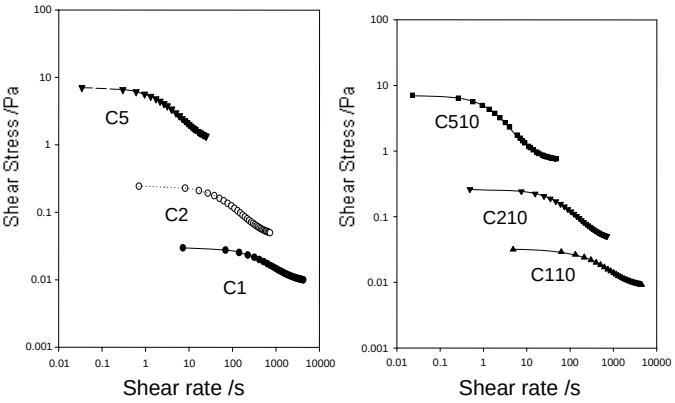

Figure 6 : Comparing samples with 0%, 5% and 10% MMT loading showed little effect on the viscosity

The increasing viscosity with molecular weight is as expected; work by Lewandowska [3] suggested that as molecular weight is increased, an increased entanglement of chains leads to a higher viscosity and a broadening of the shear thinning region. With no apparent effect on flow properties, addition of MMT may still affect the electrical properties of the composite. A Reliasoft Weibull program was used and the beta value for all samples was higher than 10. Comparison of filled and unfilled samples again showed little to no change.

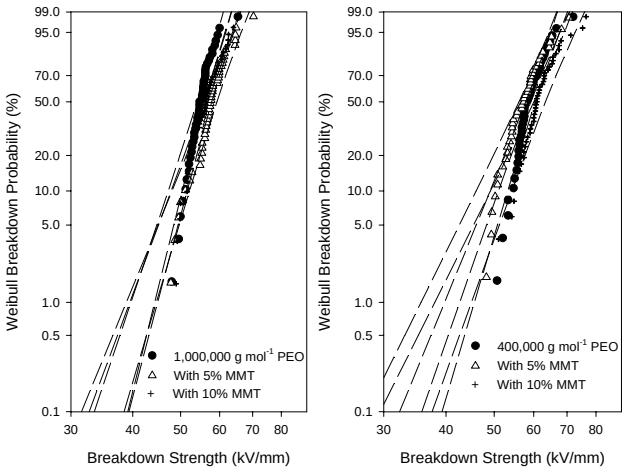

Figure 7 : Little change was observed with addition of MMT to either 1,000,000 g mol^{-1}(left) or 400,000 g mol^{-1} (right)

Despite observing no MMT effect in the breakdown data, it was hopeful that the MMT would perhaps affect the disc electrically as a whole, more than at specific points. The dielectric spectroscopy data showed a huge difference with addition of MMT. Figure 8 shows that the MMT has caused a shift in relaxations or possibly addition of a further relaxation. Also the inset shows a huge increase in real relative permittivity at low frequencies.

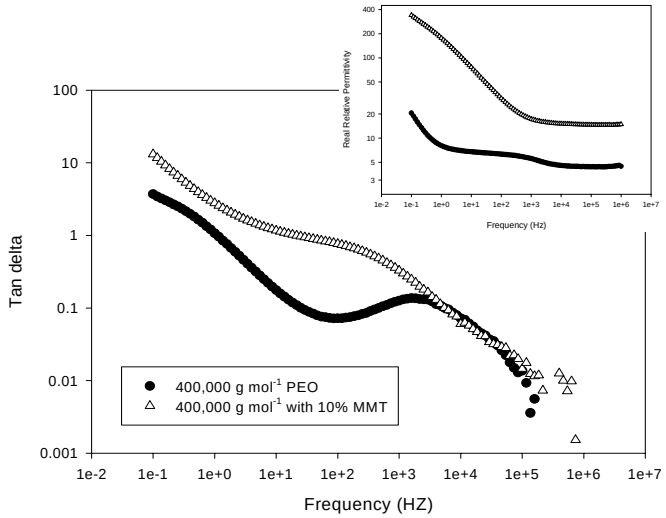

Figure 8 : Addition of MMT causes large changes in the dielectric properties when compared to unfilled samples

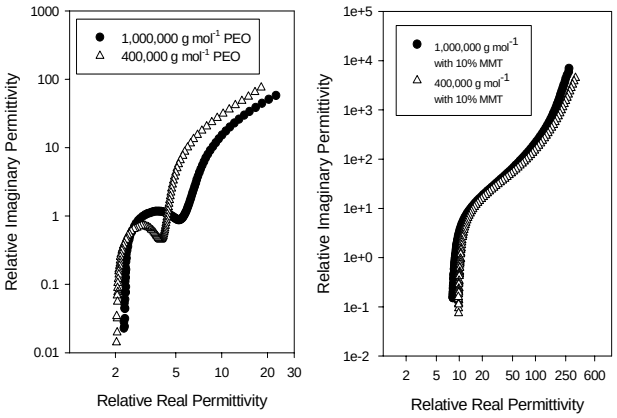

Figure 9 : Cole-Cole plots for unfilled samples (left) and MMT filled samples (right)

From the above Cole-Cole plots it is possibly suggested that the unfilled samples display a single relaxation followed by conduction. Whereas the MMT samples display two relaxations followed by conduction. However, the MMT could be shifting a relaxation rather than generating a new one. To confirm this more data and analysis are needed.

4 Conclusions

Rheology has been shown as an acceptable method for analysis of dispersion and is also seen to improve the dispersion within the system. Addition of MMT is seen to cause little change to physical flow or AC breakdown properties. This corresponds with work by Vaughan et al. [4] into the breakdown strength of PE-MMT samples with regard to dispersion. They found that poor dispersion caused a severe decrease in breakdown strength, while good dispersion caused almost no decrease. This suggests that in our PEO-MMT system, good dispersion has been achieved. Dielectrically however, a huge response was observed with addition of MMT causing either, addition of a relaxation process, or a shift to the relaxations present.

References

[1] V. K. Daga, N. J. Wagner, "Linear viscoelastic master curves of neat and laponite-filled poly(ethylene oxide)-water solutions", *Rheologica Acta*, **volume** 45, no. 6, pp. 813-824, (2006)

[2] C. Green, A. S. Vaughan, "Nanodielectrics – How much do we really understand?", *IEEE Mag.,* **volume** 24, issue 4, pp. 6-16, (2008)

[3] K. Lewandowska, "Comparative studies of rheological properties of polyacrylamide and partially hydrolyzed polyacrylamide solutions", *J. App. Poly. Sci.,* **volume** 103, issue 4, pp. 2235-2241, (2006)

[4] A. S. Vaughan, S. G. Swingler, Y. Zhang. "Polyethylene Nanodielectrics: The influence of nanoclays on structure formation and dielectric breakdown", *IEEJ Trans. FM,* **volume** 126, issue 11, pp. 1057-1063

THE EFFECTIVENESS OF FDTD MODELLING FOR REFINEMENT OF UHF PD SENSOR RESPONSE CHARACTERISTICS

A. J. Reid*, M. Stewart and M. D. Judd

University of Strathclyde
204 George St., Glasgow, G1 1XW, UK
*alistair.reid@eee.strath.ac.uk

Keywords: Partial discharge, FDTD modelling, UHF couplers, condition monitoring

Abstract

This paper explores the effectiveness of the Finite Difference Time Domain (FDTD) numerical modelling technique as a tool to aid in the design and optimisation of ultra high frequency (UHF) partial discharge (PD) couplers. The responses of two common UHF sensors – a monopole and a planar logarithmic spiral – to a step electric field have been obtained both empirically, using a gigahertz transverse electromagnetic test cell, and through software modelling by means of the FDTD technique. Results indicate that FDTD modelling can achieve sufficiently accurate prediction of UHF partial discharge sensor response provided specific environmental electromagnetic conditions are met and the model geometry is an acceptable trade-off between accuracy and simulation time.

1 Introduction

PD measurement is a well established condition monitoring technique used to detect incipient defects on strategically important electrical distribution plant such as power transformers and gas insulated substations (GIS). The UHF PD measurement technique has gained increasing popularity in recent decades due to its high sensitivity, noise immunity and the ability to install on-line monitoring systems to in-service plant. Much research has been carried out into the UHF technique over the past 25 years [1-7]. One of the key aspects of this research involves the design of UHF couplers, or antennas, to measure the radiated electromagnetic pulse emanating from the discharge site.

Although conventional antenna design theory can be viewed as a good starting point, it is not generally applicable to the design of UHF PD sensors. Due to the presence of conducting metalwork in the near field region, any derived or expected far field quantities and radiation patterns are subject to severe distortion and attenuation, greatly reducing confidence in the design. Hence, optimisation of UHF sensors is often a lengthy process involving empirical measurements and extensive refinement of design parameters.

This paper explores whether a software-based approach to UHF coupler optimisation at the design stage could provide a realistic prediction of coupler behaviour, streamlining the overall design process by reducing the need for physical construction and testing.

1.1 GTEM Calibration Cell

The frequency response of a UHF coupler can be obtained by swept-frequency methods, which can be cumbersome and costly at higher frequencies, or alternatively by using fast transient techniques. Transient calibration is achieved by injecting a step electric field, Fig. 1, into a tapered GigaHertz transverse electromagnetic (GTEM) cell onto which a UHF sensor is installed. The sensor's response to the planar electric field can then be compared to that of a reference probe with a known frequency response. Further details of the transient calibration system developed at Strathclyde are given in [8, 9]. UHF field conditions at the measurement point are designed to mimic those found at the tank wall in a transformer or GIS, the direction of travel of the TEM wave being orthogonal to the sensor's central axis.

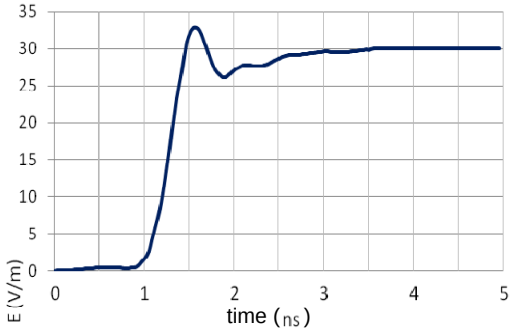

Figure 1: Step electric field applied to the UHF couplers under test for both laboratory based calibration and FDTD simulations.

1.2 FDTD Modelling

This method was first proposed by K. Yee [10]. The phrase 'Finite Difference Time Domain' and the acronym 'FDTD' were later coined by Taflove et al. [11]. The technique is based on decomposing a volume into a discrete grid of equal cells, or 'voxels', and solving Maxwell's field equations for each cell. Maxwell's equations show that the time derivative

of the change in the *E* field is dependent on the change in the *H* field across space. The solutions to these are then computed in a discrete time step manner. For the work reported here, the commercial package SEMCAD X was used.

To reduce simulation time, the model consists of a simple 500 mm x 500 mm ground plane of thickness 1 mm on which the sensor model is constructed, with the planar electric field being provided by a rectangular 300 mm x 100 mm waveguide source, as shown in Fig. 2. A short 50 Ω coaxial transmission line is connected to the base of each sensor and the voltage waveform extracted using a 50 Ω lumped element at the end of the transmission line between the two conductors. The dimensions of the line were calculated using the following equation, which relates characteristic impedance to the radii of the inner and outer conductors

$$Z_0 = \frac{138}{\sqrt{\varepsilon_r}} \log \frac{b}{a} \qquad (1)$$

where ε_r is the relative permittivity of the dielectric (PTFE), b is the radius of the outer conductor and a is the radius of the inner conductor. The FDTD model attempts to replicate field conditions in the calibration GTEM cell. The field orientation and direction of the plane wave relative to the sensor are identical in both cases. While simplification of the calibration cell's geometric structure reduces simulation time, it is noted that the use of an open waveguide source introduces finite dispersion of the electric field, affecting the model's accuracy to some extent. This is, however, deemed an acceptable compromise at this stage.

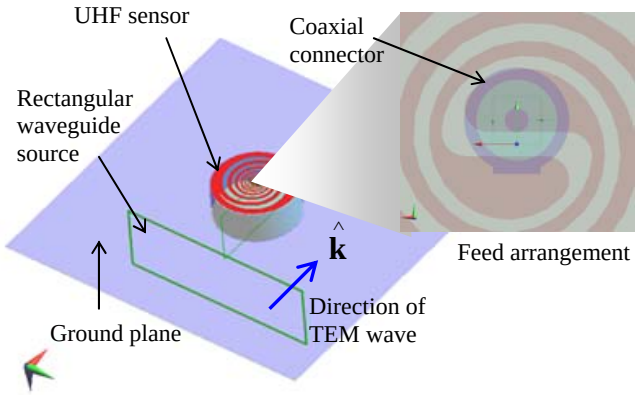

Figure 2: Example of simulation geometry for cavity-backed planar spiral sensor. The sensor under test is situated on a ground plane and subjected to a step electric field (Fig. 1) produced by a rectangular waveguide source.

2 Results

2.1 Monopole

The monopole is one of the simplest UHF sensors and also one of the most sensitive. However, a monopole is not used for PD detection in GIS since it effectively forms a sharp protrusion and may increase the likelihood of PD or breakdown in the system. Planar sensors are therefore favoured even though their sensitivity is usually lower. Monopole sensors are occasionally used on UHF transformer valve probe sensors as well as other systems, since it is possible to site the sensor in a low electric field region within the plant item. Introducing a dielectric sheath around the sensor will further reduce field concentration.

Due to its simplicity, the frequency response of the monopole can be derived theoretically [12]. A monopole is therefore used as a reference probe on the GTEM calibration cell and was chosen for FDTD modelling in this case. The measured and simulated responses of the 25 mm probe are compared in Fig. 3.

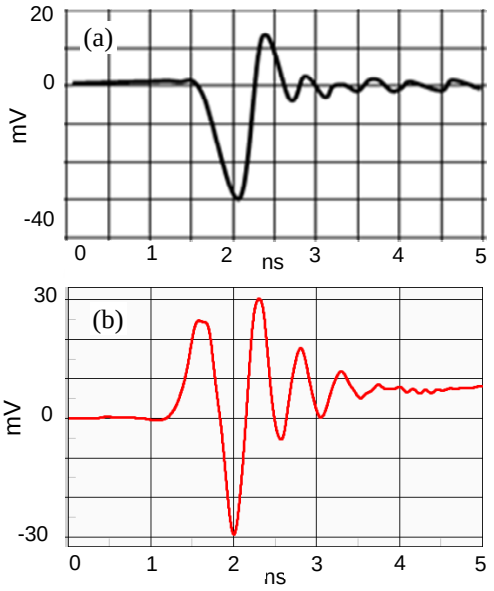

Figure 3: (a) Measured and (b) FDTD simulated response of a monopole antenna of length 25 mm and diameter 1.3 mm to a 30 Vm^{-1} step electric field.

Good agreement was found between the measured and simulated step responses in terms of amplitude. There is only 15 mV discrepancy between the peak-to-peak output voltages; 60 mV in the FDTD model as compared with 45 mV from the GTEM cell. Polarity differences are due to the orientation of the 50 Ω lumped element, representing the load in the simulation model.

2.2 Planar Logarithmic Spiral

Due to its stochastic nature, the exact frequency content of a given PD pulse is unknown. Therefore, to accurately measure UHF PD pulses it becomes necessary to use broadband sensors (bandwidth ratio of 2:1 or higher). The planar logarithmic spiral is a broadband antenna commonly installed on GIS. Since the sensor is flat, the risk of electric field enhancement is minimal.

The spiral PCB design was imported into the model from the original CAD drawing. Fig. 4 compares the measured and simulated step responses at the sensor's output.

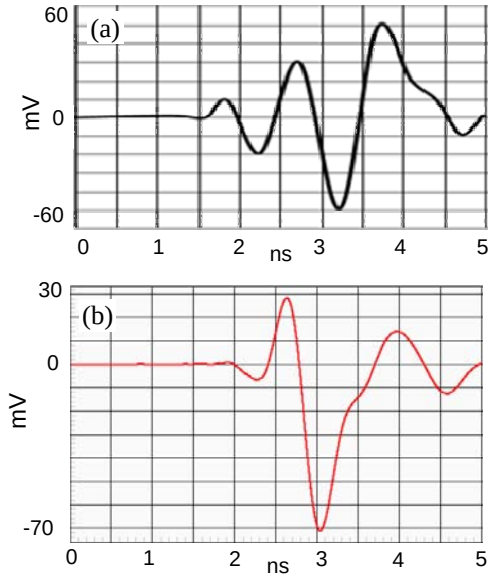

Figure 4: (a) Measured and (b) simulated response of a planar logarithmic spiral antenna to a 30 Vm^{-1} step electric field.

Simulation time in this case was around 2 hours. It can be seen that good agreement exists in the peak-peak amplitudes of the two signals (100 mV in both cases), although there is some variation in the shape of the waveform. Due to the spiral's complex structure, response time is slower than that of the simpler monopole. Fig. 5 shows a plot of the electric field in two dimensions at a point during the simulation.

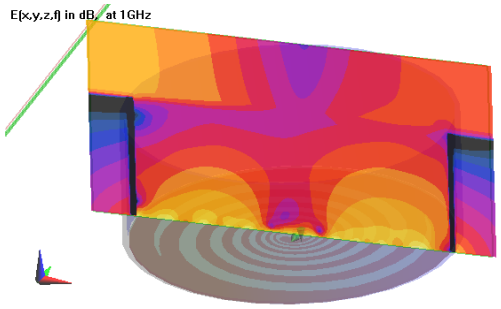

Figure 5: Electric field slice at 1 GHz during simulation of the spiral sensor.

3 Discussion

A fast response time is a desirable feature of any UHF sensor used for PD location by time-of-flight measurements. Given that the FDTD model did not predict the response time of the spiral as accurately as desired, it is recommended that caution be exercised when using the FDTD method to determine location accuracy for more geometrically complex sensor arrangements.

Variation in the shape of the spiral sensor's step response may be attributed to several factors. Firstly, FDTD techniques only allow the 3-dimensional geometric structure to be composed of rectangular voxels (finite volumetric regions). Modelling complex, non-linear structures such as the logarithmic spiral therefore introduces inaccuracies in the geometry that affect the model to a greater or lesser extent depending on the mesh density and consequently the computation time. Secondly, a number of simplifications have been applied to the model, as discussed previously. This open test configuration permits a finite radial dispersion of the electric field and will, to some extent, affect the accuracy of the simulation result. Thirdly, in the case of the spiral antenna, the step response is greatly dependent on its angular position; therefore slight differences in rotation angle can significantly affect the shape of the response.

4 Conclusions

To explore the effectiveness of FDTD modelling as a tool to aid in UHF coupler design, the responses of two common sensors – the monopole and the planar spiral – have been obtained both experimentally and through software modelling. Good agreement was found between the peak-to-peak voltages in both cases, with the spiral sensor giving the most accurate results. The predicted response time of both sensors was judged satisfactory given the variability due to other factors such as sensor orientation, although it was noted that caution should be exercised when modelling geometrically complex sensor arrangements.

Overall results indicate that FDTD methods can provide sufficiently accurate modelling of UHF PD sensors provided specific transformer-related electromagnetic conditions are met and the model geometry and mesh is sufficiently accurate. As an additional tool available in the design process, a software based approach at the initial design stage as demonstrated in this paper could provide insight as to the predicted behaviour of a coupler under realistic conditions, potentially reducing the time required for development of PD sensors for new applications.

Acknowledgements

This work is funded through the EPSRC Supergen V, UK Energy Infrastructure (AMPerES) grant in collaboration with UK electricity network operators working under Ofgem's Innovation Funding Incentive scheme; - full details on http://www.supergen-amperes.org

References

[1] S. A. Boggs. "Electromagnetic techniques for fault and partial discharge location in gas-insulated cables and substations", *IEEE Transactions on Power Apparatus and Systems*, volume 101, no. 7, pp. 1935–1941, July (1982).

[2] B. F. Hampton and R. J. Meats. "Diagnostic measurements at UHF in gas insulated substations". *IEE Proc.–C: Generation, Transmission and Distribution*, volume 135, no. 2, pp. 137–144, March (1988).

[3] J. S. Pearson, O. Farish, B. F. Hampton, M. D. Judd, D. Templeton, B. M. Pryor, and I. M. Welch. “Partial discharge diagnostics for gas insulated substations”, *IEEE Transaction on Electrical Engineering*, volume 2, no. 5, pp. 893–905, Oct (1995).

[4] M. D. Judd, O. Farish, S. G. Pearson, and B. F. Hampton. “Dielectric windows for UHF partial discharge detection”, *IEEE Transactions on Dielectrics and Electrical Insulation*, volume 8, no. 6, pp. 953–958, Dec (2001).

[5] W. R. Rutgers and Y. H. Fu. “UHF PD detection in a power transformer”, In *10th International Symposium on High Voltage Engineering*, pp. 219–222, Montreal, Canada, August (1997).

[6] M. D. Judd, L. Yang, and I. Hunter. “Partial discharge monitoring for power transformers using UHF sensors part 1: Sensors and signal interpretation”, *IEEE Electrical Insulation Magazine*, volume 21, no. 2, pp. 5–14, March/April (2005).

[7] M. D. Judd, L. Yang, and I. Hunter. “Partial discharge monitoring for power transformers using UHF sensors part 2: Field experience”, *IEEE Electrical Insulation Magazine*, volume 21, no. 3, pp. 5–13, May/June (2005).

[8] M. Judd and O. Farish. “A pulsed GTEM system for UHF sensor calibration”, *IEEE Transactions on Instrumentation and Measurement*, volume 47, no. 4, pp. 875–880, August (1998).

[9] M. D. Judd. “Transient calibration of electric field sensors”, *IEE Proc. Science, Measurement and Technology*, volume 146, no. 3, pp. 113–116, May (1999).

[10] Kane Yee. “Numerical solution of initial boundary value problems involving Maxwell’s equations in isotropic media”, *IEEE Trans. Antennas and Propagation*, volume 14, no. 3, pp. 302–307, May (1966).

[11] Allen Taflove and Morris E. Brodwin. “Numerical solution of steady-state electromagnetic scattering problems using the time-dependent Maxwell’s equations”. *IEEE Trans. Microwave Theory and Techniques*, volume 23, no. 8, pp. 623–630, Aug (1975).

[12] J. P. Karst, C. Groh, and H. Garbe. “Calculable field generation using TEM cells applied to the calibration of a novel E-field probe”. *IEEE Transactions on Electromagnetic Compatibility*, volume 44, no. 1, pp. 59–71, Feb (2002).

Monitoring System for Overhead Lines using Communications through Power Lines

S. Robson, H. Griffiths, A. Haddad

High Voltage Energy Systems Group, School of Engineering, Cardiff University, UK ,

Keywords: PLC, Fault location, Fault Prediction.

Abstract

Outlined in this paper is the concept of an Overhead Line Measuring System for use in a distribution network. In the proposed system, measuring units with the ability to measure voltage and current are placed strategically within the distribution network and its measurements are sent to a central monitoring centre via the principles of Power Line Communication. The applications of this system are discussed with particular emphasis on the potential of the system to facilitate fault location monitoring and power flow management. The major challenges facing the technology are also detailed.

1 Introduction

Power Line Communication (PLC) is a technique by which Radio Frequency (RF) signals are propagated over overhead lines primarily designed and used for power transfer. Though regarded as an established technology on transmission networks, use in Medium Voltage (MV) and Low Voltage (LV) networks has remained low and is typically restricted to commercial ventures relating to Broadband over Power Line (BPL) and 'last mile' technologies such as those promoted by the Home Plug Alliance. Recently, however, there has been renewed interest in the potential of the technology to help Distribution Network Operators (DNO) meet future requirements of sustained and/or improved customer service levels to the backdrop of increasing levels of Distributed Generation (DG) and the generally recognised need to move from a passive to an active distribution network.

Recent work has investigated a concept based on an integrated system for the monitoring, protection and control of an 11 kV network by the use of contact-less sensors and communication through the power line conductors [1]. Voltage and current is measured at various points throughout the network and processed locally within the measurement unit. A digital representation of the signals, along with a timestamp and a unique identification code, are then injected back into the conductor and transmitted to a monitoring centre and eventually the Utility's main communication infrastructure (e.g., SCADA). It is envisaged that a unidirectional implementation of this system (i.e., data flow from measuring unit to monitoring centre only) could be used to obtain a voltage and current profile of the network in real or near to real time. Clearly, analysis of this data could elucidate the location of arbitrary faults to a high degree of accuracy. In addition to this, extension of the same system could provide an early warning system for imminent line to earth faults, as is common with lines passing close to trees. Bidirectional implementation opens up the possibility of two-way communication, enabling a multitude of additional functions. Remote metering, real time network optimisation and active power flow management are three examples of applications with the potential to bring tangible benefits to DNOs, Generators, customers and the environment.

The initial aim of this paper is to examine the potential of both a unidirectional and bidirectional implementation of the aforementioned system on a distribution network. A brief explanation of how such a system could be implemented is also given, with particular emphasis on the unidirectional version. The penultimate section attempts to detail the major challenges expected to be encountered by the new system if it is to be successfully installed on a distribution network, with special consideration given to the technical limitations of using a power line conductor as a communication medium and the limitations imposed by network architecture typical of distribution networks.

2 Potential and Scope of PLC on Distribution Networks

2.1 Unidirectional implementation

i) Fault Location Monitoring: Typically, the location of faults on 11 kV networks is determined by first establishing which line has faulted at the substation and then performing a manual inspection of this length of line. Because the vast majority of interruptions observed by end users of the Electricity Supply Industry (ESI) can be attributed to the 11 kV and 400 V networks [2], expediting reconnection is an obvious way in which DNOs can improve incentivised performance. It is, therefore, unsurprising that various methods have already been developed as a potential means of determining the location of faults, with Artificial Neural Networks [3] and Bayesian Networks [4] being two models that have recently been utilised. In common with most of the developed techniques is the limitation imposed by insufficient data, pointing towards the requirement for extra measurements if a more usable technique is to be developed. Methods using voltage and current phasor measurements, as

is common in the less radial networks of the transmission system, have yet to address adequately several limiting factors inherent in the distribution system (e.g., presence of multiple feeders, taps, laterals and differences in conductor sizes [5]). A system able to measure remotely, process and transmit time and location stamped data to a centrally located monitoring centre may offer an economic solution to the fault location problem.

ii) Fault Analysis and Prediction: A common problem often encountered by DNOs is the initially unknown nature of the faults affecting the network. Access to a real-time voltage and current profile of the distribution system creates the potential to determine now only the location of a faulted section, but also its nature. In addition, the same information could facilitate an early warning system for imminent faults, notably the cases of a tree in close proximity to a conductor, faulty insulators and surge arresters.

2.2 Bidirectional implementation

i) Power Flow Management: The increased uptake of DG on distribution networks has challenged the old regime of unidirectional power flow and passive network design principles. In opposition to the current strategies designed to combat climate change is the fact that constraint of DG is often the only viable means of ensuring network security. In light of this, it is felt that active power flow management, such as that used in the transmission network, would be the most efficient and economic method of appeasing various constraints likely to arise as more DG is installed. In the absence of a suitable communication infrastructure (e.g., SCADA), the use of a Distribution Management System Controller (DMSC) has been proposed as one method of achieving active control of a distribution network [6]. A DMSC works by first feeding voltage measurement data (from local and remote substations) into a state estimator. Further processing through a control scheduler results in a series of control actions optimising network conditions. It has been demonstrated that using active network control techniques can increase DG penetration by approximately 3-5 times without the need for expensive network reinforcement [7]. At 11 kV, it has been suggested that another solution, known as Segment Controller, may be more appropriate. This is based on existing On Load Tap Changer (OLTC) transformers. Network voltages are compared with operational limits and from this Automatic Voltage Control (AVC) relays are dynamically adjusted. A practical example of a successful implementation of this system has recently been published [5]. An integrated monitoring, protection and control system, as is proposed in this paper, has the potential to provide the necessary quantity of measurements at a fraction of the cost of traditional dedicated fibre-optic or wireless methods.

ii) Role in new Distribution System Protection and Control Schemes: Distribution networks in the UK are mostly protected by non directional overcurrent and earth fault relays. Increases in DG installations are expected to undermine the prerequisite network conditions allowing such protection schemes to work. Bi-directional power flow, for instance, will cause grading problems in relays. It is envisaged that access to voltage and current measurements at various points in an 11 kV network will open up the possibility of new, flexible protection and control schemes.

3 Implementation of PLC on a Distribution Network

3.1 Operating principles

Distribution Line Carrier (DLC) is the form of PLC usually employed on MV distribution networks. DLC uses narrowband communication in the frequency range of 9 to 500 KHz. The REMPLI (Real-time Energy Management via Powerlines and Internet) system has already demonstrated the suitability of DLC in real-time applications [8].

One manifestation of DLC allowing real time fault location requires that each measurement node is given a unique identifier (UI). Associated with this UI is the measured voltage and current at a particular timestamp. Relaying of this information through the PLC channel to a remote monitoring station and subsequent central processing by appropriate software facilitates an accurate estimation of the region of the fault.

The simplest implementation of the outlined system is unidirectional. This essentially means that information is sent from Measuring Units (MUs) to a monitoring station but no information is sent the opposite way. This approximately halves both the bandwidth requirements of the channel and the equipment costs of the full system (if compared to a bidirectional system, where data is sent both ways). Figure 1 shows a sample radial 11 kV distribution network with the extreme case of a MU positioned at every node.

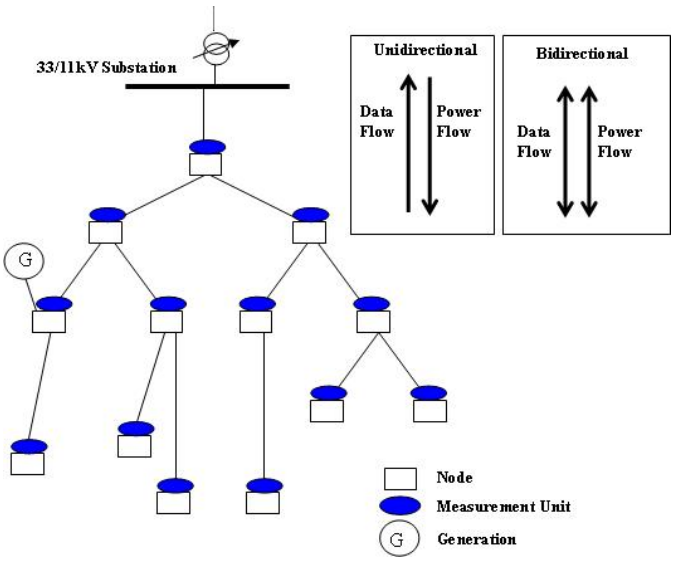

Figure 1: A sample 11 kV distribution network comprising several nodes, measurement units and a generation unit.

In the unidirectional implementation, MUs are to consist of voltage and current sensors, a DLC coupling mechanism and associated electronics e.g., Analogue to Digital Converter (ADC), modulator and control system. Figure 2 shows a simplified block diagram of an integrated DLC system with voltage and current measurement capability.

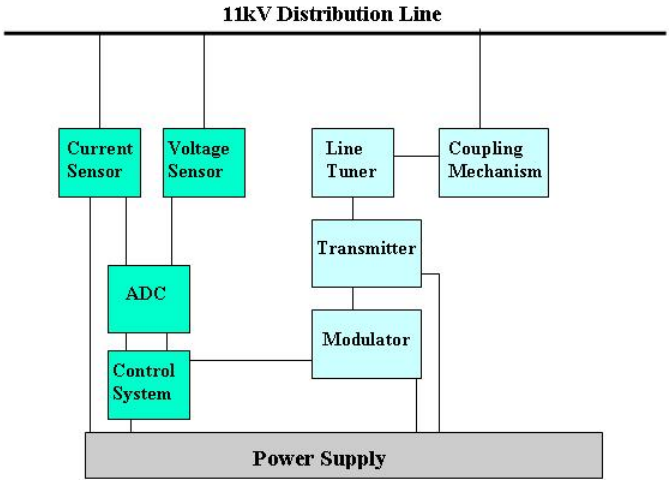

Figure 2: Simplified block diagram of a combined voltage / current sensor and DLC transmitter (unidirectional implementation).

The measuring unit, containing all the elements shown in Figure 2, would preferably be self contained and rugged with the ability to be installed onto the distribution line with minimal disruption. It has been suggested that fitting the device within, or onto the insulator could be a feasible method [1]. This utilises the structural integrity of the wood pole without adding extra weight to the suspended lines. An alternative is to 'tag' the system directly onto the line.

3.2 DLC subsystem

The DLC part of the system consists of a coupling mechanism, line tuner, transmitter and modulator.

i) Line Tuner: The line tuner and coupling mechanism must ideally act together to provide a low impedance path for carrier frequency signals and a high impedance path to power frequency signals. Typically, a tuned capacitor/inductor circuit is used for this purpose.

ii) Modulator: The modulator subsystem accepts a digital signal from the control system and conditions it appropriately. The exact nature of the modulation scheme depends on the design of the physical layer.

iii) Coupler: The coupler is responsible for injection (and extraction) of PLC signals. In the design of a coupler, consideration must be given to the type and method of coupling employed. For instance, coupling may be in the form of phase to phase or phase to ground and be of inductive or capacitive type.

3.3 Transducer subsystem

A novel approach using non-conventional transducers is currently being investigated and reported progress has been published at this colloquium (titled 'A Voltage Transducer for High Voltage Applications'). The aim of the overall project is to integrate this transducer technology into the system described in the paper.

4 Challenges and Future Work

4.1 The power line as a communication channel

The distribution network is a complex structure; Overhead lines, cables, transformers and capacitor banks are just a few of the elements making up a typical network. Invariably, these elements will have differing electrical characteristics. Furthermore, multiple branches, laterals and the presence of multiple feeders make the distribution network a relatively hostile communication channel for RF signals. Work recently carried out has reported that for an MV network (10 kV in this case); the phase and amplitude responses, even in a branchless network, tend to vary widely with frequency [9]. In related work, the amplitude response of a typical distribution network was shown to vary with frequency, time and depend on the type of coupling used [10]. Typically, these issues are resolved by the effective use of advanced digital signal processing schemes (for example, see the fledgling REMPLI standard [8]), however, little research has directly addressed the performance of a multi-node communication network on a real distribution network, and this will be addressed in this project.

4.2 Medium access control

The need for an especially robust Medium Access Control (MAC) protocol originates in part because the common Carrier Sense Multiple Access with Collision Detection (CSMA/CD) principle is difficult to implement in PLC. This is due to two main reasons [11]; Firstly, in a channel with a low Signal to Noise (SNR) ratio, the required sensitivity for effective carrier sensing is not met, and secondly, for a geographically dispersed network, it is extremely difficult for one node to 'listen' to all other nodes since network conditions will vary from place to place. Though some alternatives have been proposed (e.g., CSMA with Collision Avoidance), a more focused treatment on this particular problem is required if the full potential of a DLC channel is to be utilised.

A further option is to adopt an existing communication standard. The REMPLI standard, for example, attempts to establish an infrastructure combining PLC in the CENELEC band and IP based networks for remote control and metering access.

4.3 Clock synchronisation

In a multi-node communication system, there is often a requirement for precise clock synchronisation. Various standards for clock synchronisation in distributed systems already exist, for example the IEEE588 standard [12] provides precise time coordination in Ethernet networks. The power line, however, gives rise to time-variant channel properties and asymmetric transmission delays, rendering current master-slave techniques unsuitable for their intended purpose [13]. It is expected that further work is to be carried out to: firstly, deduce the scale of the problem clock synchronisation poses, and secondly, develop strategies to mitigate such problems.

4.4 Optimum deployment of measuring units

The cost of a fully installed system depends partly on the number of measuring units required to achieve a given level of performance. However, due to the complex nature of a distribution network, a solution as to the optimum deployment of measuring units may not be obvious.

4.5 Power supply

Providing a power supply to numerous measuring units dispersed on a network may be problematic. The obvious solution is to use battery power; however, the power consumption of a system incorporating several active devices is likely to be high, necessitating overly frequent replacements. Much attention has recently been given to 'energy scavenging' and it seems that the general idea behind this technology may find a natural application in the system described by this paper. The possibility exists, for instance, to utilise solar panels as one means of generating power. Other possibilities being explored at Cardiff University include exploitation of energy contained in the electric or magnetic fields emanating from the power line conductors.

5 Conclusion

The process of locating and characterising faults on distribution networks still mainly relies on manual inspection. With the increasing pressure to improve the level of service offered to customers, the benefits of a system able to accurately indicate the location and type of the fault would be highly valued. Given that it is uneconomical for DNOs to create a communication infrastructure in much of their network, a system utilising the already established power line network may be one way in which the traditionally passive networks can be made 'active'.

6 References

[1] B. Bale, M. Rawlings, M. O. Shahzad, R. Sidely, "Fault Location and Condition Monitoring on an 11 kV Rural Distribution Line", MEng Group Project, Cardiff University (2008).

[2] G. Strbac, N. Jenkins, T. Green. "Future Network Technologies, Report to the DTI", (2006).

[3] H. P. Khincha, D. Thukaram, P. Vijaynarasimha, "Artificial Neural Network and Support Vector Machine Approach for Locating Faults in Radial Distribution Systems", *IEEE Transactions on Power Delivery*, **Vol. 20**, pp. 710-721, (2005).

[4] S. L. Chen, C. F. Chien, Y. S. Lin "Using Bayesian Networks for Fault Location on Distribution Feeders", *IEEE Transactions on Power Delivery*, **Vol. 17**, No. 3 pp. 785-793, (2002).

[5] C. Barbier, J. Hill, N. Jenkins, P. Reay, V. Thornley, "Field Experience with Active Network Management of Distribution Networks with DG", *19th International Conference on Electricity Distribution*, Paper 0502, Vienna(Austria), (2007).

[6] T. Bopp, I. Chilvers, A. Shifiu, G. Strbac, "Active Management and Protection of Distribution Networks with Distributed Generation", *IEEE Power Engineering Society General Meeting*, **Vol. 1**, pp. 1098-1103 (2004).

[7] S. N. Liew, G. Strbac, "Maximising penetration of wind generation in existing distribution networks", *IEE Proceedings Generation, Transmission and Distribution*, **Vol. 149**, pp. 256-262, (2002).

[8] G. Bumiller, T. Sauter, A. Treytl. "Real-time Energy Management over Power-Lines and Internet", *Proceedings of the 8th International Symposium on Power-Line Communications and its Applications*, **Vol. 8**, pp. 306-411, Zaragoza(Spain), (2004).

[9] X. Yang, T. Zheng, "Investigation of Transmission Properties on 10-kV Medium Voltage Lines; Part 1: General Properties", *IEEE Transactions on Power Delivery*, **Vol. 22**, pp. 1446-1454, (2007).

[10] Y. Xiaoxian, "Research of Impedance Characteristics for Medium Voltage Power Networks", *IEEE Transactions* , **Vol. 22**, pp. 870-878, (2007).

[11] R. Gershon, D. Propp, "A Token Passing Network for Powerline Communications", *IEEE Transactions on Consumer Electronics*, **Vol. 37**, pp. 129-134, (1991).

[12] J. C. Eidson, M. Fisher, J. White, "IEEE-588 Standard for a Precision Clock Synchronisation Protocol for Networked Measurement and Control Systems", IEEE Standard 1588-2002

[13] G. Gaderer, R. Holler, T. Sauter, "Strategies for Clock Synchronisation in Powerline Networks", *Proceedings of the 2004 International Workshop on Real-Time Networks*, **Vol. 1**, pp. 77, Catania(Italy), (2004).

On-line Partial Discharge Monitoring in MV Underground Cables and Corresponding Denoising Algorithm

X. Song, C. Zhou and D.M. Hepburn

School of Engineering and Computing, Glasgow Caledonian University, Glasgow G4 0BA
Contact: x.song@gcal.ac.uk

Keywords: Partial Discharge, Cable On-line Monitoring, Wavelet Transform, Insulation diagnostics.

Abstract

For many years incipient Partial Discharge (PD) faults in power cables have been identified through off-line investigation techniques. More recently, in an effort to allow pro-active asset management of the medium voltage (MV) cable network, continuous on-line monitoring systems are being installed. This has been instigated with the aim of reducing unexpected failures. This paper presents work on the analysis and handling of acquired data from PD activity observed in on-line cable monitoring systems, from the point of view of asset management. The paper then presents the authors' experience of applying the Second Generation Wavelet Transform (SGWT) to PD data denoising. Results of a study on the on-line PD based monitoring of MV underground cables, which will be presented in later sections, demonstrate that PD activity observed in on-line monitoring is associated with strong noise and are time variant. Finally, the paper illustrates that identification and localisation of PD source(s) is possible through information that exists in PD pulse shapes after data denoising.

1 Introduction

Networks of medium-voltage (MV) cables are used to deliver electrical power at a local level in the majority of the world's utility systems. The majority of the MV distribution cables, and associated plant, in the UK's networks were installed during the 1950s and '60s [1]. As the items, typically, have a design life of 40-70 years they are approaching, or have exceeded, their expected operational life. Despite reported indications of increasing failure rate in power plant [2], the operational and cost constraints affecting utilities requires that equipment continues to operate for a considerable time. Utilities in the UK and Holland have reported that half of outages to customers are due to underground cable failure [3]. The result of faults in distribution cable is interruption of electrical supply to affected customers and inconvenience to other members of the public through roads being dug up to carry out repairs. A lack of effective power cable monitoring will lead to more frequent disruption of electrical supply to commercial and domestic customers. Companies can expect to suffer large financial penalties if they fail to address pre-existing faults and do not address poor maintenance regimes which results in customer down-time.

PD activity can be detected by using both of online and offline technique. In comparison with online testing, offline cable testing has a number of limitations as a routine cable condition diagnostics system [4]. Moreover, after initial set-up, on-line PD detection methods are less costly, as they do not require actions associated with off-line testing and are seen as an easier, faster and cheaper solution, thus potentially providing an economical advantage over off-line testing [3]. However, on-line measurement is prone to interference from airborne and internal noise e.g. electrical noise and white Gaussian noise. Over the last decade, the wavelet-based denoising algorithm has been investigated and applied to extract PD pulse from noisy background. This paper presents further results of the applications of denoising algorithms based on SGWT.

As part of ongoing research into underground cable on-line PD monitoring, the present authors investigated signals detected in cable system to ascertain whether PD activity was occurring in 4 underground cables. In this paper the authors will present the results of investigations. These will be discussed in relation to the presence of strong noise in on-line monitoring, applying newly developed denoising algorithms, observations of PD activity and the challenges facing asset managers applying on-line PD monitoring techniques.

2 PD monitoring system using HFCT sensor and PD extraction

2.1 HFCT detection system

The present authors have investigated PD activity in 4 underground cables over a 3 month period. The data has been supplied from commercially active parts of a distribution network using a standard monitoring system. All 4 cables are 11kV, 3-phase, and PILC type. The monitoring system collects data from cables at 30 minutes intervals using a high

frequency current transformer (HFCT) on the earth strap of the MV cable as it enters a substation, as shown in Figure 1. Each data set covers one AC cycle, i.e. 20 milliseconds, at an acquisition rate of 100 Mega samples per second. This results in a significant amount of data being generated from each cable being observed and requires fast data processing and large data storage to cope with the data streams which result.

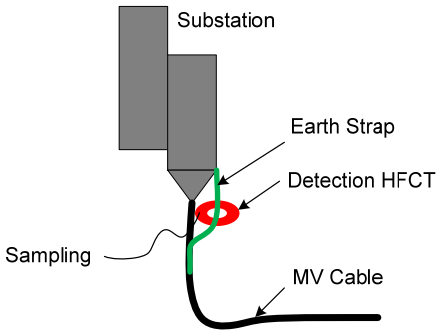

Figure 1: HFCT around the earth strap of an MV cable

2.2 Noise and Denoising

Unfortunately, as was indicated previously, on-line monitoring systems are prone to having higher levels of sinusoidal RF noise present. In addition, switching pulses and PD events from other local plant items may be detected and could be misinterpreted as coming from the cable [5]. The various challenges are evidenced in Figure 2 which shows a typical data set.

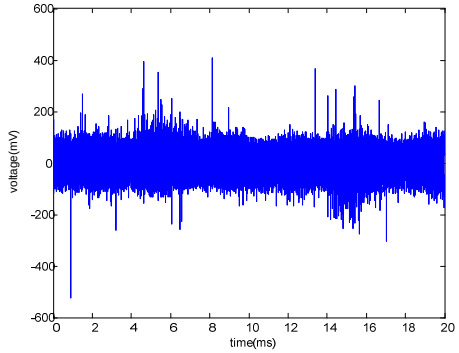

Figure 2: Data acquired from an on-line monitoring system on an 11kV underground cable. Data sampling rate is 100 MS/s.

Frequency analysis of this data, shown in Figure 3 (a) and Table 1, reveals that, in addition to white noise and impulse signals, the underground cable behaves like an antenna and picks up a significant amount of radio frequency (RF) signal. Another challenge in on-line cable PD monitoring is to distinguish PD pulse shape from other pulsative noise. Figure 3 (b) shows a typical PD pulse shape whilst Figures 3 (c) and (d) illustrate typical pulsative noise often encountered in on-line cable PD monitoring.

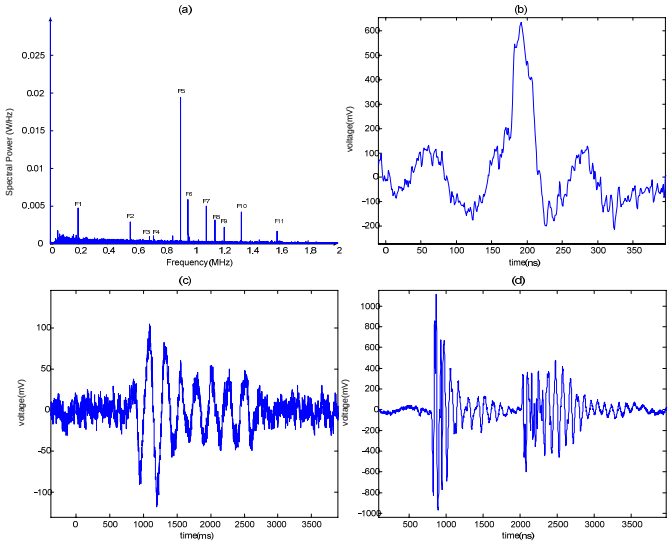

Figure 3: (a) Frequency spectrum of data segment shown in Figure 1; (b) Typical PD pulse shape with noisy background; (c) Switching noise found from data; (d) Pulses from local switchgear events

Table 1: Results of investigation into the sources of RF noise.

Frequency No.	Frequency (MHz)	Source of RF
F1	0.191	unknown
F2	0.558	Independent Local Radio Spectrum (London)
F3	0.693	National BBC R5
F4	0.720	Some BBC R4
F5	0.909	National BBC 5
F6	0.963	Local Radio Company
F7	1.089	INR3 Talk radio UK (ex BBC R1)
F8	1.152	ILR
F9	1.215	INR2 Virgin
F10	1.332	Local (BBC/ILR)
F11	1.584	Local (BBC/ILR)

The present authors earlier reported their investigations into a variety of denoising techniques, including traditional digital filters, Matched Filters and Discrete Wavelet Transform (DWT), applied to the processing of data acquired from cable PD monitoring systems [5]. The results revealed that both the matched filter and WT techniques are superior to traditional digital filters, when applied to PD detection and analysis, in terms of signal-to-noise ratio (SNR) and the number of PDs that can be identified. The matched filter [6] is the most effective technique when the waveform of the signal to be detected is perfectly known and where only white noise is present. On the other hand, the WT can be more flexible and more robust for on-site testing in the presence of other noise types and more severe noise interference. The matched filter

loses its effectiveness quickly when the acquired pulse shape is distorted by noise or due to propagation from its site of origin to the detection point. Furthermore, although the processing time required by the WT increases linearly with the data length of the wavelet, the processing time required using the matched filter increases exponentially with data length. Another important advantage of the WT over the matched filter and the traditional filters is that WT allows unambiguous reconstruction of the original pulse shapes, which are extremely useful as PD pulse shape is useful for diagnosis or validation purposes.

Most recently the authors further improved their denoising tool in the handling of the PD data by introducing the Second Generation Wavelet Transform (SGWT). In comparison with the DWT previously adopted, the SGWT has two distinct advantages. The first is that it allows for an in-place implementation of the fast wavelet transform, a feature similar to the Fast Fourier Transform. This means the wavelet transform can be implemented without allocating auxiliary memory and, as a result, the new algorithm decreases the hardware requirements while improving the speed of calculation. The second advantage which SGWT has over the classical wavelet transform is that, by using a priori information, the filter banks can be modified to allow desired PD pulses to be extracted with better accuracy. Further details with respect to the algorithms associated with the application of SGWT and its effectiveness can be found in [7, 8].

2.3 PD pulse Shapes and Patterns as Appeared in Continuous On-line PD Monitoring

After denoising data from the different sites, two types of PD patterns became apparent. Examples of the patterns which emerged are provided in Figure 4. Subsequent investigations of other cable systems has shown repetition of these two clear patterns. During the three month period of monitoring, no significant changes in pattern have been noticed though the magnitudes of individual PDs and the number of PD pulses change. Changes in PD magnitude and number will be discussed in later sections.

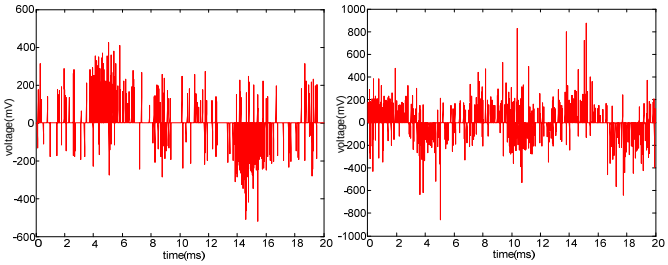

Figure 4: Typical examples of PD patterns observed from MV cable on-line PD monitoring

As many are aware, when a PD pulse travels from its origin to the site where the HFCT picks it up it may suffer attenuation, refraction, reflection and resonance effect. The appearance of the individual PD pulse shapes detected will be influenced by the type and age of insulation materials, cable configuration, joint construction, configurations in substation housing, the response of the HFCT and impedance mismatches along the propagation path. Furthermore, the individual pulses may also suffer from corruption by noise. These issues, although seen as a severe challenge to online detection, may also be useful. This will be discussed in the following section.

As an indicator of the impact of external signals upon cable signal detection, in a parallel study PD activity was measured at both ends of a cable of about 1000 metres in length. The interval between measurements was ~1 hour. The difference in data streams is shown in Figures 5 (a) and (b). The denoised data for each measurement, using the SGWT algorithm, is given in Figures 6 (a) and (b). These diagrams indicate that there is alteration of signal due to transmission characteristics between source and detection point.

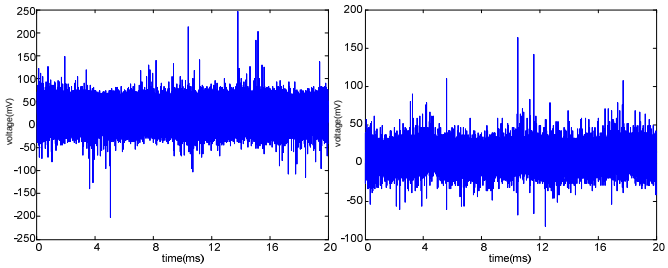

Figure 5: (a) and (b) PD signals measured at two ends of an 11kV underground cable, with a length of about 1000m.

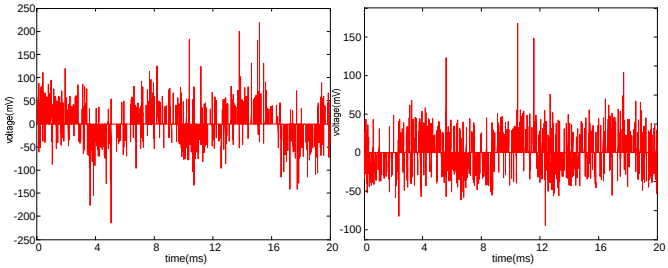

Figure 6: (a) and (b) Figures 5 (a) and (b) after denoising.

The alteration to the signal can be used for PD site localisation. Figures 7 (a) and (b) show the shapes of individual pulses extracted from the data. Figures 7(c) and (d) show a statistical analysis of the number of PDs which have given rise times. Strong indication is given of differences in characteristics for the detected signals for the two ends of the cable.

Off-line PD mapping test carried out on this cable revealed a single source which is responsible for the PD activity is approximately 220 metres away from the terminal where data shown in Figure 5(a) was acquired. Work is underway to relate the statistical information with the PD mapping results.

3 PD pulse separation

When the denoising algorithm is applied to another set of on-line PD data, an additional type of pulse shape was revealed. Figures 8 (a) and (b) show exemplars of the pulse shapes.

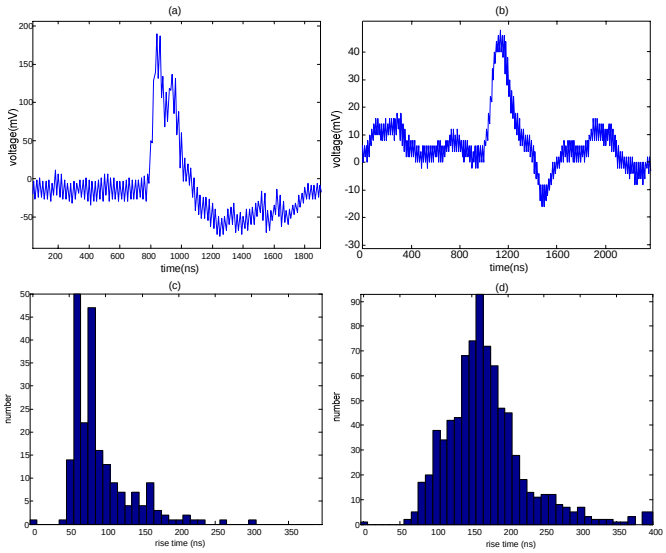

Figure 7: (a) and (b) typical pulse shapes extracted from Figs. 5(a) and (b) respectively. (c) and (d) Risetime of PD pulses vs. number of PDs having the same rise time.

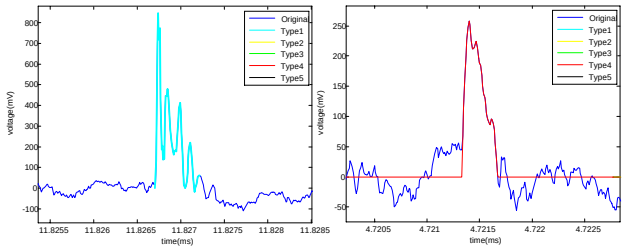

Figure 8: (a) 'new' pulse type, (b) 'standard' PD pulse

In Figure 9(a), the standard type of PD pulse is indicated in red and new type in light blue. Illustration of PD count against rise time of PD pulse, shown in Figure 9(b), suggests two sources of origins. These phase resolved clusters of PD signals (patterns), following denoising, indicate the activity is prevalent in one phase of the cable which, when confirmed, will demonstrate the effectiveness of the denoising algorithm.

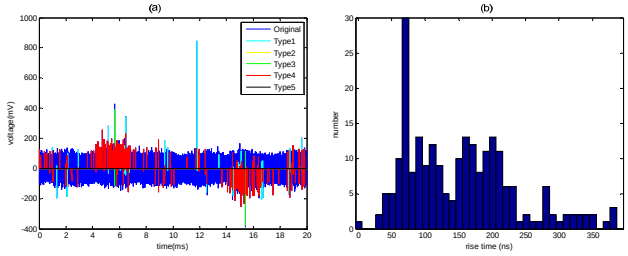

Figure 9: (a) original data and categorised PD pulses (b) Pulse Risetime vs. number of PDs having the same rise time.

4 Conclusions and discussions

An on-line cable PD monitoring systems generate, by far, larger amount of data than offline. Data may also contain significantly higher level of noise, presenting difficulty to operators of online systems. The RF interference has a similar frequency range to that of the PD pulses and, as a result, it is difficult to denoise the signal using traditional techniques.

A Second Generation Wavelet Transform-based algorithm has proved to be very effective in denoising data and capable of reconstructing PD pulse shapes for further localisation and diagnosis. Phase resolved clusters of PD signals (patterns) indicate the effectiveness of the algorithms developed by the authors. In comparison with other denoising methods, smaller PDs can be identified by SGWT based algorithms. As PD signals are attenuated during transmission in cables, this offers the possibility of more remote PDs being monitored. Successful categorisation or identification of different pulse shapes will enable better diagnosis and effective location of defect site. Despite the difficulties and challenges present in online PD monitoring, as outlined, application of the techniques being developed will reduce the risk of unexpected plant failure through more effective assessment of plant integrity. This will have significant economic and health/safety implications to an ageing plant population.

Acknowledgement

The authors would like to thank EPSRC for funding the work, under grant EP/D048133. Thanks also to Ross MacKinlay for sharing his expertise in PD monitoring and analysis.

References

[1] C. Walton and R. MacKinlay, **"**PD Monitoring: A Critical Tool For Condition-Based Assessments". Transmission and Distribution World, Dec. 2003.

[2] W.H. Bartley, "Life cycle management of utility transformer assets", presented at Breakthrough Asset Management for the Restructured Power Industry, Utah, 2002

[3] P.C.J. M.van der Wielen, E.F. Steennis and P.A.A.F. Wouters, "Fundamental aspects of excitation and propagation of on-line partial discharge signals in three-phase medium voltage cable systems", IEEE Trans.Diel.El.Ins., Vol. 10 (4), 2003

[4] L. Renforth, R. Mackinlay, and M. Michel, "MV cable diagnostics-applying online PD testing and monitoring", MNCCIRED Asia Pacific Conference on MV Power Cable Technologies, paper No. 14, 2005.

[5] C. Zhou, et al., "Comparison of Digital Filter, Matched Filter and Wavelet Transform in PD Detection". Int. Council on Large Electric Systems (CIGRE), Paper D1-111, Aug. Session 2006.

[6] J.Veen and P.C.J.M.van der Wielen: "The application of Matched Filters to PD Detectionand Localization", IEEE Electrical Insulation Magazine, Sept/Oct. 2003, Vol. 19 (5).

[7] X. Song, C. Zhou, D.M. Hepburn and M. Michel, "Second Generation Wavelet Transform in PD Measurement Denoising", IEEE Trans. Diel. El. Insul., Vol. 14 (6), 2007

[8] W. Sweldens, "The lifting scheme: A custom-design construction of biorthogonal wavelets," in Appl. Comput. Harmon. Anal, Vol. 3 (2), pp. 186–200, 1996.

TRANSIENT FAULT LOCATION IN LOW VOLTAGE UNDERGROUND DISTRIBUTION NETWORKS

Y. Tao, W.H. Siew, J.J. Soraghan

EEE Dept. University of Strathclyde, Glasgow, UK (Taoyx@eee.strath.ac.uk)

Keywords: Transient, Fault location, Arcing, Underground network

Abstract

Most power cable networks are aged and are prone to develop faults, which could lead to breakdown and loss of supply. This leads to customer minutes lost – a parameter that is monitored by the Electricity Regulator. Hence, it becomes desirable to know where in its network a major fault might be developing. For simplicity, the early stages of a fault would be classified as transient faults. Technologies to identify and locate transient faults either require access to residential homes or that they require the use of a blocking inductor to ensure that only a particular circuit is being investigated. Neither of them is preferred. This article is therefore to review some existing technologies that would be able to identify the transient faults and discuss the feasibility to overcome the restrictions or limitations posed by the existing equipment.

1 Introduction

Transient faults developed in underground cable networks are mainly caused by poor insulation. Electric arcing is the major cause of a transient fault, which is a plasma channel induced by insulation failure between conductors within the cable. The plasma channel, however, in the low voltage (LV) network, is normally self-extinguishing [1] and therefore is not an immediate hazard. Nevertheless, plasma channels during arcing have temperatures up to 25000K, which is considerably high and will damage the insulation and eventually cause a permanent fault. In some cases, an arcing fault will result in an explosion occurring in an underground cable network duct.

Self-extinguishing of arcing in LV network is due to either low driving voltage or post-arc column deionization phenomenon within the insulation decomposition gases. It was considered by some investigators that this fault may sustain for some time, or periodically reignite for minutes; thus generating much heat and gases as a result [2]. These gases could obviously be a hazard if combined with air in cable ducts to produce the minimum explosive concentration.

Many secondary LV cable networks do not have ground-failure or over-current protection, with the understanding that weak failure would be self-extinguished and high fault levels protected by the primary network protection system. However, in many cases, although weak arcing failure does self-extinguish damage caused by repeated intermittent faults would accumulate and then finally cause extensive damage to the cable or accessories nearby the fault point.

Koch et al. addressed the mechanism of arcing faults on low-voltage cables in ducts [3]. Transient faults normally begin with either a phase-to-neutral arc or phase-to-ground arc. In a wet environment, moisture infiltrates into gaps or cracks of deteriorated insulation among conductors. Conductive moisture under certain voltage will lead to a liquid breakdown that forms a plasma channel which immediately develops into a full-current arcing fault. This process turns electric energy to heat energy in a limited space around the arcing position. If the arcing fault persists, the large amount of heat energy generated will result in worse degradation of the cable insulation and evaporation of conductor material. Even though erosion (oxidation) of the conductor and creation of insulation decomposition gases will prevent or even stop arcing, adjacent insulation materials still suffer thermal degradation due to the heat and may cause the arc to reignite in the form of gas breakdown or surface discharge. The fault may result in the creation of intermittent arcing spots separated by a comparative long time, whereas, accumulated damage to the cable may lead to phase-to-phase discharge and result in a permanent three-phase fault. Thus, an effective protection system or fault location method for underground cables should possess the capability to address the disruptive aspects of transient faults.

Several investigations have been done and some methods have been developed to detect arcing faults. They can be classified into time domain analysis, frequency domain analysis and time-frequency domain analysis.

2 Methods of arcing detection

2.1 Time domain analysis

Time domain analysis is a way to examine voltage and current waveforms in the time domain. Lee utilized the ratio of zero-sequence and positive-sequence current characteristics to detect the arcing [4], while Sultan used the

half cycle current asymmetry character to address this issue. [5]. Benner detect the arcing by detecting randomness in the current behaviour of arcing [6].

Typically instantaneous phase or line current is analyzed, in order to monitor peak current caused by an arcing fault. This current has the shape of a spike with a huge magnitude compared with the magnitude of the current under normal load. However, the spike only lasts for a very short time. These techniques have the disadvantage that a similar spike also appears in the phase-current waveforms when a high-power inductive motor is being switched off.

2.2 Frequency domain analysis

For the frequency domain, phase current waveform harmonic analysis [7]-[8], or use of crest factor to evaluate waveform distortion [9] are two possible techniques to detect a fault.

Harmonic components of phase and neutral currents under normal conditions are different from those under arcing conditions. Therefore frequency domain analysis attempts to identify arcing faults by comparing harmonic contents. Harmonic contents of waveforms are derived from time domain signals by using Fast Fourier Transforms (FFT). To calculate FFT, a length of time domain data must be recorded and frequency components will be based on this length of time. W. Charytoniuk indicated that the following harmonic component values are changed by arcing faults [1]:

- DC component appearing in phase currents.
- Level of second harmonic increases sharply in phase current and neutral currents.

2.3 Time-frequency domain analysis

The time–frequency method detects the fault by interpreting transient arcing behaviour in time and frequency domain with use of wavelet transforms [10].

The purpose of time frequency analysis is to examine frequency behaviour changes over time. Bruce introduced a method of wavelet transformation that decomposes the input signal into a set of components [11]. By detecting the transient components present in a normal current, an arcing fault could be identified.

The analysis divides the transient signals into the respective components of a wavelet transformation. The transient detection capability depends on the type of wavelet family, order of the wavelet and robustness of decomposition. Fifth-order Daubechies family of wavelets are proven to produce best results in Charytoniuk's experiment.

3 Fault location

Although there are methods for detecting transient fault, location of the fault is still a mystery, this is due to unclarified frequency characteristic and unpredictable character. Accordingly, conventional fault locating methods such as synchronized complex analysis [12] [13] designed for permanent fault are no longer able to locate a transient fault which is irregular in time and sometimes non-repeatable.

Time Domain Reflectometry (TDR), which is also known as Cable Radar or Echometer technique, may be an applicable technique to locate arcing fault. In short, the TDR technique utilises a pulse sent out from a probing point of a cable, and the pulse bounces back from where there are significant changes in cable characteristic which are caused by arcing. Compared with complex analysis, TDR is faster and simple in implementation. However the success of this technique relies on the simplicity of the cable circuit being diagnosed. Another consideration would be the method chosen to filter out wide-bandwidth noise which result from arcing but retain TDR signals as much as possible.

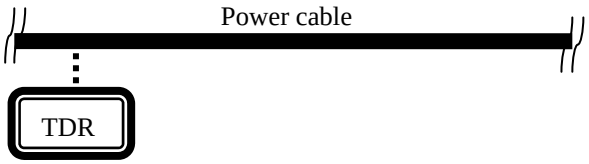

Figure 1: TDR online monitoring

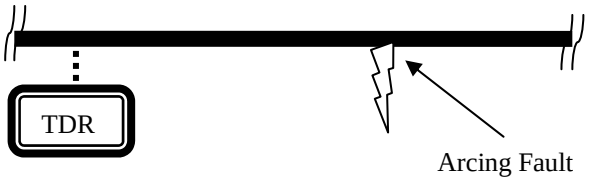

Figure 2: Arcing Fault occurring and is detected by TDR

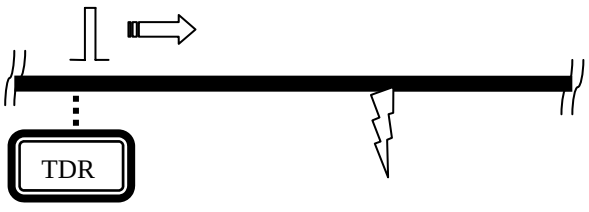

Figure 3: Upon detection, TDR sending pulse out to locate the arcing fault

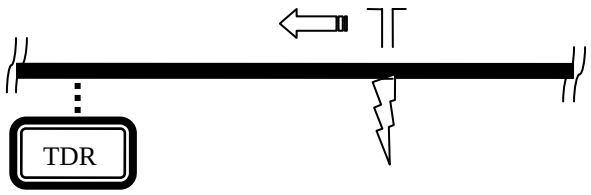

Figure 4: Reflection on point of fault due to low impedance arcing

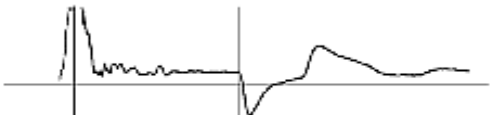

Figure 5: Captured waveform and location of fault in TDR

Figure 1 to Figure 5 show the concept of arcing fault location using the TDR technique.

4 Future work

Experiments are to be designed to address and clarify the electrical characteristics of arcing. The feasibility of applying TDR in locating transient fault will be investigated and evaluated to determine the success of the method applied.

5 Conclusions

- The most common transient fault in underground cable networks is an arcing fault, which is, in most cases, caused by insulation failure of cable network because of aging or improper work. The processes which cause damage to the cable by transient fault may be slow but cannot be neglected as they eventually develop into permanent faults.
- Detection of arcing could be considered based on time domain and frequency domain analysis. Time domain analysis is straightforward and cost-effective but requires fast monitoring systems as the faults happen over short periods of time. Moreover, setting the threshold of detection is not easy as current or voltage spike may be due to on/off operations of components that are quite normal in power systems. Frequency domain analysis has the advantage that analysis relies not only on magnitude but also on harmonic components of the signal. This method could identify uninteresting parts of the signal and focus on arcing related components. However, harmonic contents are obtained from time domain data by FFT; this may be to slow to respond to the short duration of the arcing signal and may require complex software/hardware.
- The complex analysis method for fault location is not suitable for transient fault location as it is based on mathematic models that require stable fault conditions, not relevant for transient faults. Time Domain Reflectometry may be suitable for locating transient faults, however, some issues that cause TDR technique to fail in this field should be addressed to allow it to become a mature and reliable technique.

Acknowledgements

The authors are grateful to The Scottish Funding Council for funding the studentship.

References

[1] W. Charytoniuk, Wei-Jen Lee, Mo-Shing Chen, & J. Cultrera. “Arcing fault detection in underground distribution networks - feasibility study”, *IEEE Transactions on Industry Applications,* Volume 36, Issue 6, pp. 1756-1761, (2000)

[2] J. F. Fuller,W. J. Hanna, and G. A. Kallenbach, “Arcing faults in metallic conduit at 120 and 240 V”, *IEEE Transactions on Industry Applications,* Volume IA-21, pp. 820–825, (1985)

[3] B. Koch and Y. Carpentier, “Manhole explosions due to arcing faults on underground secondary distribution cables in ducts,” *IEEE Trans. Power Delivery*, volume 7, pp. 1425–1433, (1992)

[4] R. E. Lee and M. T. Bishop, “Performance testing of the ratio ground relay on a four-wire distribution feeder,” *IEEE Trans. Power App. Syst.*, volume PAS-102, pp. 2943–2949, (1983)

[5] A. F. Sultan, G. W. Swift, and D. J. Fedirchuk, “Detecting arcing downed-wires using fault current flicker and half-cycle asymmetry,” *IEEE Trans. Power Delivery*, volume 9, pp. 461–469, (1994)

[6] C. Benner, P. Carswell, and B. D. Russell, “Improved algorithm for detecting arcing faults using random fault behaviour,” *Elect. Power Syst. Res.*, volume 17, no. 1, pp. 49–56, (1989)

[7] B. M. Aucion and B. D. Russell, “Distribution high impedance fault detection utilizing high frequency current components,” *IEEE Trans. Power App. Syst.*, volume PAS-101, pp. 1596–1606, (1982)

[8] C. J. Kim and B. D. Russell, “Harmonic behaviour during arcing faults on power distribution feeders,”

Elect. Power Syst. Res., volume 14, no. 3, pp. 219–225, (1988)

[9] C. J. Kim and B. D. Russell, "Analysis of distribution disturbances and arcing faults using the crest factor," *Elect. Power Syst. Res.*, volume 35, no. 2, pp. 141–148, (1995)

[10] S. J. Huang and C. T. Hsieh, "High-impedance fault detection utilizing a morlet wavelet transform approach," *IEEE Trans. Power Delivery*, volume 14, pp. 1401–1410, (1999)

[11] A. Bruce, D. Donoho, and H. Y. Gao, "Wavelet analysis," *IEEE Spectrum*, volume 33, pp. 26–35, (1996)

[12] M. Abe, N. Otsuzuki, T. Emura, and M. Takeuchi, "Development of a new fault location system for multiterminal single transmission lines," *IEEE Trans. Power Del.*, volume 10, no. 1, pp. 159–168, (1995)

[13] T. Funabashi, H. Otoguro, Y. Mizuma, L. Dube, and A. Ametani, "Digital fault location algorithm for parallel double-circuit multiterminal transmission lines," *IEEE Trans. Power Del.*, volume 15, no. 2, pp. 531–537, (2000)

AN INVESTIGATION INTO THE DETECTION OF PARTIAL DISCHARGE IN SUBSTATIONS

S. Xiao, P. J. Moore, and M. D. Judd

Electrical Plant & Diagnostics Group
Department of Electronic & Electrical Engineering, University of Strathclyde.
sa.xiao@eee.strath.ac.uk

Keywords: RF PD measurement, IEC PD measurement, partial discharge, substation.

Abstract

Measuring partial discharge (PD) activity in high voltage plant using radio frequency (RF) equipment is a well established technique used to monitor insulation integrity. This paper studies the partial discharges and breakdown voltage of corona PD by using both conventional measurements as defined in IEC Standard 60270 and radiometric techniques. The experiment takes the corona in point-plane gaps as example in a substation environment. The effect of corona PD on RF measurement system has been investigated by comparing with the results obtained from IEC measurement system with respect to the corona PD occurring at different high voltages. It was found that RF measurement system designed in this project is inherently unaffected by corona PD when the charges are at hundreds of pico Coulombs (pC).

1 Introduction

Corona discharge can be formed in a high electric field region caused by any sharp component or structure in a gaseous system, i.e. air-insulated substations (AIS), gas-insulated substation (GIS) [1-3]. If a charged object has a sharp point, the air around that point will be at a much higher gradient than elsewhere. Air near the electrode region can become ionized and partially conductive. When the air near the point becomes conductive, it has the effect of increasing the apparent size of the point. Since the new conductive region is less sharp, the ionization may not extend past this local region. Outside this region of ionization and conductivity, the charged particles slowly find their way to an oppositely charged object and are neutralized. If the geometry and gradient are such that the ionized region continues to grow instead of stopping at a certain radius, a completely conductive path may be formed, resulting in a momentary spark, or a continuous arc. Note that corona should not be used as a general term for all forms of PD, but refers specifically to this geometry.

The objectives of the present study are to understand the corona discharge process and the characteristics of electrical signals of corona discharge in the presence of point-plane configuration that will lead to the RF PD diagnosis. In order to study the corona discharges and the breakdown characteristics in details, two electrical detection methods were used to record the corona PD signals, which provide different diagnostic results such as the phase-resolved PD pattern, and the signal frequency spectra before breakdown.

2 Measurement of PD

2.1 Test cell

A point-plane configuration is used in the experimental study of corona PD in air under atmosphere pressure, shown in Figure 1. This configuration has been widely used to study PD phenomena because it represents a convenient way of generating sufficient electrical stress to initiate PD. The small tip radius of the needle leads to an enhancement of the electric field at the tip. In this region the physical processes are governed by the local electric field stress which is a function of the overall electrode configuration and the applied voltage [4]. By conducting experiments at voltages below air gap breakdown, the field at the needle tip will be of the level required to induce typical PD in a practical substation environment.

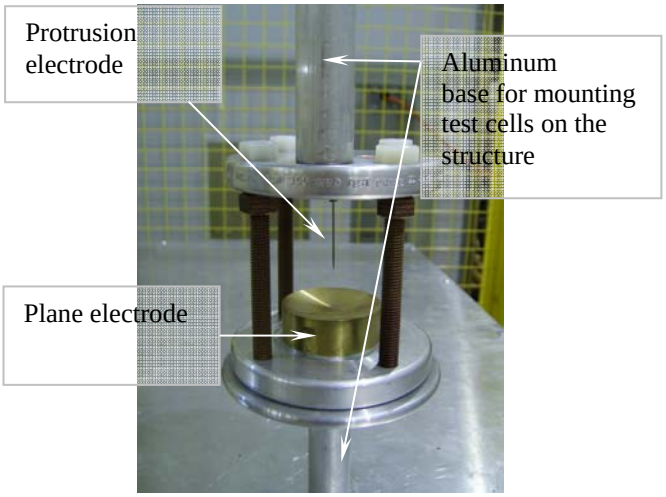

Figure 1. Point-plane test cell for corona PD.

2.2 Measurement system setup

During the progress of the present investigation, experimental measurements have been made on four air gaps - from 17 mm to 35mm – using the point-plane test cell at atmospheric pressure. All experiments have been carried out on a metallic structure at a height of 5 meter, which is the height of a busbar for a 132 kV substation. The experimental apparatus is shown in Figure 2. The purpose of the metallic structure is to provide an environment that allows the measured PD pulses to persist, simulating the response that would be observed on a busbar in the substation.

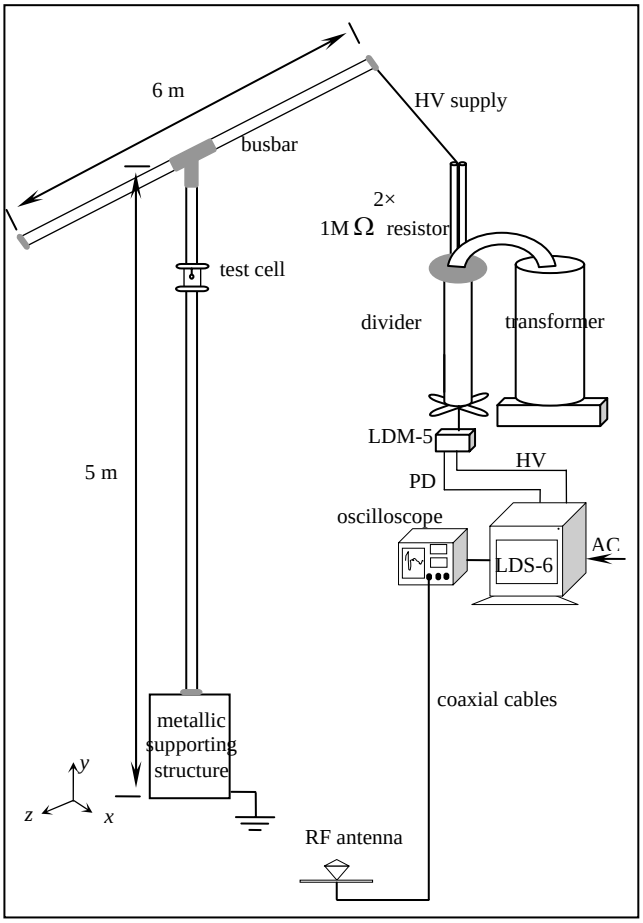

Figure 2: Experimental set-up. Test cell is mounted on a metallic busbar structure.

Corona PD patterns which consist of the number of discharges, apparent charges [5] and phase angles are recorded from IEC measurement system (Lemke LDS-6 systems) from pre-inception voltage to breakdown voltage. The LDS-6 measurement system is used to adjust the high voltage supply to energize the metallic structure and also used to store phase-resolved PD data.

A wideband antenna [6], located on the ground, was used to capture the impulsive RF signals from the corona PD. The antenna was connected to a Tektronix TDS 7104 Digital Phosphor Scope which can provide a sampling rate of 2.5 GSamples/s and has an analogue bandwidth of 1 GHz. The scope has segmented memory architecture that allows the main sampling memory of 2 M-samples per channel to be segmented into separately triggered measurement frames of 10,000 samples each, which gives the recording time duration $4\mu s$ from each recorded pulse, and it is adequate for the average length of typical PD pulses in air dielectrics.

3 Measurement results

With the four air gaps having been applied in the experimental measurements, this section goes on to describe the two measurement results of corona PD from IEC measurement system and RF measurement system, respectively.

3.1 IEC measurement results

Corona PD patterns were obtained from IEC measurement system corresponding to the number of PD pulses occurring at a given charge and phase angle. During testing, it was necessary to re-calibrate the IEC system when the gap was changed. This resulted in only a slight variation in the calibration factor for results on the test cell at same height.

The point-plane air gap produces corona PD. Free charges are created to be deposited and accelerated, which influence the electric field in the air gap when different breakdown voltages are applied subsequently. Figure 3 to 6 show that IEC patterns due to corona inception start at tens of (pC), whereas higher voltages lead to thousands of pC before the gap breakdown. Meanwhile, RF signals recorded on the oscilloscope showed that the radiated waveforms received by the antenna change from the pulseless-type to the pulse-type over this range. Table 1 to 4 show typical IEC and RF recorded data during theses stages. Note that attenuators in the LDS-6 system have to be applied to protect the measurement system from the risk of damage when the large PD charges appear, and the attenuator is also used as a factor to give a proportion of the original signal, i.e. higher attenuator, larger PD charges.

Voltage applied (kV)	Measurement Attenuator (dB)	Experiment record duration	Antenna received Max Pulse height (V)	Antenna received Pulse duration
5.5	51	4 min	None	None
7.0	57	4 min	2.763×10^{-3}	$0.75\mu s$
9.2	63	5 sec (Breakdown)		

Table 1: Record data for the air gap at 17 mm.

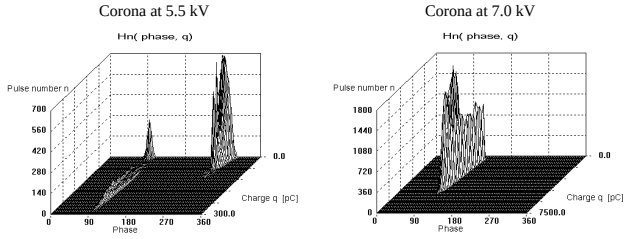

Figure 3: Typical patterns received for the air gap at 17 mm.

Voltage applied (kV)	Measurement Attenuator (dB)	Experiment record duration	Antenna received Max Pulse height (V)	Antenna received Pulse duration
7.0	51	4 min	None	None
9.0	51	4 min	None	None
11.0	51	4 min	None	None
13.8	72	4 min	4.016×10^{-3}	$1.25\mu s$
15.7	90	10 sec (Breakdown)		

Table 2: Record data for the air gap at 23 mm.

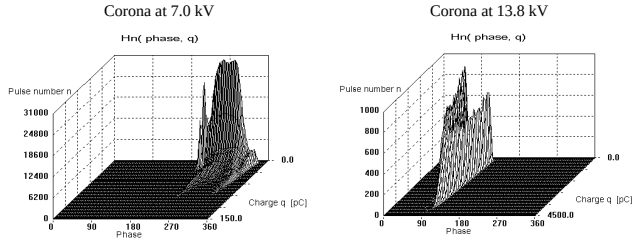

Figure 4: Typical patterns received for the air gap at 23 mm.

Voltage applied (kV)	Measurement Attenuator (dB)	Experiment record duration	Antenna received Max Pulse height (V)	Antenna received Pulse duration
9.0	51	4 min	None	None
11.0	51	4 min	None	None
12.0	51	4 min	None	None
14.0	72	4 min	None	None
16.0	87	4 min	4.481×10^{-3}	$1.75\mu s$
20.3	90	10 sec (Breakdown)		

Table 3: Record data for the air gap at 29 mm.

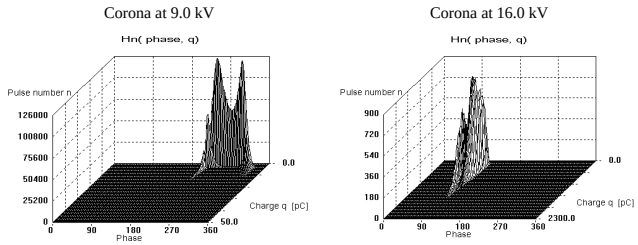

Figure 5: Typical patterns received for the air gap at 29 mm.

Voltage applied (kV)	Measurement Attenuator (dB)	Experiment record duration	Antenna received Max Pulse height (V)	Antenna received Pulse duration
11.0	51	4 min	None	None
12.0	57	4 min	None	None
14.0	57	4 min	None	None
16.0	57	10 min	None	None
19.7	81	10 min	5.448×10^{-3}	$2.25\mu s$
22.5	84	5 sec (Breakdown)		

Table 4: Record data for the air gap at 35 mm.

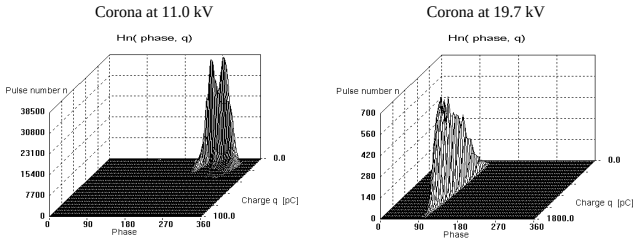

Figure 6: Typical patterns received for the air gap at 35 mm.

For the point-plane configuration, corona discharges are shown to initially occur on the negative half-cycle rather than the positive half-cycle of the a.c supply. This is due to electrode configuration, since in this case the protrusion electrode is connected to the high voltage supply and the plane electrode is connected to ground.

3.2 RF measurement results

In the RF measurement, with the repetitive nature of PD, 200 measurement frames of 10,000 samples each were recorded. Note that all RF PD signals were recorded below the breakdown voltage to avoid the risk of flashover and breakdown, which might damage the measurement system. Figures 7 to 10 show the typical pulse recorded at each air gap and their frequency spectra below 100 MHz, which is the main frequency range of interest for air insulation.

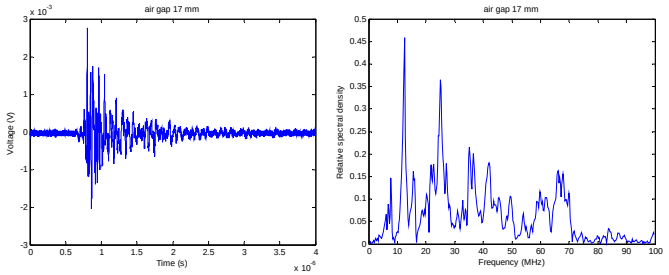

Figure 7: Typical pulse received by an antenna for the air gap at 17 mm, at 7.0 kV.

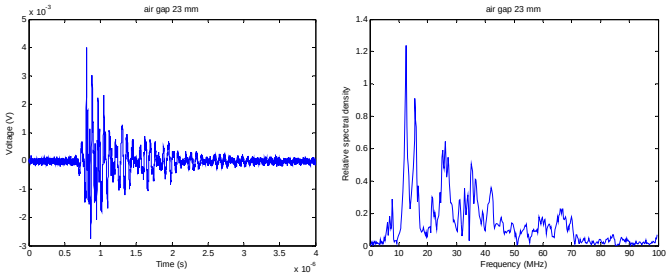

Figure 8: Typical pulse received by an antenna for the air gap at 23 mm, at 13.8 kV.

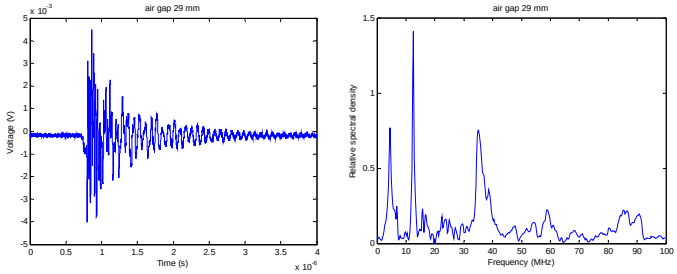

Figure 9: Typical pulse received by an antenna for the air gap at 29 mm, at 16.0 kV.

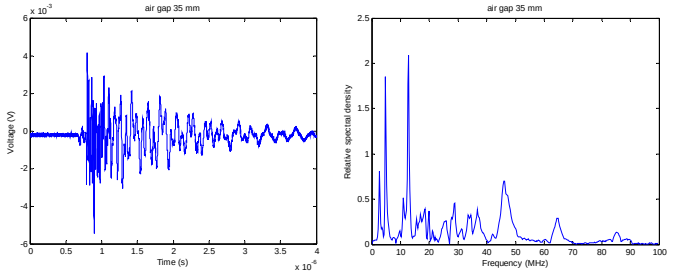

Figure 10: Typical pulse received by an antenna for the air gap at 35 mm, at 19.7 kV.

Figures 7 to 10 show PD waveforms change gradually in time domain, with the pulse duration increasing with the air gap. The frequency spectrum for large discharges is in the lower frequency region, particularly with a bigger gap. Note that when the various high voltages are supplied to energize the metallic structure, corona PD with different pC level can be obtained from IEC measurement system and RF measurement system. In the charge range of hundreds of pC, no distinct pulses were received by the antenna, demonstrating that RF measurements designed in this case are inherently unaffected by corona. This is an important conclusion for RF measurement, which is useful for the non-contact continuous monitoring in a substation environment.

4 Conclusions

This paper has described the investigation of PD and breakdown voltage of an atmospheric point – plane gap arrangement based on two different PD detection techniques. From the experimental results, it is seen that there is a significant variation in the RF pulse shape at different supply voltage. The pulse duration time as well as the pulse spectra is altered. It is also observed that the pulses can be obtained at different charge level from IEC measurement system and RF measurement system. The results demonstrate that the RF system is relatively insensitive to low levels of corona. At high levels of corona, close to breakdown, the RF system can readily detect corona impulses. When taking measurements in substations, spurious corona discharges are always present at a low level, caused by sharp protrusions on high-voltage equipment. The results indicate that the RF system will not detect practical, benign corona impulses.

Acknowledgements

This work was supported by the Overseas Research Students Awards Scheme, Higher Education Institutions, UK, and University of Strathclyde, UK.

References

[1] M. Hara, Y. Negara, M. Setoguchi, T. Kurihara, J. Suehiro, N. Haashi. “Particle-triggered pre-breakdown phenomena in atmospheric air gap under AC voltage”. IEEE Transactions on Electrical Insulation, Vol. 12, pages: 1071 – 1081, Oct. 2005.

[2] C. Chang, C.S. Chang, J. Jin, T. Hoshino, M. Hanai, and N. Kobayashi. “Source classification of partial discharge for gas insulated substation using waveshape pattern recognition”. IEEE Transactions on Dielectrics and Electrical Insulation, Vol. 12, pages: 374 – 386, April 2005.

[3] R. Bartnikas. “Detection of partial discharges (Corona) in electrical apparatus”. IEEE Transactions on Electrical Insulation, Vol. 25, pages: 111 – 124, Feb. 1990.

[4] F. H. Krueger. *Partial Discharge Detection In High Voltage Equipment*. Butterworth-Heinemann, 1989.

[5] E. Kuffel, W. S. Zaengl, and J. Kuffel. *High Voltage Engineering: Fundamentals*. Newnes, 2000.

[6] P. J. Moore, I. Portugues, I. A. Glover. A Non-Intrusive Partial Discharge Measurement System Based on RF Technology. *Power Engineering Society Meeting*, June 2003, pp 627 – 633.

Measurement and analysis of electric potential decay in corona charged low-density polyethylene films

Z. Xu*, L. Zhang† and G. Chen*

*School of Electronics and Computer Science, University of Southampton,
Southampton, SO17 1BJ, United Kingdom
†Institute of Fluid Physics
China Academy of Engineering Physics
* E-mail: zx04r@ecs.soton.ac.uk

Keywords: corona charged, potential decay, LDPE, PEA.

Abstract

In this paper, corona charged LDPE film was tested using a standard static potential monitor and the pulsed electro-acoustic (PEA) technique to observe the surface potential decay. A wide range of voltages and different corona charging times, different sample thicknesses and multi-layer films were used to demonstrate influential factors for surface potential decay. These provide a direct experimental evidence to support the bulk transport process. An important finding from the PEA results is that bipolar charge injection takes place during corona charging process and in subsequently decay process. The new evidence challenges the existing surface potential decay models which were developed based on a single charge carrier injection.

1 Introduction

In recent years there has been considerable interest in the surface potential decay characteristics of corona charged dielectrics. Various methods have been used to observe the decay including thermally stimulated discharge current, surface potential decay and the measurement of current/voltage during corona charging [**1**]. Different mechanisms have been proposed. Generally, there are three possible decaying routes for electric charge on surface, i.e. through the atmosphere, along the surface and transport through the bulk. In the present study, surface potential decay after corona charge deposition has been investigated for low density polyethylene (LDPE) films over a wide range of charging voltages and different charging times. To further understand decay process, experiments were carried out on multi-layer of LDPE films. In addition to monitor the surface potential, the pulsed electro-acoustic (PEA) technique, which has been widely used to measure space charge in solid dielectrics, has been employed to measure charge distribution and its evolution in corona charged LDPE.

2 Experimental details

In order to reduce the influence of impurities, additive-free low density polyethylene film was selected. The thin planar films were purchased from GoodFellow. Samples were cut into a disc shape with a diameter of 50mm, cleaned using methanol, raised in deionised water and dried by air.

LDPE film was charged in a conventional corona setup shown in Figure.1. The system consists of a high voltage needle, a wire mesh grid and a earth plate. The initial surface potential of corona charged film is controlled by the grid voltage applied across the needle and the rotatable earth electrode. After corona charging, the sample was moved to the static monitor (Compact JCI 140) quickly for the surface potential decay observation. The readings from the static monitor are proportional to the value of surface potential. After a calibration these readings can be easily converted into the surface potential. We use the negative corona charging in this study and the readings from the monitor were converted to absolute potential value in all the results. All experiments were carried out under a controlled environment where temperature and relative humidity were 21°C and 45%, because both the temperature and relative humidity have an influence on charge decay.

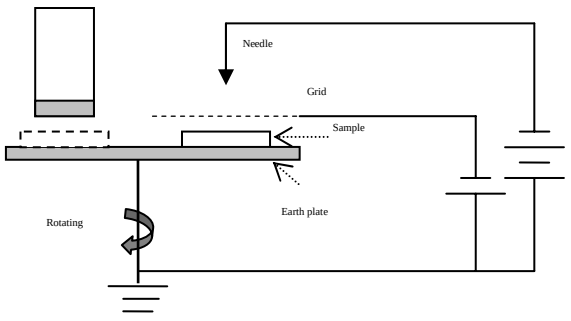

Figure 1: potential decay measurement system

The PEA technique is by far the most widely used method in space charge measurement. This technique utilizes the interaction between high voltage pulses and charge layers accumulated in the material to produce acoustic pressure waves. The pulsed acoustic waves correspond with each charge layer with respect to neutrality. The acoustic signals traverse across the material and are converted into an electrical signal by a piezo-electric transducer, amplified and captured with a digital oscilloscope. The detailed principle of PEA technique can be found in [**2**].After corona charging, both sides of sample were attached with a thin fresh LDPE film (50μm) very carefully to keep the deposited charges. The possible air bubble between films should be removed with small pressure because good contact between the films is necessary to get the good charge mapping results using the PEA method.

3 Results and discussion

The surface potential decay processes were measured for LDPE samples charged under different conditions initially. Charge distributions in the corona charged samples under the same charging condition were monitored by the PEA technique.

3.1 Surface potential decay

The potential decay result of corona-charged film (50μm) under different charging voltage for 2mins is shown in Figure 2. Surface potential shows an expected monotonic decay with time. However, we can observe clearly the crossover phenomenon; i.e. the surface potential in the sample with an initial high potential decays faster than that with a lower surface potential.

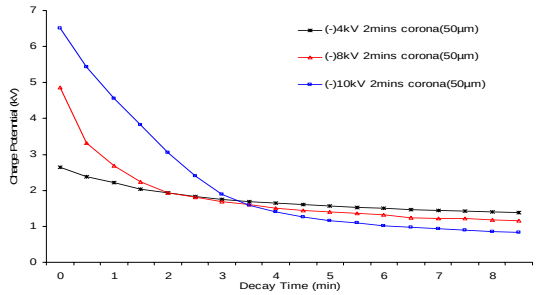

Figure 2: Potential decay under different corona voltage for thin sample (50μm)

To explain the surface charge leakage and crossover phenomenon, different mechanisms have been proposed. The decay has been attributed to various mechanisms including recombination with opposite ions in air, surface migration and bulk conduction. The bulk process has been widely accepted and several models have been proposed to explain the surface potential decay [**3-5**]. To validate the bulk process responsible for surface charge decay, samples with different thicknesses (180μm and 50μm) were used under either the same corona voltage (-8kV) and or the same electric field (~80kV/mm). The decay results were shown in Figure 3 and Figure 4. The results in Figure 3 indicate that the material thickness plays a crucial role in surface potential decay. Both results in Figure 2 and Figure 3 show us that surface potential decay faster when the sample has an initial high electric field.

Figure 4 shows the potential decay under the same initial electric field for different thickness samples. To compare two curves, we moved down the higher corona voltage charged curve parallel. Overall, it can be seen that the decay rate for two samples has no significant difference except a little faster for the thinner sample at the beginning. From the above results, it is obvious that the surface potential decay strongly depends on the initial electric field of corona charging.

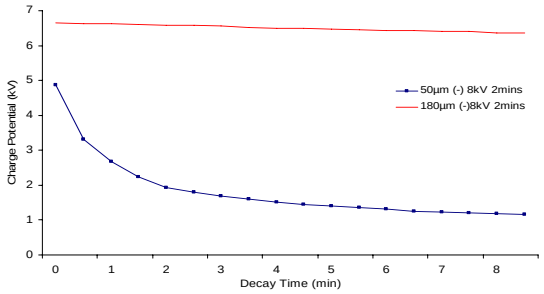

Figure 3: Potential decay under same corona voltage for different thickness sample.

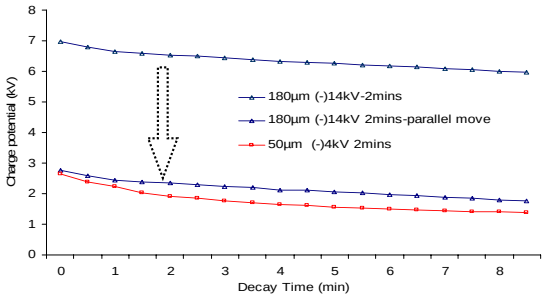

Figure 4: potential decay under same corona electric field.

Figure 5 shows the potential decay results of 50μm sample under -8kV corona charging during different times. From this figure, it seems that the longer the charging time the faster the surface potential decays. This is especially true for first a few minutes. A possible reason for the faster decay is that the longer charging time allows more charge carriers injecting into the bulk. The injected charges then may move easily towards the opposite electrodes. This fast decay result has been validated by the PEA measurement data shown in the figure later.

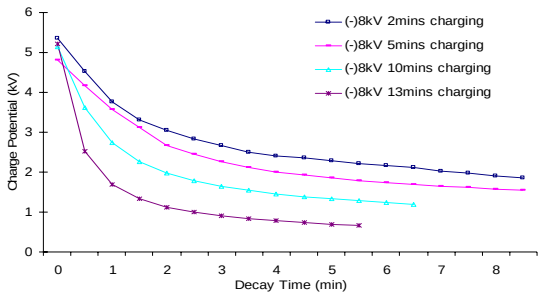

Figure 5: Potential decay during different charging period.

Figure 6 shows the surface charge decay of multi-layer LDPE sample corona-charged under -4kV for 2mins. To achieve a similar electric field, the similar sample thickness was chosen; i.e. 180µm for one layer and three layers of 50µm (150µm) as multi-layer. For the multi-layer potential decay monitoring, two measurements were carried out. In the first one the potential was continuously monitored. In the second measurement, after the potential was monitored for 3 minutes the top layer was carefully removed and surface potential produced by the middle and bottom layer was continuously observed and it shows a similar decay fashion. And after 5 minutes, the middle layer was removed and the potential produced by the bottom layer was measured as shown in Figure 6. Since surface potential is a representation of both surface charge and bulk charge, this result implies that electric charges exist either on the top surface of bottom two layers or in the bulk. No matter which case, the charges detected has to come from charge injection from the electrodes. Therefore, it provides a direct experimental evidence to support the bulk transport process.

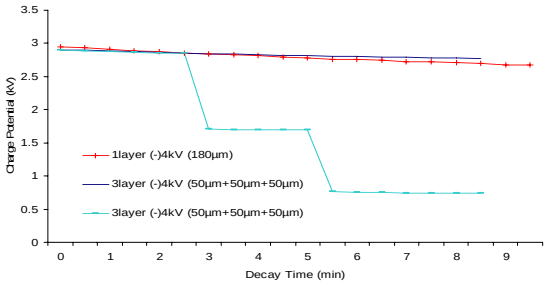

Figure 6: Potential decay for multi-layer sample (-4kV, 180µm, 50µm +50µm +50µm)

By comparing potential decay results for one layer and three layered samples, it can be noted that the surface potential from the multilayer sample with interface shows a slower decay than that from one layer sample. From the results it seems that the surface potential form a sample with an initial high field decays faster. Therefore, the surface potential from one layer sample (180µm) with an initial lower electric field should decay slower compared with the three layer sample (150µm). However, the results in Figure 6 contradict this. The only explanation lies in the presence of interfaces in the three layered sample. Interface seems to act as a barrier for charge movement therefore leading to a slow decay of surface potential.

3.2 Charge mapping results

It is clear that bulk process is responsible for the surface potential decay. As the surface potential changes relatively slow, it is possible to utilise the PEA technique to monitor space charge distribution and charge evolution. From the results of surface potential measurement, we know that the decay rate is strongly depending on the experimental setting, e.g. corona voltage, sample thickness, applied electric field, charging period and polymeric interface. Although the potential decay can give us some information about the charge decay mechanism, more interesting thing is how the charges transport inside the sample during the decay period. Figure 7 shows the charge distribution of 180µm corona-charged under 8kV for 2 minutes. The two peaks at the PEA electrodes are induced charged peaks, which is definitely due to the existence of charge in the sample. The middle two peaks at top and bottom layer of corona charged sample are the charges formed during corona charging process, protected by the attached film. Negative charges presented at the top surface are expected as a process of charge deposition. However, a significant positive peak can be observed at the bottom surface of the sample. We believe this is because the charge injection from the ground electrode happened in the corona charged process. About the detailed discussion of bipolar injection can be found in our earlier works [**6, 7**]. Charge evolution with time also shows a slow change, which is analogous to one of the potential decay curves shown in Figure 3.

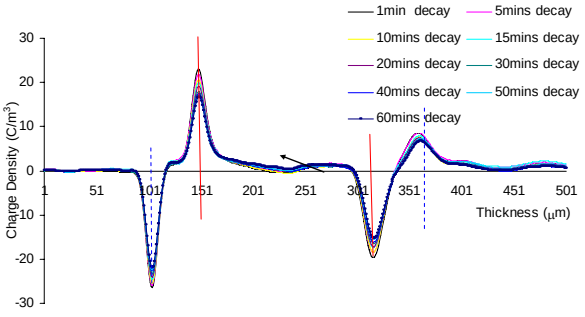

Figure 7: Space charge distribution in the corona charged sample (180µm, -8kV 2mins corona)

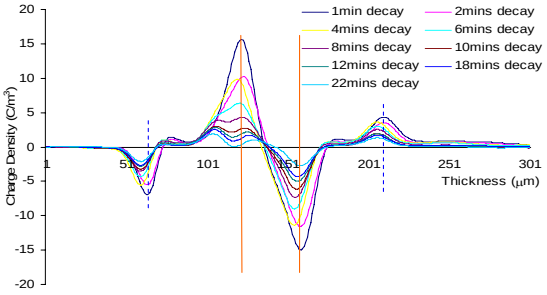

Figure 8: Space charge distribution in the corona charged sample (50µm, -8kV for 10mins corona charging)

Figure 8 shows the profile of space charge distribution decay in the corona-charged sample, under -8kV for 10 minutes, the same experimental conditions as second bottom decay curves shown in Figure 5. It is noted from the PEA results that charges decrease extremely fast. This result is consistent with the result in Figure 5.

Figure 9 shows space charge distribution and dynamics in a two-layer LDPE sample. Compared with space charge distribution in one layer corona charged sample, an extra negative charge peak is observed at the interface between the two polymer layers. This can explain the early potential results obtained from the middle and bottom layer of the multi-layer sample (see Figure 6). These negative charges measured by the PEA or potential monitor are believed to be formed due to charge injection from corona charging surfaces and then transported to the interface. To study the charge transport in the bulk or at interface after corona charging, two-layer LDPE sample was charged for a long period and the PEA result is shown in Figure 10. There is a significant difference in charge distribution inside the bulk and interface of sample compared with a short charging period.

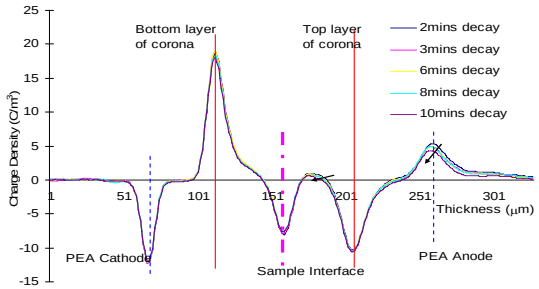

Figure 9: Space charge distribution decay in two layer corona charged sample (50μm+50μm, -4kV 2mins corona)

The negative peak at the top layer of corona charged sample is smaller than the peak shown in Figure 9 and deceased with time. Similar situation happens for the charge accumulated at the sample interface. An important result is negative charge dominated the bulk area of two corona charged layer. It seems that the negative charge deposited on the top layer moved into the bulk and overcome the interface barrier and transport in bulk of bottom layer. The longer the corona charging time the more electrons injected into the bulk. From the charge distribution evolution, it is easy to know that charge decays faster in the sample corona charged for a long time than that in the sample corona-charged for a short period. This is consistent with the results shown in Figure 5.

Using the charge mapping technique, the bipolar charge carrier injection has been observed. These new phenomenon challenges the existing surface potential decay models, which were established based on the single layer of charge carries. And interface influence factor should be considered in further research on corona charge polymeric materials as well.

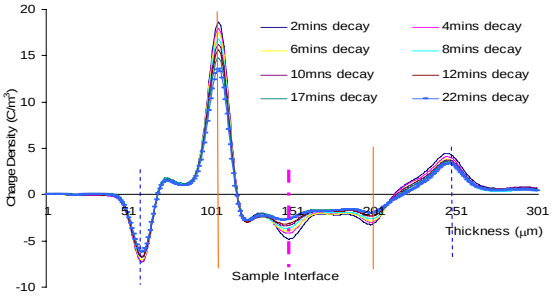

Figure 10: Space charge distribution decay in two layer corona charged sample (50μm+50μm, -4kV for 20mins)

4 Conclusion

The crossover phenomenon has been experimentally confirmed in this study. The surface potential decay is determined by several factors: corona voltage, sample thickness, charging electric field, charging period, polymer interface. The charge mapping technique used in the study of surface potential decay in polyethylene films is a valuable attempt. This technique provides an alternative way to investigate charge decay process and it allows monitoring charge migration through the bulk of corona charged film. The charge profiles obtained strongly suggest that the bipolar charge injection has taken place and interface has a special influence on charge transfer through the sample. And new surface potential decay model is required to explain the charge transport processes in corona charged LDPE film.

REFERENCES

[1] A. Kumadaa, Y. Shimizub, M. Chibab and K. Hidakab, Pockels Surface Potential Probe and Surface Charge Density Measurement, *Journal of Electrostatics* vol. 58, p. 45–58, 2003.

[2] G. Chen, Y. L. Chong and M. Fu, Calibration of the Pulsed Electroacoustic Technique in the Presence of Trapped Charge, *Measurement Science and Technology* vol. 17, p. 974-1980, 2006.

[3] T. J. Sonnonstine and M. M. Perlman, Surface-Potential Decay in Insulators with Fielddependent Mobility and Injection Efficiency, *J. App. Phys.* vol. 46, p. 3975 – 3981, 1975.

[4] R. Toomer, T. J. Lewis, Charge Trapping in Corona-Charged Polyethylene Films, *J. Phys. D: Appl. Phys.* vol. 13, p. 1343-1356, 1980.

[5] H. v. Berlepsch, Interpretation of Surface Potential Kinetics in HDPE by a Trapping Model, *J.Phys. D:Appl. Phys.* Vol. 18, p. 1155 – 1170, 1985.

[6] G. Chen, Z. Xu and L. W. Zhang, Measurement of Surface Potential Decay of Corona-Charged Polymer Films Using the Pulsed Electroacoustic Method, *Measurement Science and Technology*, 2007.

[7] L. W. Zhang, Z. Xu and G. Chen, Charge Decay of Corona-Charged Low Density Polyethylene, *Electrostatics 2007, Oxford, UK*, 2007.

Comparative Tracking Index Measurements of Materials at Reduced Atmospheric Pressures for Aerospace Applications

L. Zhang*, I. Cotton †

*PhD student, University of Manchester ,† Senior Lecturer, University of Manchester
phone: +44-161-306-8735; fax: +44-161-306-4820; e-mail: ian.cotton@manchester.ac.uk

Keywords: Comparative tracking index, tracking, creepage distance, aerospace

Abstract

Organic insulation materials are used in a variety of electrical apparatus owing to their light weight and good electrical and mechanical properties. One failure mode that can exist on such insulation is electrical tracking across surfaces, particularly those that are contaminated. This can eventually lead to electrical failure in the form of a short circuit and could pose a fire risk in some systems. For precise dimensioning of insulation within equipment, it is necessary to understand the mechanisms of electrical tracking as influenced by different environmental conditions. This paper describes work in which the Comparative Tracking Index (CTI) test is used to compare the resistance of various insulating materials to electrical tracking at different levels of air pressure. The variation of pressure is directly linked to the use of such materials in aircraft systems, particularly versions that are based on a more electric architecture and operate at higher voltages. The experiments have shown that in the range of pressures investigated, a lower pressure allows tracking damage to initiate at lower voltages and that this damage will be more severe for a given value of voltage.

1 Introduction

Electrical systems in the generation of aircraft currently in use tend to be a mix of AC and DC. DC systems are typically operated at 28 V while the AC system operates at 115 V rms (equivalent to 163 V peak phase to earth or 282 V peak phase to phase). The use of these voltages has historically provided a safe and reliable means of energy transport with the main risk being from electrical tracking. With the advent of technology such as the More-Electric-Aircraft, there are increased electrical power demands on the engines and this power must be transmitted across the airframe [1]. The increase in electrical power demand is due to the desire to eliminate heavy mechanical systems such as air-starter pipework and hot-air anti-ice systems. The replacement of such systems with electrical alternatives will provide significant aircraft efficiency benefits resulting in better environmental performance due to reduced fuel consumption.[1-3]

To prevent a significant increase in system weight through the need to transmit large currents, increased voltages are now being used in both commercial and military aircraft. In an aircraft there is also a significant tension between the desire to have a reliable power system with the need to reduce the volume and weight of equipment to the minimum possible. The control of surface discharges on items such as connectors and circuit boards is an important consideration in this regard. While much information is available for the use of organic insulating materials at atmospheric pressure, information regarding their use at low pressure is limited [4-7]. For precise dimensioning of insulation for aerospace applications, the performance of insulation materials at low pressures needs to be understood.

This paper deals with the threat to insulation systems those results from aqueous contamination being deposit on surfaces along which an electric field exists. This can lead to electrical tracking. Usually electrical tracking on insulating materials results from multiple discharges or small arcs which originate from the more conductive areas on the surface of the material and extend through the less conductive areas. Those multiple discharges or small arcs are described as scintillation.

In more detail, the process can be described as follows. In wet contaminated conditions, it is accepted that leakage current can easily be generated; meaning that the conductive contaminant evaporates as it heats and that small dry areas are produced. These formation of these dry-bands were first proposed by Obenaus[8]. The voltage across the dry-band may be high enough to cause localized breakdown since the electrical resistance of the dry band is high. These arcs can cause significant damage to the insulation surface and if carbonisation occurs can lead to eventual failure of the dielectric system.

In this paper, studies of tracking failure on different insulating materials at both ambient pressure and 100mbar (roughly equivalent to the pressure at 50,000ft) are reported. The tests have been carried out using standard CTI test methods according to IEC 60112. Through collection of voltage and

current data during the test, the mechanism of tracking failure is discussed. The relative damages to the organic materials at different pressures have been evaluated. The experiments have shown that in the range of pressures investigated, a lower pressure allows tracking damage to initiate at lower voltages and will be more severe for a given value of voltage.

2 Experimental method

The test set up conformed to the requirements of IEC 60112. Figure 1 shows the circuit diagram used for the test. The general arrangement of the test sample and the electrodes used is shown in Figure 1.

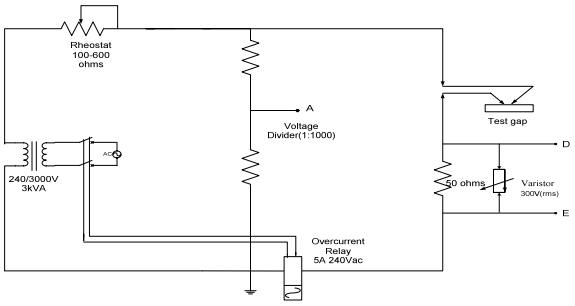

Figure 1 Sketch of the test circuit.

The power source is provided by a 240/3000V 3kVA 50Hz transformer. This is fed through a resistor that it set to keep the prospective short circuit current at a value of 1A. A voltage divider measures the voltage across the test object with a further measurement (not shown on the diagram) being taken to measure the voltage on the feed side of the transformer. A resistive shunt is used to measure the current flowing through the test sample. The output of this is displayed on an oscilloscope following filtering using a first order RC low pass filter set to have a 3dB frequency of 677Hz. An overcurrent relay is used to trip the circuit when the current flowing in the circuit is above .5A for a period of 2s. The electrodes, dripping system and test solution are placed within an environment chamber which is used to vary the pressure from 1000mBar to 100mBar and keep the temperature at a constant 20°C. The chamber has internal dimensions of 0.6m x 0.6m x 0.6m and is equipped with electrical connectors which are used to provide power to a peristaltic pump within the chamber and to make the test circuit connections..

Copper is used for the test electrodes in this paper. Although platinum is specified in the standard, some researchers still believed that copper can be more close to the real insulation-conductors in practice[9] After each test, sandpaper is used to clean the copper electrodes. The solution used to wet the specimen is a mixture of 0.1% ammonium chloride in de-ionized water. This has a resistivity of 395Ωm at room temperature. The solution is applied in drops that are xml at a rate of one drop every 30s (+/-5s). The drops are applied from a height of 40mm.

The CTI is defined as the voltage at which the specimen does not fail for 50 water drops at the set voltage at 5 sites on the specimen. In addition, the sample must withstand a further 100 drops at 25V less than this value at five additional sites.

In this paper the insulating materials tested were plain circuit board (FR4) and ABS (Acrylonitrile Butadiene Styrene Plastic). In accordance with the standard, the test specimen of the solid insulating material must be at least 3mm thick. This was achieved by laminating three 1mm thick circuit boards together. The dimension of the samples was 20mm by 20mm.

Data from the tests was recorded using a NI Labview system. Voltage and current signals were digitized using a 12-bit data acquisition card running at 10kS/s. Stored data included snap shots of the actual voltage and current waveforms and calculated RMS/peak values that were logged every 0.1s.

3 Experiment results and discussion

3.1 Testing of FR4 at standard pressure

FR4 was tested at 1000mBar and 20°C. The voltage was gradually increased from 50V and the current / voltages measured using the system described. Figure 6 shows the plot of peak current values measured during the test period of 30 minutes. The sample did not fail and no damage was observed on the surface of the sample.

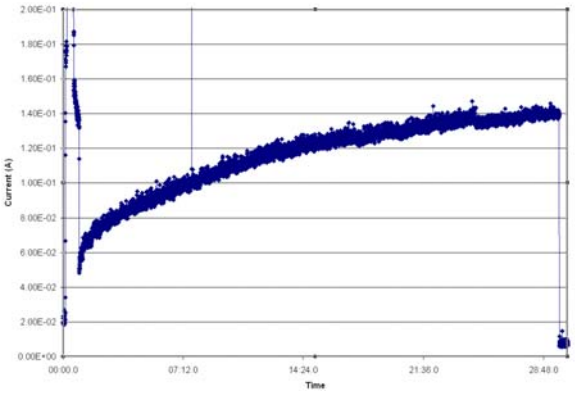

Figure 2 Peak current at 50V and 1000mbar for FR4.

The figure 2 shows that with the exception of the first few seconds of the test, the current flowing across the sample shows a gradual increase. This would suggest a gradual increase in the amount of contaminant being deposited on the surface of the sample decreasing the resistance between the electrodes. In this case, it is concluded that the current flow through the contaminant is insufficient to cause evaporation (or at least a lower rate of evaporation than the rate at which the contaminant is dropped onto the surface). As the test progresses, the quantity of liquid between the test electrodes increases and the resistance falls. While this will mean that the power dissipation in the contaminant will increase, the increased surface area of contaminant means that the temperature still does not reach boiling point.

When the test voltage is increased to 75V, the current trend as shown in Figure 3 is different. The current still initially increased but then reached a near steady state. In this case, we consider that the current flow causes sufficient heating to evaporate contaminant at the same rate of replenishment leading to a steady state current flow. Again, no damage occurs at this voltage since no arcing activity takes place on the sample.

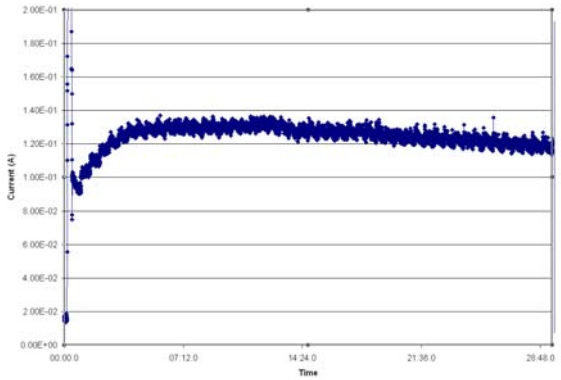

Figure 3 Peak current at 75V 1000mbar for FR4

Figure 4 shows us the peak current measured when the voltage across the test object was increased to 100V. Spikes of current are now observed. These have a peak value that is higher than that seen in the previous tests.

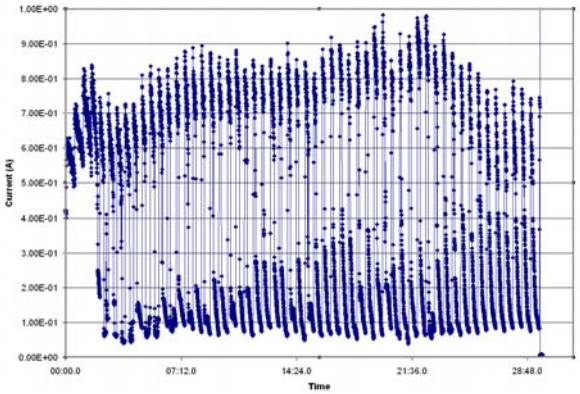

Figure 4 Peak current at 100V 1000mbar for FR4

This behaviour is characteristic of mechanisms that will be likely to cause tracking damage. Contaminant is being evaporated and in doing so will allow arcing to take place on the surface of the sample. This test level was the first at which damage was seen on the FR4 sample.

Testing at increasing voltages gave similar plots of current with the current spikes reducing in width.

We can introduce 4 different models for the aforementioned 4 different cases as follows. On the basis of the results described so far and knowledge of tracking processes, it is possible to define the following modes:

- **Mode 1 – Insignificant power:** In this mode, the current flow through the contaminant is too low to heat it sufficiently and cause evaporation. A steady increase in current flow is seen in the gap as the amount of fluid increases. No damage occurs.
- **Mode 2 – Constant current:** At a certain voltage, the current flow causes sufficient heating to evaporate contaminant at the same rate of replenishment leading to a stead state current flow. No damage occurs.
- **Mode 3 – Evaporation, arcing and no reignition:** When the contaminant evaporates owing to a high level of heating, an arc occurs in the dry band. Reignition does not take place unless reflow of the contaminant takes place if the voltage is below Paschen's minimum. This mode would not exist for cases where the voltage required to enter Mode 2 was above Paschen's minimum.
- **Mode 4 – Evaporation and significant arcing:** As the voltage is increased further, the system voltage allows re-ignitions of the arc to take place once it has initially extinguished. Severe damage is seen.

3.2 Testing of FR4 and ABS at reduced pressure

When the same material is tested at the lower pressure of 100mBar, we see a similar pattern in the plots of current. Initially, we see a current that increases as a function of time followed by one that levels off. Finally, spikes are seen indicating evaporation and arcing. However, the significant difference between this case and that of atmospheric pressure is that the transitions happen at a lower voltage. This correlates with damage being seen on the samples at a lower voltage level.

The main reason for this change in behaviour is the change in the boiling point and latent heat of vaporization of the contaminant solution. The boiling point of the contaminant drops from 101.5°C to 54.3°C when the pressure is reduced from 1000mBar to 100mBar. This will mean less heating is required to cause elevation of the solution temperature to the boiling point. This will therefore reduce the voltage at which evaporation takes place. In addition, a reduction in the latent heat of vaporization will mean that the evaporation process is more rapid. A second reason for the more severe damage being seen on the FR4 samples could be a change in the voltages at which reignition of any arcing takes place.

3.3 Visual evidence of damage

Work by other authors on the failure of organic insulating material samples exposed to discharges state that they more readily fail at low pressure than when they are at atmospheric pressure [6, 10]. Table 1 below clearly demonstrates the influence of lower pressure on tracking on the FR4 samples. The pictures are the physical evidence of a lower voltage being required to initiate tracking. In addition, damage is more severe at lower pressures, possibly due to the lower latent heat of vaporisation of liquids at low pressure and hence the longer time available for arcing.

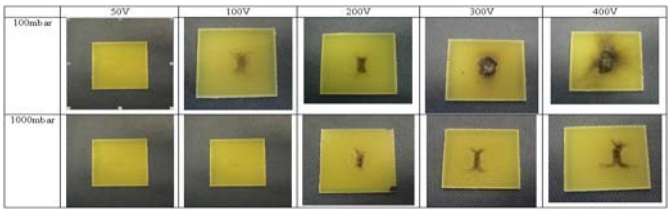

Table 1. Comparison of the damages on plain circuit board during the period of 50 drops contaminant solution

ABS has also been tested as part of this work. ABS is initials for Acrylonitrile Butadiene Styrene Plastic. ABS is a two phase polymer blend. A continuous phase of styrene-acrylonitrile copolymer (SAN) gives the material rigidity, hardness and heat resistance. The toughness of ABS is the result of sub-microscopically fine polybutadiene rubber particles uniformly distributed in the SAN matrix. Because of the good balance of the properties, ABS has been widely in electrical equipment. The current profiles observed when testing ABS were similar to those seen when testing FR4. However, while the damage started at a lower voltage at lower pressures, more severe damage occurred at atmospheric pressure as is shown in Table 2. This finding needs to be investigated further.

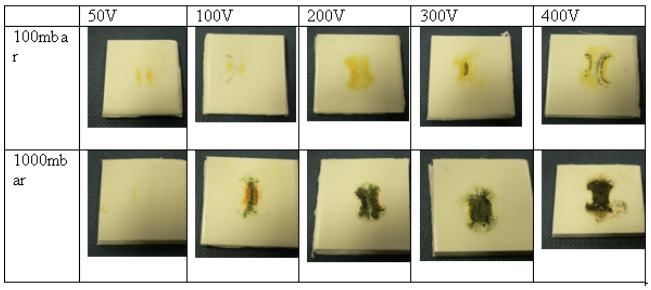

Table 2. Comparison of the damages on ABS during the period of 50 drops contaminant solution

4. Conclusion

The use of the IEC 60112 test procedure has allowed the examination of the relative tracking performance of FR4 and ABS at reduced pressures such would be found in an aerospace environment. The work has shown that the change in the boiling point of the liquid has a significant impact on the tracking performance, damage being instigated at a lower voltage at lower pressures. Increased levels of damage have been seen at lower pressure in FR4 but at higher pressures in ABS. This may be due to different mechanisms of decomposition taking place but these needs to be more clearly understood.

5. Future work

In the future, further analysis of the voltage and current waveforms collected simultaneously with the data shown in the paper will be carried out. It is hoped that this along with thermal modelling of the process and observation of the tracking mechanism using an infra-red camera will yield more useful information about tracking over insulating surfaces. In terms of minimizing dimensions of insulation for aerospace applications, this work will be used to adjust the creepage distance recommendations contained within IEC 60664[11].

References

[1] M. Howse, "All Electric Aircraft," *Power Engineer*, vol. 17, pp. 35-37.

[2] L. Faleiro, "Initial Research towards a More Electrical Aircraft," in *More Electrical Aircraft Conference*: Royal Aeronautics Society, April 2004.

[3] L. F. Faleiro, "Trends towards a More Electrical Aircraft," *Liebherr Aerospace Lindenberg GmbH and The Royal Aeronautical Society*, 2004.

[4] A. Nelms, "Electrical Discharge in More Electric Aircraft Power System," University of Manchester 2005.

[5] W. Pfeiffer, K. Richter, and P. V. Schau, "Electrical Strength of Small Creepage Distances under Natural Environmental Conditions," *IEEE Transactions on Electrical insulation*, vol. EI-19, December 1984.

[6] G. G. Karady, M. D. Sirkis, and J. R. Oliva, "Degrading Effect of High altitude Corona on Electronic Circuit Boards," *IEEE Transactions on Electrical insulation*, vol. 26, December 1991.

[7] B. X. Du, Y. Liu, and H. J. Liu, "Effects of Low Pressure on Tracking Failure of Printed Circuit Boards," *IEEE Transactions on Electrical Dielectrics and Electrical Insulation*, vol. 15, pp. 5, October 2008.

[8] F. Obenaus, "Elektrotechnische Aeitschrift," vol. 56, pp. 369, 1935.

[9] W. H. Middendorf, "The Use of Copper Electrodes for the Comparative Tracking Index Test," *IEEE Transactions on Electrical Insulation*, vol. EI-21, No.4, pp. 667-680, August 1986.

[10] R. Bartnikas and E. J. MacMahon, "Corona Measurements and Interpretation," *Engineering Dielectrics,ASTM STP669*, vol. I, 1979.

[11] "Insulation coordination for Equipment within low-voltage systems," *IEC Standard 60664*, 2003.